TAMPEREEN TEKNILLINEN YLIOPISTO
TAMPERE UNIVERSITY OF TECHNOLOGY

PAULI LOSOI

UP-SCALING OF MICROBIAL CO-CULTURES

Master of Science thesis

Examiners: Assistant Professor (tenure track) Ville Santala and Professor Jukka Konttinen

The examiners and topic of the thesis were approved on 8th August 2018

ABSTRACT

PAULI LOSOI: Up-Scaling of Microbial Co-Cultures
Tampere University of Technology
Master of Science thesis, 77 pages, 7 Appendix pages
Degree Programme in Bioengineering, MSc (Tech)
Major: Bioengineering
Examiners: Assistant Professor (tenure track) Ville Santala and Professor Jukka Konttinen

Keywords: bioengineering, scale-up, co-culture, fermentation

Microbial fermentations are used to produce pharmaceuticals, chemicals, and fuels. Side product formation along with considerable losses in productivities and yields are often encountered in transition from laboratory- to production-scale. This is mainly caused by inevitable heterogeneity of large, stirred reactors with aeration, especially in the commonly used fed-batch operation mode. Previous studies of this challenge have proposed either improving reactor homogeneity or increasing tolerance of the production host. Microbial co-cultures have also been suggested because they facilitate side-product utilization.

Purpose of this work was to examine the scale-up of microbial co-cultures. More specifically it was studied whether the adverse conditions caused by scale-up affect co-cultures less than the respective monocultures.

In this work monocultures of two bacterial species, *Escherichia coli* and *Acinetobacter baylyi*, and four co-cultures of them with and without gene deletions were cultivated in batch-mode in a 1 L aerated stirred reactor. Both batch and fed-batch operation modes were simulated with a model that incorporated a 70-compartment hydrodynamic representation of a 30 m^3 reactor, population balances, and unstructured kinetics. The simulations were performed also with an ideal reactor model at the 1 L-scale.

Due to internal recycling of acetate, which inhibited *E. coli* but was the preferred substrate for *A. baylyi*, the co-cultures had 10 % to 50 % higher specific growth rates compared to the single strain cultivations. Simulations showed more modest improvements ranging from 3 % to 20 % in both studied scales. Specific growth rates and consequently biomass productivities were consistently smaller at the simulated large-scale with both mono- and co-cultures. Based on the simulations it seems that co-cultures do not scale-up any better than the respective monocultures, but appropriate scale-down experiments are required for verification. However, they do have the potential to alleviate side-product inhibition also at industrial scale.

TIIVISTELMÄ

PAULI LOSOI: Mikrobiyhteisöjen laajentaminen tuotantomittakaavaan
Tampereen teknillinen yliopisto
Diplomityö, 77 sivua, 7 liitesivua
Biotekniikan DI-tutkinto-ohjelma
Pääaine: Bioengineering
Tarkastajat: Assistant Professor (tenure track) Ville Santala ja professori Jukka Konttinen

Avainsanat: biotekniikka, tuotantomittakaavaan laajentaminen, yhteiskasvatus, fermentaatio

Mikrobeilla tuotetaan teollisesti lukuisia tuotteita kuten lääkeaineita, kemikaaleja ja polttoaineita. Useimmiten fermentaation saannot ja tuottavuus kuitenkin pienenevät ja sivutuotemäärät kasvavat laboratoriosta tuotantomittakaavaan siirryttäessä, koska tuotantoon usein käytettävät suuret ilmastetut sekoitusreaktorit ovat heterogeenisiä erityisesti syöttöpanosprosesseissa. Ongelman ratkaisuiksi on tarjottu reaktorien heterogeenisyyden vähentämistä sekä tuotto-organismien sietokyvyn lisäämistä. Usean mikrobin yhteisviljelyä on myös ehdotettu, koska jo kahden lajin yhteisö voi pystyä luontevasti hyödyntämään toistensa sivutuotteita.

Tämän työn tarkoituksena on tarkastella yhteisviljelmien laajentamista teolliseen mittakaavaan ja erityisesti tutkia kestävätkö yhteisviljelmät suuren mittakaavan olosuhteita paremmin kuin vastaavat kannat yksin viljeltyinä. Työ suoritettiin kasvattamalla panosreaktiona ilmastetussa 1 L:n sekoitusreaktorissa *Escherichia coli*- ja *Acinetobacter baylyi*-bakteereita sekä yhteensä neljää niistä eri tavoin geenimuokattua yhteisviljelmää. Kaikkien kuuden viljelmän teollisen mittakaavan toimintaa simuloitiin mallilla, joka yhdisti 70 osastoa käsittävän mallin 30 m^3:n reaktorista, populaatiotaseen ja kineettisen kuvauksen mikrobien toiminnasta. Mallit simuloitiin sekä panos- että syöttöpanosprosesseina, ja kaikki simulaatiot toistettiin myös 1 L:n reaktoria kuvaavan ideaalireaktorimallin kanssa.

Yhteisviljelmien spesifi kasvunopeus oli 10–50 %:a suurempi kuin vastaavien yksittäisviljelmien. Simulaatioissa vastaava tulos toistui pienempänä, noin 3–20 %:n suuruisena. Suuremman kasvunopeuden selittää *A. baylyi*:n tapa suosia *E. coli*:n toimintaa haitanneen etikkahapon käyttämistä hiilenlähteenään. Simuloidussa suuren kokoluokan reaktorissa kasvunopeudet ja vastaavasti myös biomassan tuotto olivat johdonmukaisesti pienempiä sekä yhteis- että yksittäisviljelmillä. Simulaatioiden perusteella yhteisviljelmät eivät näytä siirtyvän tuotantomittakaavaan vastaavia yksittäisviljelmiään helpommin. Teollisen mittakaavan olosuhteita jäljitteleviä kokeita pitäisi kuitenkin tehdä ennen kuin asiasta voi vetää lopullisia johtopäätöksiä. Joka tapauksessa yhteisviljelmät kykenevät helpottamaan sivutuotteiden aiheuttamia ongelmia teollisessakin mittakaavassa.

PREFACE

This thesis work began on 1st of June in 2018 and it was conducted in the Laboratory of Chemistry and Bioengineering under the supervision of Assistant Professor (tenure track) Ville Santala. This work was independent in the sense that it was not part of any particular research project. However, it served as a natural extension to some of my earlier works at the laboratory.

My supervisor and examiner Ville Santala contributed by reviewing my research methodology and by giving practical suggestions for design of experiments. He also proposed a very educational book on bioreactor modelling by Jérôme Morchain, which led me to familiarize myself with research on biological population balance models and compartmental reactor models. In hindsight, I do not know whether I could have done much of an estimation of large-scale operation without getting in touch with these subjects first. My second examiner Jukka Konttinen contributed to this thesis by assessing my modelling methodology and by giving a valuable reminder on limiting the amount of parameters that are fit to measurements. Both Ville Santala and Suvi Santala are acknowledged for designing the four co-cultures used in this thesis and guiding me through constructing the strains during Summer 2017.

I give my thanks to Ville and Jukka for supervision and examination of my thesis, and all the trust in letting me do a rather independent piece of work. I am also grateful to the members of the synthetic biology group, and particularly Suvi, Tapio, and Milla for teaching me practices around the laboratory during the past two of years I have been involved in laboratory work. Last but not least, I thank my dear wife Sara, for without her respect and invaluable efforts in taking care of our daughter at home I could not have devoted so much of my time on this work.
Soli Deo gloria.

In Tampere, Finland, on 21th November 2018

Pauli Losoi

CONTENTS

LIST OF FIGURES

LIST OF TABLES

LIST OF ABBREVIATIONS AND SYMBOLS

Abbreviations

FI	Fluorescence intensity
OD_{600}	Optical density at 600 nm

Physico-chemical symbols

n	Amount
A	Area
C	Concentration
O	Dissolved oxygen concentration
μ	Dynamic viscosity
O_2	Gaseous oxygen concentration
ρ	Density
d	Diameter
D	Diffusivity
N_F	Flow number
ϕ	Gas holdup
g	Gravitational acceleration
H	Height
H	Henry's constant
Π	Hydrostatic pressure correction factor
R	Ideal gas constant
k_L	Liquid-phase mass transfer coefficient
m	Mass
M	Molar mass
pO_2	Oxygen tension
p	Partial pressure
pH	pH, negative 10-based logarithm of hydrogen ion concentration
P	Power
N_P	Power number
P	Pressure
q	Reaction rate
R	Reynolds number
N	Speed
σ	Surface tension
T	Temperature
t	Time
v	Velocity

ν	Kinematic viscosity
a	Specific or interfacial area
h	Specific height
k	Turbulence kinetic energy
ε	Turbulence power dissipation
V	Volume
F	Volume flow
Q	Volumetric productivity

Biological symbols

X	Biomass concentration
G	Glucose concentration
N	Gluconate concentration
A	Acetate concentration
E	ATP concentration
S	Substrate concentration
Y_{ij}	Yield of i on j
m_{S}	Maintenance
K	Affinity constant
I	Inhibition constant
μ	Specific growth rate
N	Number density or amount
ξ	Internal state vector in a population balance

Economic symbols

Γ	Capital investment
D	Depreciation
r	Discount
τ	Downtime
G	Gross profit
NPV	Net present value
t	Annual operating time
E	Operating costs
ω	Operating costs proportion
p	Price
W	Product amount
R	Revenues
δ	Summed discount term
T	Total production time
χ	Tax

1. INTRODUCTION

Microbial fermentations have been utilized by man for thousands of years by now. Most of the traditional applications have been related to food, such as bread baking, beer brewing, and wine making to name a few. Nowadays, however, fermentations are also used in producing fuels, chemicals, and pharmaceuticals alike, constituting what is known as the biochemical industry [60]. Global production volumes of the biochemical industry range from everything under $50\,\mathrm{kt\,a^{-1}}$ of high-value products, such as pharmacuticals or specialty chemicals, up to $1\,\mathrm{Mt\,a^{-1}}$ to $100\,\mathrm{Mt\,a^{-1}}$ of commodity chemicals, such as citric acid or ethanol [143].

Unfortunately, scale-up from laboratory to production scale often makes it difficult to provide adequate mass and heat transfer at a reasonable cost. Therefore the reactions start occurring in a physical regime, where mass transfer is the rate-limiting step [101]. In a chemical context this mostly just slows down the desired reaction, potentially leading to side-product formation, but when cells are involved, the adverse effects are easily more disruptive and less predictable as well. Microbial biomass constantly adapts to its surroundings unlike chemical catalysts, which in the ever fluctuating conditions of an industrial-size reactor leads to product yield losses.

Two approaches are readily devised as an answer to the aforementioned scale-up issues: either reactor heterogeneity should be decreased or biological tolerance to it increased. Improved reactor design with better mixing and oxygen transfer has been provided by chemical engineering, whereas genetic engineering has enhanced performace of production hosts in the adverse conditions of an industrial reactor. Biological tolerance to heterogeneous conditions, however, can be increased also by deliberately co-culturing such strains which could for example recycle the inhibitory side-products [131].

Given the general demand for products of microbial fermentations [143] and the issues of scale-up, this thesis assesses the scalability of microbial co-cultures as an alternative to the conventional monocultures. More specifically it is examined whether co-cultures could scale-up with smaller productivity losses than the respective monocultures, as illustrated in Figure 1.1.

To meet the objectives, two bacterial species, *Escherichia coli* and *Acinetobacter baylyi*, are cultivated together and in isolation in a 1 L aerated stirred reactor. In order to test various community dynamics, single-gene knock-out strains of both strains are co-cultured with the other, yielding altogether four co-cultures (one with the two wild-type strains, two with one wild-type and one knock-out strain, and one with two knock-out strains). Known

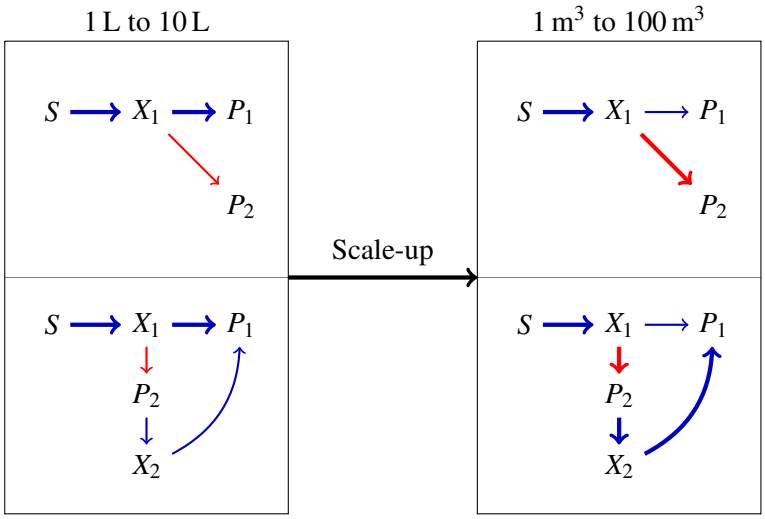

Figure 1.1 *Fermentation scale-up and co-cultures. Upon transition from small-scale (*1 L *to* 10 L*) to large-scale (*1 m^3 *to* 100 m^3*) the yield of the side-product P_2 is increased at the expense of the desired product P_1. This is indicated by increased thickness of the arrow pointing to the side-product. In one of the few studies conducted in an industrial sized reactor, a* 20 % *loss in* E. coli *biomass yield was realized in transition from* 15 L *to* 30 m^3 *[165]. It is proposed that co-cultures could help in recovering some of the effort lost in undesired side-product formation. Ideally such co-cultures could endure scale-up better than the respective monocultures do. X_1 and X_2 denote the microbial biomasses, and S stands for the substrate.*

to be unable grow on their own in the experiment conditions, the two knock-out strains are not cultivated in isolation. To estimate the effect of scale-up, both batch and fed-batch operation modes of the six cultures are then simulated with a model that couples a validated 70-compartment representation of a 30 m^3 reactor [151, 152], population balances, and unstructured kinetics [120]. The population balance models are simulated for reference also in an ideal reactor model corresponding to the 1 L-scale. To evaluate industrial relevance of performance differences across scales, a simple method for estimating the net present value of a fermentation relative to another one is derived.

Chapter 2 of this thesis lays out theoretical background concerning the research questions, and Chapter 3 presents the research methodology and materials used to answer the questions. Results are then presented in Chapter 4 and discussed in Chapter 5. Finally, the conclusions of this work are drawn in Chapter 6. Appendix A contains numerical summary tables of both experiments and simulations.

2. BACKGROUND

To understand the potential issues in fermentation scale-up and how co-cultures might be a beneficial approach to treat them, it is necessary to first consider fermentations in general (Section 2.1), and mass transfer phenomena in particular (Section 2.2). Scale-up itself along with its consequences are then treated in Section 2.3, and Section 2.4 presents microbial co-cultures and the potential benefits associated with them. This chapter concludes by reviewing some relevant modelling frameworks in Sections 2.5 and 2.6, which focus on biological and physical aspects of bioreactors, respectively.

2.1 Industrial fermentation bioprocesses

Applying a retro-design perspective, bioprocesses and chemical processes alike involve a product, downstream processes required for its purification, the main conversion process itself, upstream processes required to render chosen feedstocks more usable, and a feedstock [112]. In bioprocess industry the conversion is catalyzed by either enzymes or cells [31, 143]. This work focuses on up-scaling of microbial fermentations themselves, and therefore the products and feedstocks are presented here only briefly, and the various up- and downstream processes will not be covered at all.

Microbial fermentations are used in producing high-value compounds and bulk or commodity chemicals as well. In biochemical terms, these various products are either the microbial biomass itself, proteins produced by the microbes, or end-products of either primary or secondary metabolism. The more valuable products include pharmaceuticals, antibiotics, and specialty chemicals, for example [7], and biochemically these products tend to be recombinant proteins of very high value, such as insulin, human growth hormone, or secondary metabolites like penicillin [60]. Almost by definition, high-value products tend to have a smaller global demand and consequently smaller production volumes than products lower in value. Vice versa, the so called commodity or bulk chemicals are produced in larger quantities, and the most notable examples in terms of production volume are ethanol, L-glutamate, and citric acid, which were produced by microbial fermentations in quantities of 99 $\mathrm{Mt\,a^{-1}}$, 2.5 $\mathrm{Mt\,a^{-1}}$ and 1.7 $\mathrm{Mt\,a^{-1}}$ in 2014 [143].

Published studies include many more examples of potential products, some of which have not entered large-scale commercial production by fermentation. These include ethanol from lignocellulosic sources after gasification or hydrolysis [87, 97], fatty acid methyl esters [10], hydrogen [92, 136, 150], methyl halides [6], nanocellulose [93, 132],

polyhydroxybutyrate [30], and propionic acid [142], to name just a few. It is worth noting that some of these would have to compete with existing petrochemical routes.

As to the operating modes and conditions used in industrial fermentations, stirred tanks are the most conventional reactor type according to literature, and consequently this work focuses on them in particular. Alternatives to stirred tanks are bubble columns and airlift reactors, which do not involve mechanical agitation but rely on aeration only instead [1, 31]. Literature reports reactor volumes ranging from 0.05 m^3 to 800 m^3 [31, 60], temperatures within 20 °C to 40 °C [1, 31], mostly neutral pH conditions near 7, ranging from 4 to 8 [1], and mild pressures between 1 bar to 2.5 bar [167]. This is in contrast to the much more extreme temperatures, pressures, and pHs that can be found in chemical industry.

Fermentations themselves are often categorized as batch, continuous, or fed-batch processes. According to literature, fed-batch is the most applied production mode in industry due to its ability to achieve higher titers and productivities by appropriate environmental control than purely batch or continuous processes [60, 109]. Fed-batch fermentation contol by limiting the carboneous substrate is cited as the most common method, but recent studies have suggested various alternatives to this, such as limiting temperature below the level of fastest growth [62], controlling substrate feed to keep temperature constant [144, 145], limiting oxygen availability [23], and regulating substrate feed to hold dissolved oxygen concentration constant [17].

In addition to reactor configuration and operating conditions, a significant choice in any fermentation design is the host organism catalyzing the actual conversion from feedstocks to products. There is a vast amount of possible microbial hosts, ranging from bacteria to fungi, but only some are suitable to industrial fermentations. The host organism is ultimately determined by what it is capable of producing, how it performs in a bioreactor, and how amenable it is for genetic engineering if required. Obviously, when the product is the microbial biomass itself, the species must have some use as itself, such as the probiotic bacterium *Lactobacillus rhamnosus* [155, 156] or baker's yeast *Saccharomyces cerevisiae*. Hosts for recombinant protein production must be suitable for genetic engineering, and an often cited organism for these purposes is the easily modifiable bacterium *Escherichia coli* [60, 95]. Some other notable examples include the xanthan gum -producing bacterium *Xanthomonas campestris*, the fungus *Aspergillus niger* used in both enzyme and citric acid production, and the bacterium *Corynebacterium glutamicum* used in producing L-glutamic acid [60, 143].

One more requirement for any chosen production host is its ability to utilize the chosen feedstocks. Notably, almost all microbial fermentations convert renewable carbon sources into the products of interest [143]. In industry these carboneous feedstocks are often complex in composition, and they consist of polymers such as starch or cellulose, their hydrolysates, or the constituent carbohydrate monomers themselves. The use of synthesis gas (syngas) derived from lignocellulosic sources as a feedstock has also been proposed

[86, 97, 123, 143]. Theoretically, CO_2-based bioproduction is also possible with algae or other autotrophic organisms, but such schemes are not considered in this work. A distinct advantage of some microbial processes is that they can utilize waste streams [30], as is done in biogas production and in waste-water treatment, but this is often limited to mixed cultures of unknown composition. With pure cultures of single strains, coutilization of different substrates present in feedstock is often challenging [113].

Altogether, the performance of an industrial-scale fermentation process involving the aforementioned combination of a product, host organism, feedstock, and the necessary pre- and post-treatments, is mainly determined by the fermentation yield, productivity, and titer along with efficiency of any downstream processes [112]. The yield of substrate to product signifies the conversion efficiency, and it ranges mostly from $0.11\,\mathrm{g\,g^{-1}}$ to $1.0\,\mathrm{g\,g^{-1}}$, depending on products, substrate, and exact definition of yield [143]. Product titers should also be high to avoid excessive product loss during purification, and like yield, the achievable titers depend on the type of product in question: titers of only $1\,\mathrm{g\,L^{-1}}$ may be sufficient to high-value products, but some bulk chemicals are produced even in titers of $106\,\mathrm{g\,L^{-1}}$ to $504\,\mathrm{g\,L^{-1}}$ [60, 143]. Productivities, on the other hand, dictate the process times required of fermentations. They generally are greater than $2\,\mathrm{g\,L^{-1}\,h^{-1}}$, but values even up to $150\,\mathrm{g\,L^{-1}\,h^{-1}}$ have been demonstrated [143].

2.2 Mass transfer phenomena

Before the scale-up of fermentations is considered, the various mass transfer phenomena occurring in a bioreactor need to be reviewed first, and in order to treat mass transfer, the different phases present in a bioreactor must also be characterized. This work considers microbial fermentations carried out in stirred tanks with aeration, which gives a total of three phases to account for: liquid medium, gas, and microbial biomass. This would give a total of six mass transfer situations to consider: mixing within the three phases and transfers across the three phase interfaces. Mass transfer within the gas and biotic phases and between them are excluded, which leaves mixing within the liquid phase (Section 2.2.1), and mass transfer through gas-liquid interface (Section 2.2.2) and liquid-cell interface (Section 2.2.3). Emphasis is given also to the characteristic time-scales involved in these phenomena, because ultimately they govern which of the transfer processes limits the overall rate [78, 100, 101]. Considering a reaction or phenomenon rate as a function of a concentration C, its characteristic time-scale t is identified by approximating the reaction rate as [101]

$$q(C) \approx \frac{1}{t}C. \tag{2.1}$$

2.2.1 Mixing and turbulence within liquid phase

Liquid-phase mixing in a bioreactor can be classified to three main scales, which from largest to smallest are macromixing, mesomixing, and micromixing, and each of these is associated with characteristic scales of time and length [101]. The basis for any considerable mixing to occur in the first place is mechanical agitation, which induces a flow field in the reactor. Flow fields in turn are usually categorized according to laminar, transition, and turbulent regimes, of which only the turbulent regime is relevant to fermentations [31]. In a stirred tank equipped with an impeller of diameter d_i (m) rotating at speed N_i (s^{-1}), and filled with a liquid of density ρ_L ($\mathrm{kg\,m}^{-3}$) and viscosity μ_L (Pa s), the criterion for turbulent flow is conventionally expressed by the dimensionless impeller Reynolds number R_i

$$R_\mathrm{i} = \frac{N_\mathrm{i} d_\mathrm{i}^2 \rho_\mathrm{L}}{\mu_\mathrm{L}}, \tag{2.2}$$

which describes the ratio of inertial to viscous forces [31]. The flow induced by an impeller is considered turbulent when $R_\mathrm{i} > 10^4$ [31]. A further distinction in aerobic fermentations is whether the liquid-phase flow field is homo- or heterogeneous, or equivalently whether it is defined by mixing or gas flow [107].

The most common impeller type to provide for mechanical agitation in microbial fermentations is the Rushton turbine, a flat disc to which six blades are attached perpendicular to the disc plane. Some alternatives exist, such as hydrofoils or pitched blade systems [44, 139], to name a few, but strength of the Rushton turbine is its efficient gas dispersion in aerobic fermentations [31]. Given then a Rushton turbine, the power P (W) input to the liquid by the impeller is [31, 110]

$$P = N_\mathrm{P} \rho_\mathrm{L} N_\mathrm{i}^3 d_\mathrm{i}^5, \tag{2.3}$$

where N_P is the power number characteristic to the impeller type in turbulent flow regime ($R_\mathrm{i} > 10^4$). Volume specific power inputs in industrial fermentations are reported to range from $0.5\,\mathrm{kW\,m}^{-3}$ to $5\,\mathrm{kW\,m}^{-3}$ [31]. It should be noted that some host organisms are more sensitive to shear stresses created by stirring, which may impose limits to power input [31]. For example, the penicillin-producing fungus *Penicillium chrysogenum* was found to lyse 20 % more with 600 RPM stirrer speed than with 400 RPM, which corresponded to industrially relevant volume specific powers in the study conditions [158].

The performance of mechanical agitation is influenced not only by equipment geometry and stirrer speed, but also by aeration and rheology. Depending on the gas flow rate, impeller type, and stirrer speed, the power input may decrease even up to 70 % due to gas accumulation behind impeller blades in aerated reactors [42, 122]. In a large reactor with multiple impellers, only the bottom impeller is usually affected significantly by gas input [27]. As is evident from Equation 2.2, the liquid viscosity μ_L also affects the nature of

liquid flow. In general, both polymeric substrates and products, such as starch and xanthan gum, and also microbial biomass, increase liquid viscosity [31, 164]. Some substances and microbes exert a Newtonian effect on viscosity, which means that they merely increase broth viscosity linearly as a function of concentration, but especially gums and fungi also exhibit a non-Newtonian shear thinning behaviour [31, 89], in which the apparent viscosity of the fermentation broth actually decreases with increased power input [42]. Non-Newtonian liquids are therefore particularly challenging to homogenize effectively, because the shear thinning effect readily results in stagnant zones in regions further away from the impeller.

Within the flow fields induced by mechanical agitation there are several scales of mixing superimposed, namely macromixing, mesomixing, and micromixing [101]. Macromixing has the largest spatial and temporal scales and it corresponds to the convective transport of fluid with a characteristic length comparable to cubic root of total liquid volume. Mesomixing is caused by turbulent vortices and it is of smaller scale in both length and time. The smallest of mixing scales is further divided into micromixing caused by incorporation and micromixing by diffusion. Micromixing by incorporation happens at the Kolmogorov length scale, i.e. the length scale of the smallest turbulent vortices present, in which the fluid flow is considered to be laminar. The smallest of mixing scales is that caused by molecular diffusion, which is characterized by the Batchelor length scale. Equations of the characteristic spatial and temporal scales associated with the mixing types are shown in Table 2.1. Industrially relevant characteristic times of macromixing, mesomixing, micromixing by incorporation, and micromixing by diffusion are in the scales of 13 s, 0.2 s, 0.015 s and 0.008 s in a reactor of 22 m^3 working volume [85].

2.2.2 Oxygen transfer from gas to liquid

Many industrially relevant micro-organisms are aerobic respirers, but oxygen solubility in fermentation media is quite low, in the order of only 2 mg L^{-1} to 8 mg L^{-1}. Therefore oxygen has to be continuously supplied when aerobic organisms are used, and all of this makes oxygen transfer from gas- to liquid-phase an important topic to consider [43]. The volumetric oxygen transfer rate into liquid phase is expressed in terms of an overall transfer coefficient and a driving force [31, 43, 101]

$$\frac{\mathrm{d}O}{\mathrm{d}t} = k_{\mathrm{L}}a\,(O^* - O), \tag{2.4}$$

where the overall mass transfer coefficient $k_{\mathrm{L}}a$ (s^{-1}) is constituted by liquid-phase mass transfer coefficient k_{L} (m s^{-1}) and gas-liquid interfacial area a (m^2 m^{-3}), and where the driving force $O^* - O$ (mg L^{-1}) is defined by dissolved oxygen concentration in equilibrium O^* and actual dissolved oxygen concentration O. Industrially relevant characteristic time-scales of oxygen transfer range from 4 s to 50 s, given that the overall mass transfer coefficients are reported to range from 0.02 s^{-1} to 0.25 s^{-1} [31]. Comparing with the mixing

Table 2.1 *Length and time scales associated with main mechanisms of mixing, as defined in [101, Table 2.1]. To define the characteristic scales, a liquid volume V_L (m^3), impeller flow number (assuming turbulent regime) N_F, stirrer speed N_i (s^{-1}), impeller diameter d_i (m), mass specific turbulence kinetic energy k ($J\,kg^{-1}$), mass specific power ε ($W\,kg^{-1}$), kinematic viscosity ν ($m^2\,s^{-1}$) of liquid, and diffusivity D ($m^2\,s^{-1}$) in liquid are required. Taking the* 30 m^3 *(liquid volume* 22 m^3*, diameter* 2.09 m*, and impeller diameter* 0.7 m*) reactor studied by Vrábel, Lans, Cui, and Luyben [151] as an example, Linkès, Fede, Morchain, and Schmitz identified the characteristic times as* 13 s*,* 0.2 s*,* 0.015 s *and* 0.008 s *[85].*

	Characteristic length	Characteristic time
Macromixing	$V_L^{1/3}$	$\frac{V_L}{N_F N_i d_i^3}$
Mesomixing	$\frac{k^{3/2}}{2\varepsilon}$	$\frac{k}{2\varepsilon}$
Micromixing by incorporation	$\left(\frac{\nu^3}{\varepsilon}\right)^{1/4}$	$\left(\frac{\nu}{\varepsilon}\right)^{1/2}$
Micromixing by diffusion	$\left(\frac{D^2\nu}{\varepsilon}\right)^{1/4}$	$2\left(\frac{\nu}{\varepsilon}\right)^{1/2}\operatorname{arsinh}\left(0.05\frac{\nu}{D}\right)$

time-scales (Section 2.2.1), it is concluded that oxygen availability should not be limited by micromixing relevant to single cells [84, 85], but it is limited by the phase-interface transfer instead.

A plenty of empirical correlations have been derived to estimate the overall transfer coefficient $k_L a$ in different settings [42–44], but they are almost invariably derived at relatively small reactors in a homogeneous flow regime. This limits their applicability in estimating oxygen transfer in heterogeneous conditions [107]. Another limitation of such lumped correlations is that a and k_L are not necessarily in the same way proportional to different factors [71]. Nevertheless, some general remarks are that reactor configuration, input gas flow rate, and other operating conditions influence $k_L a$ [42, 43, 63].

Based on the concept of interfacial surface renewal, liquid-phase mass transfer coefficient k_L ($m\,s^{-1}$) has been correlated with power input P (W) and liquid diffusion constant D ($m^2\,s^{-1}$) of the transferred species [71]

$$k_L = 0.301\sqrt{D}\left(\frac{P}{V_L \mu_L}\right)^{1/4}, \tag{2.5}$$

where μ_L (Pa s) is the liquid viscosity. Antifoam agents and both polymeric products and substrates may increase mass transfer resistance in the gas-liquid boundary, decreasing k_L [17, 18, 70, 164]. Likewise it should be noted that in large reactors the turbulence energy dissipation is heterogeneously distributed with up to 100-fold differences between regions near and far from the impeller, which inevitably leads to heterogeneity in k_L across the

entire reactor [29].

The interfacial area a ($m^2\ m^{-3}$) in turn depends on the amount of air bubbles within the liquid phase and on the size and shape of them. The volume fraction of gas is defined

$$\phi = \frac{V_G}{V_L + V_G}, \tag{2.6}$$

where V_G (m^3) is the gas phase volume. Given then a gas volume fraction ϕ, and assuming the bubbles are spherical and their size can be expressed in terms of a mean diameter d_b (m), the liquid volume specific area becomes [101, 107]

$$a = \frac{6\phi\,(1-\phi)}{d_b} \tag{2.7}$$

Inferring the interfacial area a is then only a matter of estimating the gas holdup ϕ and mean diameter of bubbles d_b [43, 101, 107]. It is worth considering that bubble sizes are affected by bubble breakage and coalescence [44, 106, 162], and the effective interfacial area may be diminished by surface-active substances such as antifoam agents [70] or extracellular polymers [17, 18, 164]

The equilibrium concentration O^* depends on oxygen gas partial pressure, which makes it possible to augment the transfer driving force by increasing reactor pressure [22]. Another alternative is to enrich the input air with oxygen, but both of these approaches are limited by costs and possible inhibitory effects of excessively high oxygen concentrations to some host organisms [19].

2.2.3 Transfer at liquid-cell interface

Microbial biomass is often considered as a dissolved species within the liquid phase, but it is more correct to consider it as a suspended solid, as a phase of its own [84, 101]. Particularly substrate assimilation and product excretion are in fact mass transfer through a phase interface, the cellular membrane. It has been shown that at high cell-densities the characteristic time-scales of micromixing may overlap with those of substrate assimilation, which distincts a biological regime where the bioreactions are limited by biological capacity of the cells themselves, and a physical regime where the bioreactions are limited by micromixing instead [84, 101]. In the physical regime, transport towards the cells is the rate-limiting step, whereas in the biological regime the overall rate is limited by cellular uptake capacity. As an example: the substrate assimilation time-scale of $50\,g\,L^{-1}$ of biomass consuming $2\,g_S\,g_X^{-1}\,h^{-1}$ substrate present in an average concentration $10\,mg\,L^{-1}$ is 0.36 s, which already is close to the mesomixing and micromixing by incorporation time-scales (0.2 s and 0.015 s).

Another point to consider in liquid-cell transfer is that it involves several mechanisms. The main types of transport are diffusion, facilitated transport, and active transport [101].

Interestingly, even a simple theoretical calculation shows how a substantial portion of total cell membrane area is taken up by transport proteins [119]. This leads to the conclusion that there should be an actual physical maximum to cellular transport, imposed by available membrane area. The transporters present and their time-dependent relative contributions in given settings should therefore be accounted for.

2.3 Fermentation scale-up

Fermentation scale-up refers to the process of transferring a given fermentation from laboratory-scale (e.g. 1 L to 10 L) to industrial production-scale (e.g. 1 m^3 to 100 m^3). This 1000 to 100 000 -fold increase in volume has inevitably physical and biological consequences (Sections 2.3.1 and 2.3.2), which mostly relate to mass transfer. Heat transfer is another potential issue, but it is not considered in this work.

2.3.1 Physical consequences of scale-up

Physical scale-up consequences relate all to mass transfer either through mixing or aeration, and as was stated in Section 2.2.1, all of mass transfer is preceded by mechanical agitation. Considering only the power inputs required to mix a large reactor, it is seen from Equation 2.3 that the power P (W) is proportional to the fifth power of impeller diameter, d_i^5 (m). Already this observation sets a challenging objective: one should be able to provide sufficient mixing at both macro- and microscales without a prohibitive cost.

Indeed it is often found that both macro- and micromixing may become the rate-limiting steps in production scale reactor [100], leading to locally heterogeneous substrate concentrations within the reactor. Addition of concentrated acids and alkali and feeding of substrates into reactor invoke concentration gradients along the reactor in the macromixing space-time-scale [26, 37, 51]. In addition, efficient micromixing in the whole reactor is challenging due the heterogeneity of turbulent power dissipation ε found in reactors: up to 100-fold differences have been reported between regions near and far away from the impeller [29]. This implies that in a given instant the physical regime may limit substrate assimilation in regions further away from the impeller whereas the biological regime limits assimilation closer to impellers (see Sections 2.2.1 and 2.2.3).

Large reactors also require high gas flow rates for sufficient oxygen transfer, but the power input discussed earlier limits the amount of gas that can actually be effectively dispersed throughout the reactor. Non-uniform gas holdup ϕ distributions are common within large reactors [167] in addition to the already heterogeneous distribution of mass specific power ε [29], which by Equations 2.4, 2.5, and 2.7 implies a heterogeneous oxygen transfer capacity. Indeed, persistent gradients of dissolved oxygen concentration have been found [77] along with completely oxygen limited zones [37, 165]. A further complication regarding aeration of over 10 m^3 reactors is that even modest microbial

biomass concentrations ($10\,\mathrm{g\,L^{-1}}$) tend to require gas inputs so large that a heterogeneous flow regime is almost guaranteed [107]. Considering that laboratory-scale experiments are more often than not performed in homogeneous flow regimes, predicting production-scale performance from laboratory-scale is questionable [107].

2.3.2 Biological challenges in scale-up

The aforementioned physical heterogeneity in large-scale reactors has biological consequences as well [37]. Some organisms are more susceptible these heterogeneities and extremes of substrate concentration, dissolved oxygen, dissolved carbon dioxide, pH, and temperature than others. Due to insufficient mixing, aeration, and mass transfer, growth rates decrease [85, 120], side products such as acetate, formate, and ethanol form [18, 24, 35, 37, 69, 85, 90, 120, 153, 165], and transcription of some genes is toggled back and forth resulting in waste of cellular resources [16, 37, 76, 88, 111, 138, 155, 156], In addition, some properties of biological systems, such as foaming [67], release of outer membrane lipopolysaccharides, phospholipids, and carbohydrates [47], and morphology of fungi [148], to name a few, are challenging in themselves.

Probably one of the most studied biological challenges in fermentation scale-up is the acetate overflow metabolism of *E. coli* and its inhibitory effect [35, 90]. The general observation is that given glucose as a carbon source, some of it is converted to acetate regardless of oxygen availability, and even quite low acetate concentrations inhibit growth on glucose in *E. coli* [90, 124]. Glucose being the preferred substrate, *E. coli* does not usually efficiently utilize acetate either in such situations because acetate-utilization genes have not been expressed [38, 39]. Acetate overflow was associated with certain growth regimes [35], but recent research has confirmed that it is produced and consumed simultaneously [3, 37, 39, 120, 153, 165], which constitues a somewhat futile cycle. Acetate accumulation is then observed only when the production rate consistently exceeds consumption. Other observations are that the overflow in fed-batch operation depends on cultivation history prior to feeding [13], and that the rate of acetate anabolism depends likewise on cultivation history [38]. These observations make sense with the overflow definition in [120]: if *E. coli* can take up more glucose than it has adapted for to anabolize and catabolize, it does so, but the overconsumed glucose is dissimilated straight into acetate.

To complicate the scale-up further, microbial populations are inherently heterogeneous [5, 45, 76], even regardless of culture scale [5]. These geno- and phenotypic differences are problematic especially with genetically engineered organisms, if the microbial hosts have the load of additional gene expression [20]. Considering the amount of generations required to reach the final cell-density in large-scale reactors, the cell populations are susceptible to a large amount of potentially disruptive mutations. In a population carrying additional gene expression load, this gives rise to non-producing mutants with improved fitness, which eventually leads to the population losing its producitivity. Reaching the final

cell-density in a 1 m^3-scale reactor may require over 60 generations since initial inoculation, and depending on mutation rate and the gene expression load, even 95 % of recombinant protein productivity could be lost [126].

2.4 Microbial co-cultures

Challenges of fermentation scale-up were categorized as physical and biological. To the extent it is possible, physical adversities are tackled by reactor design. An applicable method to solve biological challenges is genetic engineering of the production strain, but given the potential instability of genetical constructs, this approach also has its limits. Microbial co-cultures provide an alternative way to increase tolerance to the physical heterogeneity encountered. Inspired by natural microbial communities, co-culture systems enable efficient utilization of several substrates simultaneously, easier culture of certain strains by cross-feeding, removal of inhibitory substances such as acetate, and also specialization of tasks within community [14, 40, 54, 64].

Efficient substrate coutilization is generally challenging to a single strain, even though it has been facilitated by genetic engineering [113]. Another approach is to co-cultivate strains with altogether different preferences or capabilities for substrate utilization, which also has the advantage of eliminating competition over resources within a co-culture. Coutilization of hexose-pentose mixtures has been succesfully demonstrated with the important observation that the community structure, or strain proportions, adapted according to the feed composition [36, 163, 168]. In addition to simultaneous utilization of different substrates, co-culture systems may be enhanced by strains providing substrates to one another [6, 32, 58, 98, 99, 131, 150, 169, 172].

The third listed benefit associated with co-cultures, removal of inhibitory substances, is readily coupled to the previous one, cross-feeding, and like cross-feeding, it drives commensialistic or mutualistic population dynamics. The undesired, often inhibitory side products, such as acetate and ethanol, are potential substrates to other strains which prefer them as carbon sources, and consequently many studies have shown the positive effect of inhibitor removal by a co-cultured strain [6, 131, 169]. Relating to inhibitory side products, pH stabilization has also been shown to enhance performance in co-cultures [10, 131]. Yet another type of inhibition removal can be demonstrated by co-cultivating aerobic and anaerobic strains, where the aerobe consumes all input oxygen effectively enough to keep the environment sufficiently anoxic to the anaerobic strain [66, 172].

The simultaneous substrate utilization and cross-feeding mentioned earlier were both examples of metabolic specialization in community [64]. The rationale in such approaches is to mimick natural communities, in which differnent functions are also carried out by specialized community members. Research has demonstrated two potential applications: cultivating a cellulolytic strain together with a strain producing ethanol, isobutanol, hydrogen, or even methyl iodine [6, 32, 99, 150, 172], or a strain capable of converting

an intermediate compound to a challenging product with a strain providing that particular intermediate efficiently [160, 168, 169]. Both applications share the benefit of achieving a challenging conversion in a single fermentation process step. Using a cellulolytic strain to provide soluble carbohydrate monomers to the culture additionally makes the producing strain dependent of the cellulolytic one. Given that genetically engineered organisms are susceptible to mutational instability [126], a properly designed co-culture system has the benefit of requiring less genetic engineering of individual strains to achieve the desired goal.

2.5 Biological models

To further understand bioreactor functioning, appropriate simplifications and models are required. Some of the most common ways to model the microbiological aspects are kinetic models (Section 2.5.1) and genome-scale metabolic models (Section 2.5.2). Often left unstated, however, is that most modelling attempts are carried out with an implicit assumption of a perfectly homogeneus population. This simplification is somewhat problematic given the studies proving heterogeneity of microbial populations [5, 45, 76]. At best it neglects an inherent property of the system subject to modelling, and at worst it leads to model failure. To deal then with biological heterogeneity, the concept of population balances is reviewed in Section 2.5.3.

2.5.1 Kinetic models

Kinetic models come in two main forms: unstructured and structured models. The distinction is in that unstructured models do not consider intracellular variables, whereas structured models do [102, 147], and consequently they are simpler in nature. At the heart of all biokinetic models lies the growth rate of biomass. Considering a biomass of concentration X ($\mathrm{g\,L^{-1}}$), the rate of its formation is conceptually an autocatalytic first-order reaction, leading to the expression

$$\frac{\mathrm{d}X}{\mathrm{d}t} = \mu X, \tag{2.8}$$

where μ is the specific growth rate ($\mathrm{h^{-1}}$). To be precise, this formulation holds true only at a metabolic steady-state where growth of cellular mass is equivalent to growth in cell number, such as during the exponential phase of a batch cultivation [94, 121]. In such conditions where μ is essentially constant, growth is exponential. Already this step has implicitly assumed an identical specific growth rate μ for the entire population, making the kinetic models population averaged unless heterogeneity of population is somehow accounted for, for example by coupling to a population balance [101]. The characteristic time-scale of growth is usually between 1 h to 5 h (equal to μ^{-1}), making growth the slowest phenomenon occurring in a bioreactor. As such, growth does not compete with any of the

mixing scales.

Considering biomass X ($\mathrm{g\,L^{-1}}$) growth (Equation 2.8) as an autocatalytic reaction with first-order kinetics is misleading in the sense that the specific growth rate μ ($\mathrm{h^{-1}}$) is by no means a constant independent of prevailing conditions. The most common formulation of specific growth rate μ is the so-called Monod model

$$\mu = \mu_{\max} \frac{S}{K_S + S}, \tag{2.9}$$

where the introduction of substrate concentration S ($\mathrm{g\,L^{-1}}$) and a substrate affinity constant K_S ($\mathrm{g\,L^{-1}}$) makes growth kinetics vary between zero- and first-order, depending on substrate concentration S. A point worth making is that this commonly [3, 48, 61, 73, 118, 120, 134, 153, 166] used formulation implicitly has assumed homogeneous catalysis, and as such neglects possible micromixing limitations to substrate uptake and subsequent growth [84, 85, 101, 121].

With the specific growth rate μ ($\mathrm{h^{-1}}$) established, the biomass specific substrate uptake ($\mathrm{g_S\,g_X^{-1}\,h^{-1}}$) is then usually directly associated with it by a yield coefficient Y_{XS} of biomass produced on consumed substrate ($\mathrm{g_X\,g_S^{-1}}$)

$$\left(\frac{\mathrm{d}S}{\mathrm{d}t}\right) X^{-1} = \frac{\mu}{Y_{XS}}. \tag{2.10}$$

This modelling step in turn couples substrate uptake rate directly to growth rate, which implies immediate adaptation of both uptake and growth to the prevailing substrate concentration. Equations 2.8, 2.9, and 2.10 constitute a basic unstructured kinetic model, which despite all the simplifications involved provides a good estimate as long as the population is not facing any considerable environmental changes. Unstructured models are therefore applicable in modelling the exponential phase of a batch cultivation or steady-states of continuous operations.

2.5.2 Genome-scale metabolic models

The basic unstructured model presented earlier merges numerous biochemical processes into a couple of simple reactions, which makes it impossible to include or infer the effect of any single enzyme-catalyzed step on the overall reaction rates. Metabolic models, on the other hand, employ a genome-scale reconstruction of all known enzyme-catalyzed reactions enabled by the particular micro-organism's genome.

Kinetics of all enzyme-catalyzed reactions are not available, though, so the metabolic models are studied using flux balance analysis, which assumes steady-state kinetics, or in other words that the concentration of compounds is not changed. Mathematically this is expressed by collecting all known reaction stoichiometry into a matrix, which maps

reaction fluxes (mol L^{-1} h^{-1}) into metabolite concentration change rates (mol L^{-1} h^{-1}), and studying the null-space of the resulting stoichiometry matrix [114]. Once exchange flux reactions importing and exporting extracellular compounds have been added, all possible steady-state solutions to the genome-scale metabolite mass balance are contained in the null-space. To infer something applicable, mathematical optimization is used with bounds imposed on chosen reactions. The most common optimization target is to maximize flux through a growth reaction representing biomass assembly, which leads to the following optimization problem given a stoichiometry matrix $\mathbf{S}$, reaction flux vector $\mathbf{v}$, lower bounds $\mathbf{v_l}$, and upper bounds $\mathbf{v_u}$:

$$\begin{aligned} &\text{Maximize} && \mu, \\ &\text{such that} && \mathbf{Sv} = \mathbf{0}, \\ &\text{where} && \mathbf{v_l} \leq \mathbf{v} \leq \mathbf{v_u}. \end{aligned} \tag{2.11}$$

Flux balance analysis can be used to estimate the effects of genetic engineering [135] or to deduce general reaction network properties [2]. It has also been used in studying functioning of and interactions within microbial co-cultures [21, 49, 72, 141, 146, 171]. Another extension, also applied in co-culture studies, is dynamic flux balance analysis, which is used to simulate the time-course of batch cultivations by sequential flux balance analyses [57, 170].

Despite their merits, flux balance analyses have some drawbacks as well. Firstly, they generally do not treat intracellular concentrations nor do they generally impose any bounds on intracellular reaction fluxes apart from the notion of reversible and irreversible reactions. The recently formulated demand-directed dynamic flux balance analysis provides a framework for including intracellular bounds linked to gene expression demand [161]. A drawback of applying flux balance analyses to co-cultures is the fact that if direct inter-species metabolite exchange is possible, the mathematical optimization step treats the whole community as a single entity, which may result in unrealistic metabolite exchange with the community [74]. However, this drawback can be circumvented in dynamic flux balance analyses by formulating the extracellular mass balance and stoichiometry matrix such that direct exchange between different species is not possible within optimization steps. Like kinetic models, flux balance analyses also implicitly assume a homogeneous population which instantly adapts to the most optimal performance allowed by the modelled reaction network.

2.5.3 Population balance models

Considering that not all individuals in a microbial population share the same physiological state [5, 45], even regardless of cultivation scale [5], there is a need to distinguish individuals of a population from one another also in modelling. Population balance models utilized in process engineering can also be applied to biological population modelling [101]. In a

bioprocessing context, air bubble size distribution modelling along with cellulose hydrolysis modelling have already been demonstrated [44, 79, 106]

Describing the number density N, or probability equivalently, of a particle with internal properties ξ residing in position x of physical space, the general form of a population balance equation is [101, 103–105]

$$\frac{\partial N(\xi,x,t)}{\partial t} + \frac{\partial N(\xi,x,t)\, v_\xi}{\partial \xi} + v_i \frac{\partial N(\xi,x,t)}{\partial x_i} - D_i \frac{\partial}{\partial x_i}\left(\frac{\partial N(\xi,x,t)}{\partial x_i}\right) = R(\xi,t)\,. \tag{2.12}$$

First of the left-side equation terms translates to the overall rate of change with respect to time. The second term describes change of internal properties, with a transport velocity v_ξ. The third and fourth terms both translate to tranport in physical space, with the third describing convective, and the fourth diffusive transport, respectively. The right-side term stands for production and consumption of particles with the internal state ξ.

The challenge in utilizing population balances in cell modelling is the same as in the use of structured kinetic models (Section 2.5.1): the amount of potential intracellular variables is huge. Therefore, the choice of an appropriate state vector ξ is far from trivial. Population balances for cell mass, age, and composition have been derived, but from such properties it is difficult to infer the reaction rates catalyzed by the cell population [101]. An alternative is to apply the specific growth rate μ as the discriminating factor in a one-dimensional population balance, demonstrated in recent works [103–105, 120]. This recent approach has the advantage that μ relates more naturally to the metabolic rates of cells than cellular size or age do [101].

Considering then

1. Biomass concentration X representing number density N
2. Specific growth rate μ as the only internal state variable ξ
3. Biomass growth (Equation 2.8) as the source term R without cell death
4. Only convective tranport in physical space x

and assuming daughter cells inherit the mother cell's growth rate [103, 120], the general population balance (Equation 2.12) simplifies to

$$\frac{\partial X(\mu,x,t)}{\partial t} + \frac{\partial X(\mu,x,t)\, v_\mu}{\partial \mu} + v_i \frac{\partial X(\mu,x,t)}{\partial x_i} = \mu X(\mu,x,t)\,. \tag{2.13}$$

The velocity in internal variable space corresponds now to velocity of growth rate adaptation v_μ [102–105, 120, 121]

$$v_\mu = \left(\frac{\mu_{\max}}{1.25} + \mu\right)(\mu^* - \mu), \tag{2.14}$$

where $\left(\frac{\mu_{\max}}{1.25} + \mu\right)^{-1}$ corresponds to the characteristic time-scale of growth adaptation in the order of 1 h to 3 h. Here μ^* is the specific growth rate at biological equilibrium, which is

defined as the population averaged growth rate a completely adapted microbial population would have. This definition allows a natural way to couple population balances with unstructured kinetic models (Equations 2.9 and 2.10), which are then taken to describe the behaviour μ^* the population is adapting to [103, 104, 120].

Modelling frameworks presented in previous sections implicitly assumed that the whole population adapts immediately to local concentrations. It has been shown and discussed thoroughly that this is not the case [38]. To model biological delays, such models need to incorporate lag constants, such as in [73, 149]. A strength of population balances is that they can be used to decouple actual growth rates from local concentrations [103–105, 120, 121], which renders delay or lag contants obsolete by introducing the concept of biological disequilibrium driving adaptation towards equilibrium. Further improvements have been demonstrated by decoupling substrate uptake rates from growth rates and by formulating the source term (right-hand side in Equation 2.12) such that growth gives rise also to daughter cell's with a growth rate different of their mother [105, 121].

2.6 Reactor models

Physical aspects of a bioreactor are generally modelled by either ideal reactor models, compartment models, or computational fluid dynamics. Ideal models are by far the simplest of these, computational fluid dynamic models the most complex, and compartment models in between. Regardless of the chosen modelling technique, it must provide a description of mass transfer between and withing the phases, throughout the reactor [100]. Regarding large-scale reactor modelling, an unfortunate complication in model validation is that only few studies available in open literature have been carried in a scale truly relevant to production, from 15 m^3 to 30 m^3 [125, 152, 165].

The simplest of the models, ideal reactors, assume that an aerated stirred reactor is perfectly mixed and homogeneous. Such a simplification is applicable as long as the characteristic mixing times do not interfere with characteristic reaction times. Well-stirred laboratory-scale (1 L to 10 L) reactors are usually sufficiently well described by these models.

The perfect mixing assumption becomes unjustified and misleading at large scale and especially much so in the case of fed-batch processes. An applicable extension of the ideal homogeneous reactors is then to consider a given reactor as a network of interconnected ideal reactors. Such models are usually known as networks-of-zones or compartment models [28, 106, 151, 167]. The advantage is that they simultaneously enable a heterogeneous description of mixing and other relevant physical characteristics, such as gas holdup, but without denying integration of a complex biokinetic model of the microbial biomass [120, 153]. Compartment models are derived either by general knowledge of hydrodynamics [151, 167] or by computational fluid dynamics [28, 106], and they generally consist of around 100 compartments, but even 9216 have been used.

The experimental validation of these models is usually done by verifying that the simulated and experimentally observed macroscopic mixing times match [28, 151, 152].

Computational fluid dynamics in turn involve solving fluid velocity fields with Navier-Stokes equations throughout the reactor [31, 100]. The solving process resembles compartment models in the sense that the reactor is first discretized into a computational mesh. However, the amount of compartments is much larger here, often between 100 000 to 1 000 000. Biokinetic models have also been integrated to computational fluid dynamics, but model complexity is limited by computational costs [50–52, 104]. At small-scale it has been possible to validate the resulting flow fields by optical methods, and the simulation correctness has been found to depend on the chosen physical boundary conditions [137]. Like with the previously presented compartment models, validation of large-scale reactor models is hampered by the lack of experimental data. Nevertheless, rigorously performed simulations provide a description of fluid dynamics based on fundamental physics, which probably is the best that can be achieved by any simulations.

3. METHODS AND MATERIALS

To answer the research questions, batch experiments were carried out, the obtained samples were analyzed, and both small- and large-scale fermentations were simulated. Finally, performance of the different cultures had to be quantified in order to compare them. Section 3.1 explains the conducted experiments, whereas Section 3.2 explains the analytics performed. Simulations and comparisons are explained in Sections 3.3 and 3.4, respectively.

3.1 Batch fermentation experiments

The six culture settings, two monocultures and four co-cultures, were each batch-cultivated in a 1 L bioreactor. The bacterial strains used in this work are described in Section 3.1.1, cultivation media and conditions in Section 3.1.2, and the bioreactor configuration and experiment performance in Section 3.1.3

3.1.1 Bacterial strains and genetic constructs

This work was conducted with altogether four bacterial strains consisting of two *Escherichia coli* and two *Acinetobacter baylyi* strains, which were constructed by the author in an earlier work. The used strains and their parent strains are characterized in Table 3.1, and a wild-type and glucose-utilization knock-out strain of both were utilized in this work. To facilitate identification of individual strains in co-cultures, all of the used strains had also a genomically integrated constitutive fluorescent protein expression cassette, a so-called capacity monitor [20]: *A. baylyi* strains expressed the red fluorescent protein mScarlet [11], and *E. coli* strains expressed the superfolder green fluorescent protein sfGFP [116]. The green fluorescent protein sfGFP [116] has excitation-emission maxima at 485 nm and 510 nm, respectively, whereas mScarlet [11] has its excitation-emission maxima at 569 nm and 594 nm, respectively. The genomic integrations of sfGFP and mScarlet were confirmed visually, by antibiotic resistances, and also by fluorescence measurements in the earlier work. Construction of the strains and compositions of the expression cassettes are briefly described below.

Genomic integration of the sfGFP expression cassette into *E. coli* was based on the conditional-replication, integration, and modular (CRIM) plasmids [46]. The CRIM plasmids Burden Monitor phi80 version (henceforth pBM) and pAH123 were gifts from Tom Ellis (Addgene plasmids #66074 and #66077, respectively) [20], and genomic integrations into *E. coli* strains were conducted as described in the original publication [46].

Table 3.1 *Bacterial strains used in this work, and their parent strains. BM(int) and mS(int) are shorthands to the constitutively expressed fluorescent protein constructs integrated into genome. BM(int) is the construct for green fluorescent protein sfGFP expression, and mS(int) for the red fluorescent protein mScarlet. Integration of mS(int) into* A. baylyi *resulted in* ΔpoxB *deletion, but this was not found to have any distinct effect. The gene deletion* ΔptsI *renders* E. coli *uncapable of importing glucose, and deletion* ΔgntT *makes* A. baylyi *uncapable of importing gluconate. P(G) denotes whether the strain is capable of growing on glucose. The observable fluorescence is designated by P(F). CGSC stands for Yale University Coli Genetic Stock Center, whereas DSMZ stands for Deutsche Sammlung von Mikroorganismen und Zellkulturen.*

Strain	Genotype	P(G)	P(F)	Source
EC	*E. coli* BM(int)	+	+	Earlier work by author
EC*Δptsl*	*E. coli Δptsl*	−	+	Earlier work by author
AB	*A. baylyi* mS(int)	+	+	Earlier work by author
AB*ΔgntT*	*A. baylyi ΔgntT* mS(int)	−	+	Earlier work by author
K-12 BW25113	*E. coli*	+	−	CGSC no. 7636
K-12 JW2409	*E. coli Δptsl*	−	−	CGSC no. 9918 [4]
ADP1	*A. baylyi*	+	−	DSMZ (DSM no. 24193)
ADP1 *ΔgntT*	*A. baylyi ΔgntT*	−	−	[8]

The sfGFP expression cassette was contained in the pBM plasmid, and it was composed of the synthetic constitutive promoter BBa_J23100, a synthetic ribosome binding site, the sfGFP protein coding sequence codon-optimized for *E. coli*, and a synthetic terminator.

Integrations of the mScarlet expression cassette into *A. baylyi* genome were conducted similarly to [129]: the gene cassette [130] overwriting the *poxB*-locus (ACIAD3381) of *A. baylyi* genome was utilized, but with the mScarlet cassette inserted into it. As a consequence, none of the *A. baylyi* strains used in this work expressed the pyruvate dehydrogenase poxB (EC:1.2.5.1). The mScarlet cassette was ordered from GenScript (New Jersey, United States) with a design similar to the sfGFP cassette:

1. MunI restriction site
2. BBa_J23100 synthetic constitutive promoter [20]
3. Synthetic ribosome binding site [20], shortened 3 bp from 3'-end
4. NdeI restriction site
5. 6H-tag [59]
6. Glycine-serine-glycine-linker
7. mScarlet coding sequence [11] codon-optimized by GenScript for *E. coli*
8. 2 stop codons
9. XhoI restriction site.

After the mScarlet construct had been extracted and purified from its initial *E. coli* host and plasmid with GeneJET Plasmid Miniprep Kit (Thermo Fisher Scientific, USA), MunI and XhoI restriction enzymes (Fermentas, Lithuania), gel electrophoresis, and GeneJET Gel Extraction Kit (Fermentas), it was ligated into the MunI-XhoI-digested integration plasmid

Table 3.2 *Mineral salt medium (MSM) composition used in all liquid cultivations. The only difference to original [53] is a doubled concentration of phosphate buffer (K_2HPO_4-NaH_2PO_4). The medium was prepared by diluting sterilized phosphate buffer, ammonium sulfate, and salt stock solutions in sterilized ion-exchanged water. A carbon source (glucose, gluconate, or acetate) was always added to cultivation media.*

Component	Concentration / mg L^{-1}	Component	Concentration / mg L^{-1}
K_2HPO_4	3880	$ZnSO_4 \cdot 7\,H_2O$	2
NaH_2PO_4	1630	$CaCl_2 \cdot 2\,H_2O$	1
$(NH_4)_2SO_4$	2000	$MnCl_2 \cdot 2\,H_2O$	1
$MgCl_2 \cdot 6\,H_2O$	100	$CoCl_2 \cdot 6\,H_2O$	0.4
EDTA	10	$CuSO_4 \cdot 5\,H_2O$	0.2
$FeSO_4 \cdot 7\,H_2O$	5	$Na_2MoO_4 \cdot 2\,H_2O$	0.2

and transformed into *E. coli* XL1. The resulting mScarlet-integration plasmid was then amplified and extracted for integration into *A. baylyi*. The cassette was integrated into *A. baylyi* genome by natural transformation [115] and homologous recombination [154]. The transformation was conducted in solid phase, directly on a single *A. baylyi* colony on an LA plate, as described by Barrick Lab (UT Austin, USA).

3.1.2 Culture media and conditions

Prior to liquid cultivations, strains stored in 10 $\%_{m/v}$ glycerol at −80 °C were plated on lysogeny-broth-agar (LA) plates that consisted of 15 g L^{-1} agar, 10 g L^{-1} glucose, 10 g L^{-1} tryptone, 10 g L^{-1} yeast extract, 1 g L^{-1} NaCl, and antibiotics (5 µg mL^{-1} gentamicin for *E. coli* (sfGFP cassette), 20 µg mL^{-1} chloramphenicol for *A. baylyi* (mScarlet cassette)). *E. coli* plates were incubated at 37 °C and *A. baylyi* plates at 30 °C

All liquid cultivations were performed in a mineral salt medium (MSM), described in [53] but with doubled concentration of phosphate buffer (K_2HPO_4-NaH_2PO_4). The contents of the medium are reported in Table 3.2. No antibiotics were used in liquid media in order to prevent residuals ending up in eventual co-cultivations. Either glucose, gluconate, or acetate was used as a carbon source, depending on the cultivation.

Precultivations to reactor experiments were carried out in two stages: the first stage was a 5 mL culture in a 14 mL tube, and the second stage was a 50 mL culture in a 250 mL flasks. The tube-cultivations were inoculated from LA-plates, and the flask-cultivations by transferring 4 mL of tube-cultivations to flasks with 50 mL of fresh medium. The cultures were incubated with 250 RPM to 300 RPM shaking in temperatures of 37 °C for *E. coli* and 30 °C for *A. baylyi*. The tube-cultivations were inoculated 24 h to 36 h prior to reactor inoculation, and the tube-cultivations were then transferred to flasks 12 h to 18 h before to reactor start-up.

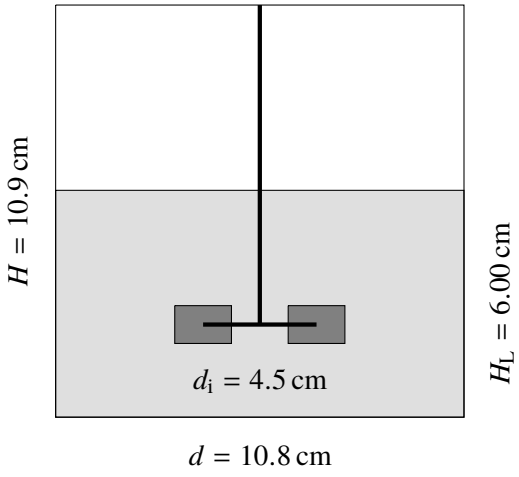

Figure 3.1 *Geometry of the* 1 L *bioreactor used in experiments. Room for foaming was left by keeping working volumes at approximately* 0.55 L. *H and H_L denote reactor and liquid heights, whereas d and d_i stand for reactor and impeller diameters.*

Table 3.3 *Bioreactor geometry and operating conditions. Substrate was not fed, antifoam was not used, and pH was not adjusted during cultivations.*

Quantity	Unit	Value
Air flow rate	$L\,min^{-1}$	0.55
Air flow rate, specific	VVM	1
Impeller diameter	cm	4.5
Impeller speed	RPM	350
Initial glucose	$g\,L^{-1}$	10
Initial pH		7
Reactor diameter	cm	10.8
Temperature	°C	30
Working volume	L	0.55

3.1.3 Bioreactor configuration and operation

The bioreactor was a 1 L UniVessel Glass Culture Vessel connected to a Biostat B plus control tower (Sartorius, Germany). Reactor geometry and the used operating conditions are summarized in Figure 3.1 and Table 3.3. The control tower monitored continuously culture temperature, pH, and pO_2 (oxygen tension). Stirring was set to 350 RPM. According to manufacturer's instructions, pH sensors were calibrated prior to reactor sterilization and pO_2 sensors after preparing the medium in sterilized reactor and saturating the liquid with air.

The working volume was kept at approximately 0.55 L, but slight variance occurred due to sterilization. The low volume was chosen to accommodate foam without having to use antifoams. Inocula volumes were in total 50 mL of precultivations such that the

initial optical density would not exceed 0.1. In case of co-cultures, the inocula were also balanced to include approximately the same amount of biomass in terms of optical density. The filtered air input rate was adjusted to 0.55 L min^{-1} (refers to gas at 20 °C temperature, 1.2 bar absolute pressure), which approximates 1 vvm specific flow. Temperature was kept at 30 °C.

Filled with 475 mL of ion-exchanged water, the reactor was sterilized at 121 °C for 30 min in an autoclave. Slight changes in the water volume occurred due to sterilization, but they were considered neglicible. The medium (Table 3.2) was then finalized in reactor by adding appropriate amounts of stock solutions and adding glucose to a concentration of 10 g L^{-1}. After medium preparation, the initial pH in reactor was always approximately equal to 7.

After medium preparation and calibrations, an initial sample was taken before inoculating the reactor. The reactor was sampled again right after inoculation, and subsequent samples were taken approximately hourly. The batches were run from 12 h to 18 h.

3.2 Sample analysis

The reactor was sampled approximately once per hour. A 2 ml sample was drawn and divided into two aliquots of 1 ml. Optical density was measured from one aliquot (Section 3.2.1), and the other one was centrifuged to separate cells from medium with a Centrifuge 5417 R (Eppendorf, Germany). The centrifuge was run for 1 min at 25 kRCF. Supernatants and cells were stored separately in freezer (−20 °C) for later analysis. The supernatants and cell pellets were thawed prior to analyses (Sections 3.2.2 and 3.2.3).

3.2.1 Biomass quantification

Optical densities at 600 nm and 700 nm (OD_{600} and OD_{700}, respectively) were measured with a Ultrospec 500 pro -spectrophotometer (Amersham Biosciences, UK) right after samples were taken. The wavelength 700 nm was additionally used, because the mScarlet expressed by the engineered *A. baylyi* strains has an absorption maximum at 569 nm, and could therefore have biased measurements at the conventional 600 nm wavelength [56].

Due to relatively low expression level of the 1-copy genomic mS-construct, the bias caused by mScarlet remained at a neglicible level. Therefore, biomass was ultimately quantified by OD_{600} despite the presence of a red fluorescent protein.

3.2.2 Concentration quantification

Sample supernatants were analyzed with a high-performance liquid chromatograph (HPLC) for glucose, gluconate, and acetate concentrations. The HPLC consisted of LC-20 AD Prominence liquid chromatograph, SIL-20 AC Prominence auto sampler, and RID-10 A refractive index detector (Shimadzu, Japan). A 30 cm Rezex RHM-Monosaccharide

H^+ (8 %) column (Phenomenex, USA) was used with 40 °C operating temperature and 0.6 mL min^{-1} flow. The mobile phase was 5 mM H_2SO_4 prepared in ion-exchanged water and filtered through a 0.2 µm filter.

Reactor sample supernatants were diluted 10-fold in ion-exchanged water. Glucose, gluconate, and acetate standards of 0.1 mM, 0.25 mM, 0.5 mM, 1.0 mM, 2.5 mM, 5.0 mM and 10.0 mM were prepared in ion-exchanged water. All samples and standards were filtered through 0.2 µm filters.

Chromatograms were analyzed with the LCsolution software, version 1.24 (Shimadzu). Peaks were identified by a slope of 200 µV s^{-1} and a width of 5 s. The peak integration program was given a slope of 20 µV s^{-1} from 16.5 min to 18.5 min to increase sensitivity to acetate (retention time about 17 min). Both peak areas and heights were calculated by the software. Areas and heights alike were found to correlate linearly with standard compound concentrations and with each other. To quantify metabolites, linear fits of area to concentration were made.

Glucose and gluconate had almost identical retention times (about 10.8 min), but they had different area-to-height-ratios. Therefore, reactor samples which were expected to include both glucose and gluconate, showed only a single peak with the retention time of glucose. The single peaks detected in samples at about 10.8 min were therefore treated followingly: Assuming both the peak area A (m^2) and height H (m) are sums of contributions by glucose and gluconate, the specific area a ($m^2\ m^{-1}$) is written as

$$a = \frac{A}{H} = \frac{A_G + A_N}{H_G + H_N}, \tag{3.1}$$

where subscripts G and N denote glucose and gluconate, respectively. Recognizing that a height H_i can be expressed as a function $H_i = h_i A_i$ of its corresponding area A_i and a compound-specific area-specific height h_i ($m\ m^{-2}$) leads to

$$A_G + A_N = a\,(h_G A_G + h_N A_N), \tag{3.2}$$

from which either area is readily solved as a function of the other. Considering $A = A_G + A_N$ and using Equation 3.2, the peak area caused by glucose is

$$A_G = A\left(1 + \frac{1 - a h_G}{a h_N - 1}\right)^{-1}. \tag{3.3}$$

To prevent glucose areas becoming greater than the actually measured peak areas, the following formulation was adopted:

$$A_G = \min\left(A,\ A\left(1 + \frac{1 - a h_G}{a h_N - 1}\right)^{-1}\right). \tag{3.4}$$

Knowing the area contributed by glucose, gluconate area was then calculated

$$A_{\mathrm{N}} = A - A_{\mathrm{G}}. \tag{3.5}$$

Glucose and gluconate concentrations were ultimately calculated according to these areas (Equations 3.4 and 3.5). As it should, the above formulation predicts zero concentration of gluconate, if the peak's specific area a is equal to characteristic area-to-height of glucose ($a = a_{\mathrm{G}}$), or equivalently if it is the inverse of specific height of glucose ($a = h_{\mathrm{G}}^{-1}$).

3.2.3 Fluorescence measurements

Prior to analysis, sample cell pellets were resuspended in sterile 10 mM Tris-HCl with 150 mM NaCl. The resuspension buffer was adjusted to pH 8 with HCl.

The samples were transferred to 200 µl microwell plates with an OT-One Hood -pipetting robot (Opentrons, USA), which were then read with a Spark multimode microplate reader (Tecan, Switzerland). Duplicates and duplicate 10-fold dilutions in resuspension buffer were transferred. Gain was manually set to a fixed value of 50 for all readings. All measurements were performed with the instrument temperature at 25 °C, and the microwell plates were allowed to set into this temperature prior to measurements.

Fluorescence intensities were measured using excitation-emission filters 485 nm and 510 nm, and 580 nm and 610 nm, corresponding to sfGFP and mScarlet excitation-emission maxima, respectively. Optical densities at 600 nm and 700 nm were also measured simultaneously with the fluorescence intensities.

3.3 Modelling framework

The modelling framework is very similar to that presented Pigou and Morchain [120], and altogether it integrates population balances, to which an unstructered kinetic model is coupled, and reactor hydrodynamics. The population balance models are described in Section 3.3.1 and the reactor models in Section 3.3.2. The simulations are explained in Section 3.3.3.

3.3.1 Population balance models of *E. coli* and *A. baylyi*

Following previously published works [103–105, 120], the population balance is developed by utilizing specific growth rate μ as the discriminating variable. The adaptation term (second term in left side of Equation 2.12) was formulated as in [103, 105, 120]. The biomass growth term (right-hand side of Equation 2.12) became μX, assuming that daughter cells inherit the growth rate of their mother [103, 120]. Altogether, the general population balance (Equation 2.12) simplified to Equation 2.13 describing adaptation, convective transport, and growth, and Equation 2.14 describing adapation rate of specific growth rate.

The population balance was solved with the method of discrete classes [103–105, 120], and the amount of classes was chosen to be 60 [120]. Biological reaction rates were then sums of rates over all classes (specific rates weighted by respective biomass concentrations) [103–105, 120]. Discretized over classes, the adaptation term (second term on left-hand side of Equation 2.13) was then approximated by [103]

$$-\frac{\partial X_i v_\mu(\mu_i)}{\partial \mu} \approx \frac{v^{\mathrm{u}}_{\mu i-1} X_{i-1} - v^{\mathrm{u}}_{\mu i} X_i}{\Delta\mu} + \frac{v^{\mathrm{d}}_{\mu i} X_i - v^{\mathrm{d}}_{\mu i+1} X_{i+1}}{\Delta\mu}, \tag{3.6}$$

where $\Delta\mu$ is the difference between two adjacent classes of specific growth rate.

Biomass (X) was considered as a dissolved species with a composition of $C_5H_7NO_2$ (molar mass 113.1 g mol^{-1}) [120], leading to a kinetic approach. Other considered species were glucose (G), gluconate (N), acetate (A), dissolved oxygen (O), and cellular energy in the form of ATP (E). Gaseous oxygen was not involved in the biologial model.

The metabolic reactions $q^{\mathrm{j}}_{\mathrm{i}}$ (mol g$^{-1}_{\mathrm{X}}$ h^{-1}) modelled are divided into anabolic and catabolic reactions. Both *E. coli* and *A. baylyi* have anabolic and oxidative reactions. *E. coli* has additionally fermentative and overflow reactions. Stoichiometric yield coefficients (mol mol^{-1}) of i formed per j consumed in a reaction of type k are denoted by $Y^{\mathrm{k}}_{\mathrm{ij}}$.

Anabolic reactions involve consumption of a substrate and energy to form biomass:

$$\mathrm{G} + Y^{\mathrm{a}}_{\mathrm{EG}}\,\mathrm{E} \xrightarrow{\mathrm{q}^{\mathrm{G}}_{\mathrm{ana}}} Y_{\mathrm{XG}}\,\mathrm{X} \tag{3.7}$$

$$\mathrm{N} + Y^{\mathrm{a}}_{\mathrm{EN}}\,\mathrm{E} \xrightarrow{\mathrm{q}^{\mathrm{N}}_{\mathrm{ana}}} Y_{\mathrm{XN}}\,\mathrm{X} \tag{3.8}$$

$$\mathrm{A} + Y^{\mathrm{a}}_{\mathrm{EA}}\,\mathrm{E} \xrightarrow{\mathrm{q}^{\mathrm{A}}_{\mathrm{ana}}} Y_{\mathrm{XA}}\,\mathrm{X}. \tag{3.9}$$

Catabolic reactions are divided into oxidative, fermentative, and overflow reactions. Oxidative and fermentative reactions produce energy from substrate, but in oxidative reactions an input of oxygen is required as well:

$$\mathrm{G} + Y^{\mathrm{o}}_{\mathrm{OG}}\,\mathrm{O} \xrightarrow{\mathrm{q}^{\mathrm{G}}_{\mathrm{oxy}}} Y^{\mathrm{o}}_{\mathrm{EG}}\,\mathrm{E} \tag{3.10}$$

$$\mathrm{N} + Y^{\mathrm{o}}_{\mathrm{ON}}\,\mathrm{O} \xrightarrow{\mathrm{q}^{\mathrm{N}}_{\mathrm{oxy}}} Y^{\mathrm{o}}_{\mathrm{EN}}\,\mathrm{E} \tag{3.11}$$

$$\mathrm{A} + Y^{\mathrm{o}}_{\mathrm{OA}}\,\mathrm{O} \xrightarrow{\mathrm{q}^{\mathrm{A}}_{\mathrm{oxy}}} Y^{\mathrm{o}}_{\mathrm{EA}}\,\mathrm{E}. \tag{3.12}$$

There is additionally oxidation of glucose to gluconate, but the energy obtained is not modelled for:

$$\mathrm{G} + Y^{\mathrm{gcd}}_{\mathrm{OG}}\,\mathrm{O} \xrightarrow{\mathrm{q}^{\mathrm{G}}_{\mathrm{gcd}}} Y_{\mathrm{NG}}\,\mathrm{N}. \tag{3.13}$$

Fermentative reactions, which do not require oxygen, apply only on glucose and gluconate:

$$\mathrm{G} \xrightarrow{\mathrm{q}^{\mathrm{G}}_{\mathrm{ferm}}} Y^{\mathrm{f}}_{\mathrm{EG}}\,\mathrm{E} + Y_{\mathrm{AG}}\,\mathrm{A} \tag{3.14}$$

$$\mathrm{N} \xrightarrow{\mathrm{q}^{\mathrm{N}}_{\mathrm{ferm}}} Y^{\mathrm{f}}_{\mathrm{EN}}\,\mathrm{E} + Y_{\mathrm{AN}}\,\mathrm{A}. \tag{3.15}$$

Overflow reactions also apply only on glucose and gluconate, and they describe a direct dissimmilation of substrate to a side product, in this case acetate:

$$\mathrm{G} \xrightarrow{\mathrm{q}^{\mathrm{G}}_{\mathrm{over}}} Y_{\mathrm{AG}}\,\mathrm{A} \tag{3.16}$$

$$\mathrm{N} \xrightarrow{\mathrm{q}^{\mathrm{N}}_{\mathrm{over}}} Y_{\mathrm{AN}}\,\mathrm{A}. \tag{3.17}$$

E. coli employs all of the above reactions except glucose oxidation to gluconate (Equation 3.13). *A. baylyi* has anabolism and oxidative catabolism of gluconate and acetate (Equations 3.8, 3.9, 3.11, and 3.12). *A. baylyi* is strictly aerobic and cannot therefore fermentate gluconate. *A. baylyi* cannot utilize glucose directly, but rather oxidizes it to gluconate first, which it then utilizes.

The unstructured metabolic reactions defined above were coupled to the population balance according to [120], and therefore only the deviations are outlined here. The only major difference to [120] is the addition of gluconate to the model. Gluconate was treated like glucose, with the exception that in *E. coli* model growth on it was inhibited by glucose, but gluconate was not modelled to inhibit glucose or acetate utilization, however. The *A. baylyi* model was formulated similarly to *E. coli*, with the expections that no fermentation or overflow reactions were considered and consequently the concept of biological oxygen uptake limit was neglected, and that acetate did not inhibit oxygen uptake or glucose oxidation to gluconate.

The maximal specific growth rates, affinity constants, yield coefficents, and other model parameters used in this work are shown in Tables 3.4 and 3.5 for *E. coli* and *A. baylyi*, respectively. Yield coefficients for both *E. coli* and *A. baylyi* were estimated by flux balance analysis (see Section 2.5.2) due to lack of published kinetic parameters for *A. baylyi*. The genome-scale models iAF1260 [41] (*E. coli*) and iAbaylyiv4 [33] (*A. baylyi*) were used for these purposes, and the derived *E. coli* yield coefficients were fairly similar to those in [120]. Growth associated maintenace was set to 59.8 $\mathrm{mmol\,g^{-1}\,h^{-1}}$ (*E. coli* model default), and non-growth associated maintenance to 0 in both genome-scale models. The conventional growth rate maximation was used as the optimization objective.

Table 3.4 *Constants in the* E. coli *kinetic model. EC*ΔptsI *was simulated by setting maximum specific growth rate on glucose to zero, and by relieving glucose inhibition on gluconate and acetate utilization. Affinity constants K_i corresponding to the definition in Equation 2.9 were assumed to equal the values in [120]. The acetate inhibition constant I_A exerts a non-competitive inhibition to growth on glucose and gluconate by a factor of $I_A/(I_A + A)$, and glucose correspondingly inhibited gluconate and acetate utilization by its respective inhibition constant I_G. Acetate additionally inhibited oxygen uptake by the constant I_{OA}. Glucose inhibition constant was kept the same as in [120], but the acetate inhibition constants were estimated instead from the results by [124]. The maintenance rate m_S was assumed to be the same as in [120], but the yield coefficients were estimated by flux balance analysis. The estimated yield coefficients were in agreement with the values used in [120]. The maximal specific growth rate on glucose μ_G^{max} was approximated by experimental growth rate and an estimation of acetate inhibition effect. On the other hand, μ_N^{max} was scaled down from μ_G^{max} by the ratio of respective maximal biomass yields (Y_{Xi}^m). μ_A^{max} and maximal oxygen uptake q_O^{max} were kept equal to the values in [120].*

	Value	Unit
Affinity and inhibition constants		
K_G	0.05	$g\,L^{-1}$
K_N	0.05	$g\,L^{-1}$
K_A	0.05	$mg\,L^{-1}$
K_O	0.10	$g\,L^{-1}$
I_G	0.20	$g\,L^{-1}$
I_A	0.47	$g\,L^{-1}$
I_{OA}	0.71	$g\,L^{-1}$
Yield coefficients		
m_S	0.25	$mmol_S\,g_X^{-1}\,h^{-1}$
Y_{EG}^a	10.81	$mol_E\,mol_G^{-1}$
Y_{XG}^m	0.85	$mol_X\,mol_G^{-1}$
Y_{OG}	6.00	$mol_O\,mol_G^{-1}$
Y_{AG}	2.00	$mol_A\,mol_G^{-1}$
Y_{EG}^o	17.64	$mol_E\,mol_G^{-1}$
Y_{EG}^f	2.67	$mol_E\,mol_G^{-1}$
Y_{EN}^a	11.77	$mol_E\,mol_N^{-1}$
Y_{XN}^m	0.78	$mol_X\,mol_N^{-1}$
Y_{ON}^o	6.00	$mol_O\,mol_N^{-1}$
Y_{AN}	2.00	$mol_A\,mol_N^{-1}$
Y_{EN}^o	14.36	$mol_E\,mol_N^{-1}$
Y_{EN}^f	3.16	$mol_E\,mol_N^{-1}$
Y_{EA}^a	3.54	$mol_E\,mol_A^{-1}$
Y_{XA}^m	0.22	$mol_X\,mol_A^{-1}$
Y_{OA}^o	2.00	$mol_O\,mol_A^{-1}$
Y_{EA}^o	7.17	$mol_E\,mol_A^{-1}$
Reaction rate limits		
μ_G^{max}	0.47	h^{-1}
μ_N^{max}	0.40	h^{-1}
μ_A^{max}	0.03	h^{-1}
q_O^{max}	15.60	$mmol\,g^{-1}\,h^{-1}$

Table 3.5 *Constants in the* A. baylyi *kinetic model. AB*Δ*gntT was modelled by setting maximum specific growth rate on gluconate to zero. Affinity constants K_i correspond to the definition in Equation 2.9, and their values were assumed to equal the* E. coli *model values. The inhibition constant I_A exerts a non-competitive inhibition to growth in gluconate by a factor of $I_A/(I_A + A)$, and it was assumed to equal I_G of* E. coli. *Apart from the assumed maintenance rate m_S , the yield coefficients were estimated by flux balance analysis. The maximal specific growth rate on gluconate μ_N^{max} was estimated by the conducted experiments, and μ_A^{max} was assumed to equal μ_G^{max} of* E. coli.

	Value	Unit
Affinity and inhibition constants		
K_G	0.05	$g\,L^{-1}$
K_N	0.05	$g\,L^{-1}$
K_A	0.05	$mg\,L^{-1}$
K_O	0.10	$g\,L^{-1}$
I_A	0.20	$g\,L^{-1}$
Yield coefficients		
m_S	0.25	$mmol_S\,g_X^{-1}\,h^{-1}$
Y_{NG}	1.00	$mol_N\,mol_G^{-1}$
Y_{OG}^{gcd}	0.50	$mol_O\,mol_G^{-1}$
Y_{EN}^{a}	11.73	$mol_E\,mol_N^{-1}$
Y_{XN}^{m}	0.73	$mol_X\,mol_N^{-1}$
Y_{ON}^{o}	6.00	$mol_O\,mol_N^{-1}$
Y_{EN}^{o}	20.15	$mol_E\,mol_N^{-1}$
Y_{EA}^{a}	3.53	$mol_E\,mol_A^{-1}$
Y_{XA}^{m}	0.21	$mol_X\,mol_A^{-1}$
Y_{OA}^{o}	2.00	$mol_O\,mol_A^{-1}$
Y_{EA}^{o}	8.18	$mol_E\,mol_A^{-1}$
Reaction rate limits		
μ_N^{max}	0.24	h^{-1}
μ_A^{max}	0.47	h^{-1}
q_{gcd}^{max}	12.00	$mmol\,g^{-1}\,h^{-1}$

3.3.2 Laboratory- and production-scale bioreactor models

The laboratory-scale 0.55 L reactor was modelled as an ideal perfectly homogeneous reactor, and the production-scale 22 m^3 reactor as a network of 70 ideal reactor compartments (5 columns, 14 rows). Additionally, the effect of hydrostatic pressure on gas phase is taken into account. Given liquid density ρ_L ($kg\,m^{-3}$), gravitational acceleration g ($m\,s^{-2}$), liquid height H (m), and atmospheric pressure P_0 (Pa), the pressure correction factor Π is

$$\Pi = \frac{\rho_L g H + P_0}{P_0}. \tag{3.18}$$

Figure 3.2 *Flow fields in a production-scale reactor with* $22\,\mathrm{m}^3$ *working volume. The flow names and values are the same as in [120]. The reactor was considered axisymmetrical, such that the left edge of the compartment model corresponds to the reactor center. Each compartment was assumed to hold an equal volume, and the effect of gas presence on volumes was neglected. Compartments holding impellers are denoted by a black fill. To build the whole reactor flow field, the bottom three row block is repeated three times more, yielding altogether four impellers and impeller flow regions of 15 compartments each. Each arrow corresponds to a single unit of the designated flow, and the total flow field is the sum of the three depicted flow fields.*

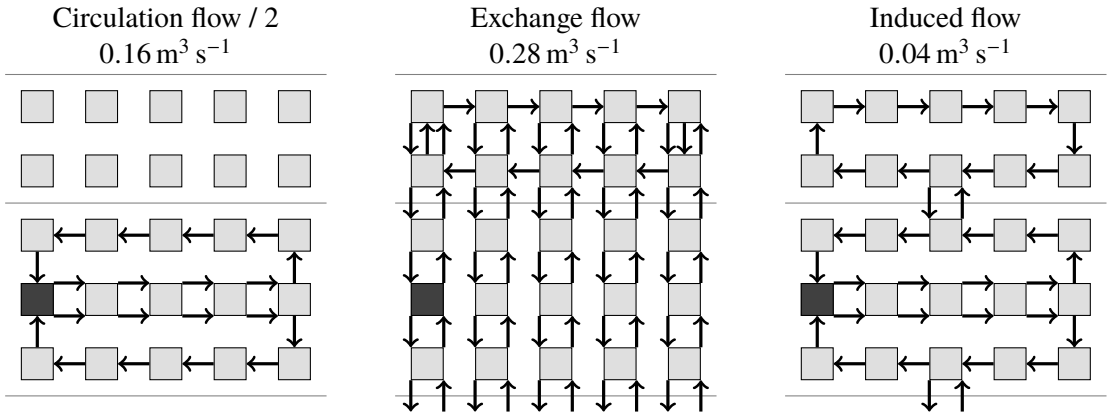

In each compartment the effective liquid height is assumed to equal the height at the middle of the compartment.

Production-scale reactor model was adapted from [151–153] as was done in [120]. The 70-compartments were assumed to be equal in volume, and perfectly homogeneous as in [120]. The flows were considered to be composed of three underlying flows: circulation flow caused by the mechanical agitation ($0.32\,\mathrm{m}^3\,\mathrm{s}^{-1}$), exchange flow ($0.28\,\mathrm{m}^3\,\mathrm{s}^{-1}$) caused by turbulence, and flow induced by aeration ($0.04\,\mathrm{m}^3\,\mathrm{s}^{-1}$). The flow names and values are the same as in [120], and the resulting flow field is illustrated in Figure 3.2. The small-scale reactor was modelled with a stirrer speed of 350 RPM, which is equal to the stirring in experiments, whereas the large-scale reactor was modelled with a stirrer speed of 60 RPM as in [120].

In each compartment a mass balance of compounds is set up, taking convective transport and reactions into account. Considering a compound i in compartment n of volume V_n (m^3), the rate of change of concentration C_i^n ($\mathrm{kg\,m}^{-3}$) is expressed

$$\frac{\mathrm{d}C_i^n}{\mathrm{d}t}V_n = q_i^n V_n + \sum_{m=1}^{N}\left(F_{m,n}C_i^m\right) - C_i^n\sum_{m=1}^{N}F_{n,m}, \tag{3.19}$$

where q_i^n ($\mathrm{kg\,m}^{-3}\,\mathrm{h}^{-1}$) represents the net effect of all reactions affecting i in compartment n and $F_{m,n}$ ($\mathrm{m}^3\,\mathrm{h}^{-1}$) is the volumetric flow rate of liquid from compartment m to compartment n. The biomass population balance models as well as gas-liquid transfer of oxygen are

coupled to the mass balance through the reaction term.

Oxygen transfer from gas to liquid phase is calculated with Equation 2.4. Liquid-phase mass transfer coefficient k_L was determined from 2.5, and it was considered to be constant throughout the reactor. Interfacial area a, on the other hand, was made to change as a function of height. The interfacial area a was calculated according to Equation 2.7, and the gas holdup ϕ (Equation 3.21) was pressure-corrected by Π according to liquid height H above compartments (Equation 3.18). The specific surface area in connection with reactor headspace was alse added to interfacial area in all applicable compartments (top row of large reactor and the small-scale ideal reactor itself). To define the gas holdup ϕ, the concept of superficial gas velocity v_s ($m\,s^{-1}$) is required:

$$v_s = \frac{F_G}{A}, \tag{3.20}$$

where F_G ($m^3\,s^{-1}$) is the volumetric gas flow and A (m^2) is the reactor's cross-section. With the superficial gas velocity defined, the average gas holdup in reactor is calculated according to [107]

$$\phi = \frac{v_s}{v_b}, \tag{3.21}$$

by assuming that the rising velocity of bubbles v_b ($m\,s^{-1}$) is known. As proposed [107], $0.15\,m\,s^{-1}$ was used here for v_b, and the gas holdups were estimated to range on average from 1 % to 2.5 %. Consequently, the estimated k_La values were below $0.01\,s^{-1}$, which corresponds to a characteristic time-scale of 100 s.

The oxygen concentrations at equilibrium O^* were estimated with Henry's law, which relates equilibrium concentration and partial pressure. With ideal gas assumption this leads to the relation

$$O^* = \frac{\phi}{1-\phi} RTHC_{O_2} \tag{3.22}$$

between dissolved oxygen concentration at equilibrium O^* and the gaseous oxygen concentration C_{O_2}. The Henry's constant H was taken to be $10.2\,\mu mol\,m^{-3}\,Pa^{-1}$ at temperature T of 303.15 K [128]. The value has been deliberatly reduced by a 15 % solute factor (original $12\,\mu mol\,m^{-3}\,Pa^{-1}$) to estimate the effect of solutes on equilibrium concentration [31].

The aeration was modelled by adding an input flow of gaseous oxygen below the lowest impeller in the large reactor model. The input flow of gaseous oxygen by sparging is considered as rate of change in gaseous oxygen concentration C_{O_2} ($mg\,L^{-1}$)

$$\frac{dC_{O_2}}{dt} = \frac{F_G}{V_L}\frac{m_{O_2}}{V_G}. \tag{3.23}$$

The liquid volume V_L refers here to the compartment's volume, and therefore volume specific flow F_G/V_L (h^{-1}) into a sparged compartment is not equal to the specific flow into reactor in a multi-compartment model. The oxygen density in gas m_{O_2}/V_G ($kg\,m_G^{-3}$) is

calculated by rearranging the state equation of ideal gas:

$$\frac{m_{O_2}}{V_G} = \frac{P n_{O_2}}{R T n_G} M_{O_2}, \tag{3.24}$$

where P (Pa) is the gas pressure (corrected by hydrostatic pressure effect), n_{O_2} (mol) the amount of O_2, R ($J\,K^{-1}\,mol^{-1}$) the universal gas constant, T (K) temperature, n_G (mol) the amount of air, and M_{O_2} ($kg\,mol^{-1}$) the molar mass of oxygen. The molar proportion of oxygen in air n_{O_2}/n_G was assumed to be 21 %. Reactor-averaged air inputs were $0.55\,L\,min^{-1}$ for the small reactor and $1\,m^3\,min^{-1}$ for the large reactor, which led to characteristic aeration time-scales of about 1 s and 25 s in the small and large reactor, respectively.

In addition to convective transport, air is transported in the reactor by buoyant rising. Similar to gaseous oxygen input, the flow of gaseous oxygen out of a compartment is

$$\frac{dC_{O_2}}{dt} = \frac{1-\phi}{\phi} C_{O_2} \frac{F_G}{V_L} \tag{3.25}$$

where the specific gas flow F_G/V_L is due to rising air bubbles:

$$\frac{F_G}{V_L} = \frac{v_b \phi A}{V_L}. \tag{3.26}$$

The liquid area A in Equation 3.26 is the compartment's area through which gas rises. Due to equal volumes of compartments, the compartment cross-section areas from which gas rises are equal as well. Therefore, in the production-scale reactor model, the area of a compartment through which gas rises is one fifth of the reactor's cross-section. Equation 3.26 was derived by rearranging the definitions of superficial gas velocity (Equation 3.20) and gas holdup (Equation 3.21) and dividing both sides by the considered compartment's liquid volume V_L. To maintain mass balance at the reactor level, the compartment right above receives the risen amount of oxygen. The topmost compartments in a reactor release gases out of the system.

To close aeration and oxygen transfer, the mean bubble diameter d_b was estimated according to [9], as proposed by [107]

$$d_b = 0.7 \frac{\sigma^{0.6}}{(P/V_L)^{0.4} \rho_L^{0.2}} \left(\frac{\mu_L}{\mu_G}\right)^{0.1}, \tag{3.27}$$

where σ ($N\,m^{-1}$) is the surface tension, P (W) the power input to reactor (Equation 2.3), ρ_L ($kg\,m^{-3}$) the liquid density, and μ_L and μ_G (Pa s) the liquid and gas viscosities, respectively.

One final aspect to consider is the substrate (glucose) feed in fed-batch mode. An exponential feed pattern was chosen, with an initial feed F_0 ($g\,L^{-1}\,h^{-1}$), exponential coefficient β (h^{-1}) which corresponds to a specific growth rate, and a maximal feed F_{max}

($\mathrm{g\,L^{-1}\,h^{-1}}$). Altogether, these lead to the equation

$$\frac{\mathrm{d}S}{\mathrm{d}t} = \min\left(F_0 e^{\beta t}, F_{\max}\right), \tag{3.28}$$

where t is time (h). In this work the effect of substrate feed on liquid volume was not taken into account.

3.3.3 Monoculture and co-culture simulations

Batch- and fed-batch-production modes were simulated according to [120], and the presented population balance models with unstructured kinetics (Section 3.3.1) were incorporated to the hydrodynamic models (Section 3.3.2), leading to a system of ordinary differential equations. Simulations were carried out on both scales, both production modes, and all 6 strain configurations, giving a total of 24 simulations. All computations and data analyses were performed with the Python programming language (`www.python.org`) utilizing `cobrapy` [34], `numpy` [157], `pandas` [96], and `scipy` [65] libraries. The initial value problems were solved with `scipy.integrate.solve_ivp` using the provided Runge-Kutta explicit 23 method (based on [12]). The constants and parameters used in modelling are compiled in Table 3.6.

All simulations were 50 h in length. The initial biomass concentration was $0.1\ \mathrm{g\,L^{-1}}$, and in co-culture simulations it was divided evenly between the two strains. The biomasses were initialized always on the lowest class in the population balance model. Initial glucose levels were set to $10\ \mathrm{g\,L^{-1}}$ in batches and $0.1\ \mathrm{g\,L^{-1}}$ in fed-batches. Initial concentration of gaseous and dissolved oxygen was set according to an estimates of equilibrium concentrations. Each batch simulation had identical initial concentrations, and accordingly each fed-batch simulation had also identical initial concentrations. The feeding parameters β and $F_{\max}$ of fed-batch simulations were chosen individually for each of the 6 strain configurations according to small-scale batch performance, and they were then used in simulating small- and large-scale fed-batches. The exponential coefficient β was set to 50 % of the maximal specific growth rate, and $F_{\max}$ was set to 1.15 times the averaged glucose conversion rate achieved by the respective small-scale batch culture.

3.4 Fermentation performance quantification

An objective of this work was to compare performance of monocultures and co-cultures across laboratory- and production-scales. Section 3.4.1 describes the conventional growth rates and biomass yields used in comparing performance, and Section 3.4.2 defines the economic concepts used in assessing performance in monetary dimensions.

Table 3.6 *Constants used in bioreactor modelling. The physical constants were the same in both reactors, and therefore they are not repeated on the* $30\,\mathrm{m}^3$ *column. Gas holdup and mass transfer coefficient are given as averages over whole reactor.*

	Unit	1 L	$30\,\mathrm{m}^3$	Source
Physical constants				
Atmospheric pressure P_0	kPa	101.325		
Density (liquid) ρ_L	$\mathrm{kg\,m^3}$	996		[127]
Diffusivity D	$\mathrm{cm^2\,s^{-1}}$	2.42×10^{-5}		[127]
Gas constant R	$\mathrm{J\,mol^{-1}\,K^{-1}}$	8.31		[127]
Gravitational acceleration g	$\mathrm{m\,s^{-2}}$	9.81		
Henry's constant H	$\mathrm{\mu mol\,m^{-3}\,Pa^{-1}}$	10.2		[128]
Solute factor	%	15		[31]
Surface tension σ	$\mathrm{mN\,m^{-1}}$	72.1		[127]
Viscosity (air) μ_G	µPa s	18.5		[127]
Viscosity (water) μ_L	µPa s	853		[127]
Reactor geometry				
Impeller diameter d_i	cm	4.5	70	
Reactor cross section A	$\mathrm{m^2}$	9.2×10^{-3}	3.43	
Reactor diameter d	m	0.108	2.09	
Working volume V	$\mathrm{m^3}$	0.55×10^{-3}	22	
Number of compartments		1	70	
Number of impellers		1	4	
Operating conditions				
Gas holdup ϕ	%	1.0	2.5	
Mass transfer coefficient $k_\mathrm{L}a$	$\mathrm{s^{-1}}$	0.008	0.004	
Mean bubble diameter d_b	mm	5.0	9.1	
Power number N_P		5	5	[31]
Stirrer speed N_i	$\mathrm{s^{-1}}$	5.83	1	
Specific gas input F_G/V	VVM	1	0.045	
Specific power input P/V	$\mathrm{W\,m^{-3}}$	352	35.3	
Temperature T	°C	30	30	

3.4.1 Growth rates and yields

Specific growth rates and yields of biomass on substrate were calculated for both experimented and simulated cultivations using the same definitions. Taking the Monod equation's (Equation 2.9) integral form and applying natural logarithm on it yields

$$\ln X = \mu t + \ln X_0, \tag{3.29}$$

a linear function of time t. Specific growth rates μ ($\mathrm{h^{-1}}$) were then calculated similar to [55]: the linear function (Equation 3.29) was fit on each available measurement time point centered on a window of 5 h using a linear least squares method (`scipy.stats.linregress` [65]). Biomass concentration X was expressed in terms of $\mathrm{OD_{600}}$ in experimental data and in units

of $\mathrm{g\,L^{-1}}$ in simulations. This procedure was applied to both experimental and simulated biomass concentrations to facilitate comparison.

It is worth noting that OD_{600} linearization by taking natural logarithms could have distorted the underlying distribution of experimental error, which in turn would have affected the growth rates obtained by linear least squares fit [31]. This aspect had no practical significance in this work, though.

Biomass yields per substrate consumed Y_{XS} were calculated as

$$Y_{XS} = \frac{\max(X) - \min(X)}{\max(S) - \min(S)} \tag{3.30}$$

for both simulated and experimented batches, and as

$$Y_{XS} = \frac{\max(X) - \min(X)}{S_{\text{converted}}} \tag{3.31}$$

for simulated fed-batches. The amount of substrate converted was inferred from the initial substrate concentration, the amount of substrate fed (Equation 3.28), and residual concentration. These yield calculations were performed with biomass in terms of either measured OD_{600} or simulated concentration, and substrate in terms of glucose concentration. This definition of biomass yield on substrate has the disadvantage that in all cultures with *A. baylyi*, glucose is also converted to gluconate, which inevitably makes the biomass yield appear smaller if some gluconate is left unconverted.

3.4.2 Relative economic potential

To define measures for profitability of fermentation processes, total production time T (a), total capital investment Γ (€), discount rate r (unitless), and the annual net profit N ($\mathrm{€\,a^{-1}}$) are required. Using these constructs and assuming that annual net profits and costs are constant, net present value NPV (€) is defined [117]

$$\mathrm{NPV} = \sum_{t=1}^{T} \left(\frac{N_t}{(1+r)^t} \right) - \Gamma. \tag{3.32}$$

Other measures, such as internal rate of return, payback period, or return on investment could have been used as well.

Neglecting inflation and assuming that production is profitable and depreciation is tax-deductible, net profit is expressed as a function of revenues R ($\mathrm{€\,a^{-1}}$), operating costs E ($\mathrm{€\,a^{-1}}$), tax rate χ (unitless), and annual depreciation D ($\mathrm{€\,a^{-1}}$):

$$N = (1 - \chi)(R - E) + \chi D. \tag{3.33}$$

Considering all of the product (measured in mass units) is sold at a fixed price, revenues

are are calculated as the product

$$R = Wp \tag{3.34}$$

of annual production W ($\mathrm{kg\,a^{-1}}$) and product price p ($€\,\mathrm{kg^{-1}}$). Volumetric productivity Q ($\mathrm{kg\,m^{-3}\,h^{-1}}$), total production volume V ($\mathrm{m^3}$), and the amount of annual operating time t ($\mathrm{h\,a^{-1}}$) define then the annual production

$$W = QVt_\mathrm{e}. \tag{3.35}$$

It is evident from the definitions above that some assumptions and simplifications need to be made in order to analyse profitability of the fermentation settings studied in this thesis. The major issues to be resolved are that

1. There is no obvious unit price of product, p, because culture productivity Q is quantified in terms of optical density (biomass concentration)
2. Estimating investment and operating costs (Γ and E) would require knowledge of a comparable industrial plant.

Additionally, total production time T, annual effective operating hours t_e, production volume V, tax rate χ, annual depreciation D, and discount rate χ need also to be set. The yearly effective reaction time t_e is then directly estimated as a function of yearly operating hours t, time per batch Δt, and process downtime per batch τ:

$$t_\mathrm{e} = \left\lfloor \frac{t}{\Delta t + \tau} \right\rfloor \tag{3.36}$$

To circumvent cost estimation and need for product prices, the performance of large-scale fermentations is fixed as a reference point by forcing their net present values NPV to equal zero:

$$\sum_{t=1}^{T} \left(\frac{N_t}{(1+r)^t} \right) - \Gamma = 0. \tag{3.37}$$

Annual net profits are assumed to be constant, hence they can be removed from the summation term. To facilitate subsequent net profit analysis, a linear depreciation model with a recovery period equal to total production length T is adopted:

$$D = \frac{\Gamma}{T}. \tag{3.38}$$

By letting the discounting term $\sum_{t=1}^{T} = \delta$ and substituting net profits (3.33), Equation 3.37 becomes

$$((1-\chi)(R-E) + \chi D)\,\delta = \Gamma. \tag{3.39}$$

Now the issue of operating costs E is circumvented by assuming that at the reference

fermentation they are a fraction $\omega \in (0, 1)$ of revenues:

$$E = \omega R, \tag{3.40}$$

which simplifies Equation 3.39 to

$$((1 - \chi)(1 - \omega) R + \chi D) \delta = \Gamma. \tag{3.41}$$

Recalling definitions of revenue (Equation 3.34), production (Equation 3.35), and depreciation (Equation 3.38), Equation 3.41 becomes

$$\left((1 - \chi)(1 - \omega) QVpt_e + \chi \Gamma T^{-1}\right) \delta = \Gamma, \tag{3.42}$$

or equivalently

$$(1 - \chi)(1 - \omega) QVpt_e \delta = \Gamma - \chi \Gamma T^{-1} \delta, \tag{3.43}$$

from which the unit price p is solved:

$$p = \frac{\Gamma\left(1 - \chi \delta T^{-1}\right)}{(1 - \chi)(1 - \omega) QVt_e \delta}. \tag{3.44}$$

Therefore, a reference price in units of € per OD_{600} can be obtained from reference fermentation data given investment costs, tax rate, discount rate, opex fraction, total production length, total production volume, process downtime per batch, and annual working hours. The price can then be used to estimate the volumetric economic potential of large-scale cultivations relative to small-scale.

Production costs are assumed to equal the costs at reference states. Even if productivity is enhanced from the reference, upstream costs and labour and mainentance costs should not change considerably. As for downstream processing, the costs are likely to be higher if productivity has been increased, but the analysis is done under the equal-costs assumption nevertheless.

Due to the large amount of parameters required, and the broad ranges of values they might obtain, a parameter space was set up and sampled (151 200 samples) to obtain distributions of economic potentials. The process-economic parameters and their value ranges are compiled in Table 3.7. The parameters were considered followingly: total capital investments ranged from 10 M € to 100 M €, discount rates ranged from 10 % to 50 %, income tax rates from 20 % to 40 %, and total operation times from 5 a to 25 a. Total costs range from 20 % to 80 % of reference revenues. Yearly operating times were assumed to range from 7200 h to 8400 h, which correspond to 300 d to 350 d. Total production volume of the hypothetical plant was assumed to range from 10 m^3 to 1000 m^3. Process downtimes between subsequent batches ranged from 4 h to 24 h. Both lower and upper bounds of all parameters were included, and the rest of the samples were taken with equal

Table 3.7 *Economic potential parameters. A total of* 151 200 *samples within the shown bounds were drawn from parameter space. Both upper and lower bounds were included, and the rest of samples were drawn with equal intervals in between.*

Quantity	Unit	Lower bound	Upper bound	Samples
Discount rate r	%	10	50	5
Process downtime τ	h	4	24	6
Tax rate χ	%	20	40	3
Total capital investment Γ	M€	10	100	4
Total cost proportion in reference ω	%	20	80	4
Total production length T	a	5	25	5
Total production volume V	m^3	10	1000	7
Yearly operating time t	h	7200	8400	3

intervals in between.

It worth restating, that the economic potential evaluated as described above is by no means a plant cost estimation, but rather a way to express differences in culture productivities as a fermentation's economic potential relative to another culture. True cost and price estimations would of course be required to evaluate absolute profitability of fermentation processes, such as in [25, 86, 87, 91, 97, 123, 142].

4. RESULTS

To assess the up-scaling of microbial co-culture fermentations, the two bacterial species *Escherichia coli* and *Acinetobacter baylyi* were studied in mono- and co-cultures. Using additionally glucose-utilization knock-out mutants of both in co-cultures, a total of two monocultures and four co-cultures was examined in this work. Results of batch experiments are presented in Section 4.1. Batch- and fed-batch simulations are shown in Sections 4.2 and 4.3, respectively. Concluding this chapter, Section 4.4 describes the relative economic potentials of the studied strain configurations.

4.1 Batch experiments

Sections 4.1.1 to 4.1.6 present the results of EC, AB, EC:AB, ECΔ*ptsI*:AB, EC:ABΔ*gntT*, and ECΔ*ptsI*:ABΔ*gntT* cultures. Batch experiments of the six cultures were carried out for 12 h to 18 h with 0.55 L working volume in a 1 L bioreactor. The aim was to start each fermentation with an OD_{600} of 0.1, but due to precultivation variability this was not achieved with EC:AB and ECΔ*ptsI*:AB. Therefore concentrations of neither biomass nor metabolites are directly comparable between the cultivations. Regarding the calculated specific growth rates, it should be noted that due to the formulation (Section 3.4.1) the first and last 2.5 h of each cultivation show no change in specific growth rate. Biomass titers, yields on glucose, and productivities are quantified in terms of OD_{600}, leading to units L^{-1}, g^{-1}, and $L^{-1}\,h^{-1}$, respectively. The conducted batch experiments are summarized in Table A.1.

4.1.1 *E. coli* monoculture

The course of 0.55 L-EC cultivation is shown in Figure 4.1. Within 11.9 h, the culture reached an OD_{600} of 0.90 with a yield 0.38 g^{-1} and time-averaged productivity 0.08 $L^{-1}\,h^{-1}$. The EC cultivation entered exponential phase without a noticable lag phase, and the maximal specific growth rate was 0.29 h^{-1}. The exponential phase declined to stationary phase after 9 h, and growth came to halt at 10 h as the culture pH approached 5. At the same time, the previously steadily decreasing pO_2 started a sharp ascent for a short time, after which it increased at a gentler rate until the end. This was accompanied by a drop in the rate of pH-decrease; the culture pH had decreased constantly since inoculation. Biomass in terms of OD_{600} decayed slightly between 11 h and 12 h. Glucose concentration decreased whereas

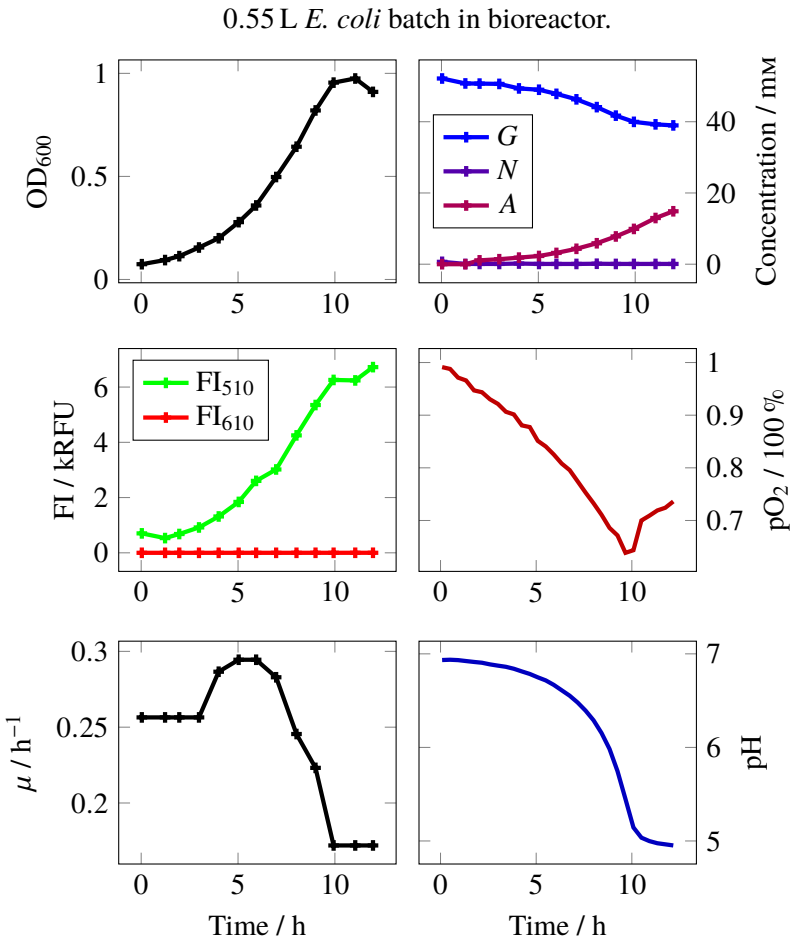

Figure 4.1 *EC-batch displayed a typical batch growth curve: exponential growth until the accumulated acetate and medium pH became inhibitory. It is noted that the sharp inverse peak of pO_2 signal corresponds very accurately to the observed cease of growth. Another point worth noticing is that EC could achieve only about a* 20 % *conversion of glucose substrate before the conditions became inhibitory. If the cultivation were continued over the* 12 h*, the calculated specific growth rate (lower left corner) would have fallen to 0 and possibly below at the end. G stands for glucose, N for gluconate, and A for acetate. FI_{510} denotes fluorescence intensity corresponding to sfGFP wavelengths and FI_{610} corresponds to mScarlet.*

acetate accumulated steadily troughout the cultivation almost up to 15 mM (0.885 g L^{-1}). FI_{510}- and OD_{600}-signals correlated in a linear way, but with some slight deviations.

The EC cultivation exhibited no unexpected properties apart from an unidentified additional peak in the chromatogram with a retention time of 15.5 min. Growth cease due to too high acetate concentration, too low pH, or the combination thereof was expected, and it demonstrates a natural limitation of *E. coli* monocultures, which can acidify their growth environment beyond tolerance. Additionally, both the pO_2 and pH signals were in agreement with the growth cease. Likewise as expected, the culture did not fluoresce at the mScarlet wavelengths at all and practically no gluconate was predicted by the glucose-gluconate separation methodology (Section 3.2.2). Consequently FI_{610} signal can

be used as a marker for *A. baylyi* presence, and the glucose-gluconate separation is at least partly validated.

Of the samples drawn from reactor for fluorescence measurements, only the last two samples were certainly 1 ml due to sampling errors. Then on resuspension most of the samples have been too concentrated. It is estimated that those samples were originally 1.25 ml, which would have resulted in 25 % too high fluorescence readings apart from the last two samples. Indeed an otherwise unexpected drop in FI_{510} is observed after 10 h, but at the same time growth also ceased, so the effect of sampling errors may have been masked.

4.1.2 *A. baylyi* monoculture

Figure 4.2 displays the AB cultivation. Monoculture of AB exhibited a lag phase for the first 3 h of cultivation, but grew thereafter exponentially to the end. Again, a correlation between fluorescence intensity and biomass concentration was found: both FI_{610}- and FI_{510}-signals correlated almost linearly with OD_{600}. The FI_{510}-signal remained low, corresponding only to the background fluorescence caused by biomass itself, unlike in *E. coli* which also expressed the green fluorescent protein sfGFP. Glucose was consumed steadily, and as expected, estimated gluconate concentration built up. Predictions of gluconate not being present with EC but accumulating with AB imply that the derived glucose-gluconate separation (Section 3.2.2) is valid at least at a qualitative level. Interestingly the medium pH rose after reactor inoculation, but altogether it stayed within the narrow range of 6.9 and 7.1.

With a final OD_{600} of 1.04 and only a low amount of glucose converted, the AB culture had a considerably high OD_{600} yield on glucose (0.79 g^{-1}) compared to EC (0.38 g^{-1}). The productivity of 0.09 $L^{-1}\,h^{-1}$, however, was not much higher than with *E. coli* (0.08 $L^{-1}\,h^{-1}$). It seems then that the two species, *A. baylyi* and *E. coli*, have different biomass-to-OD_{600}-ratios, with a unit of *A. baylyi* OD_{600} corresponding probably to about half the biomass *E. coli* would have. On the other hand, oxygen tension decreased steadily below the minimum reached by EC, implying that the obligate aerobe *A. baylyi* respired at a higher specific rate than *E. coli*. This implication is valid if the culture aerations were equal. The low FI_{510} background signal of *A. baylyi* means that a strong FI_{510} signal can be attributed solely to *E. coli* presence, whereas all FI_{610} signal is due to *A. baylyi*. Therefore the two fluorescence signals can be used to detect the presence of both strains in co-cultures.

4.1.3 *E. coli*:*A. baylyi* co-culture

The course of EC:AB cultivation is shown in Figure 4.3. The co-culture seems to have started exponential growth immediately after inoculation and continued it to the end. The inocula of co-cultured EC:AB-batch had a considerably much lower OD_{600} than

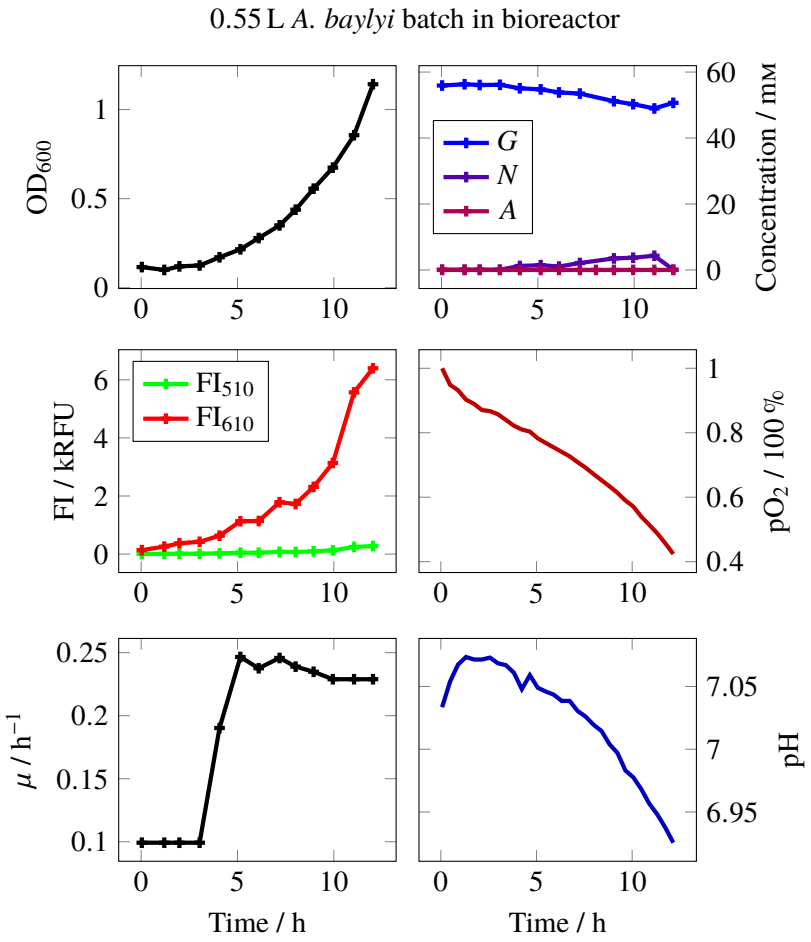

Figure 4.2 *AB-batch reached an OD_{600} higher than EC, but the amount of glucose converted is much lower. Likewise the change in culture pH was very small. It seems therefore that* A. baylyi *cells have a higher optical density than* E. coli. *On the other hand, oxygen tension decreased well below the minimum found in EC culture, which indicates that the obligatorily aerobic* A. baylyi *consumed oxygen at a higher rate than* E. coli*, provided the aeration in both cultures was equal. G stands for glucose, N for gluconate, and A for acetate. FI_{510} denotes fluorescence intensity corresponding to sfGFP wavelengths and FI_{610} corresponds to mScarlet.*

the corresponding monoculture experiments, and therefore it reached an OD_{600} of only 1.65 despite its high specific growth rate. Both FI_{610}- and FI_{510}-signals were strong and correlated almost linearly with OD_{600}, but with lower slopes than in the monocultures, which is in accordance with the fact that the OD_{600} signal was now caused by both strains present. Like in the AB monoculture but unlike in EC cultivation, no acetate was found, but gluconate accumulated instead as glucose was consumed. EC being present, acetate accumulation could have been expected, but its absence implies utilization by AB instead. At first both pH and pO_2 rose minutely, but from 5 h onwards they both started to decrease exponentially.

As was stated, EC:AB reached an OD_{600} fo 1.65, which was higher than that reached by either of the constituing single strains. Batch productivity was also higher than with the

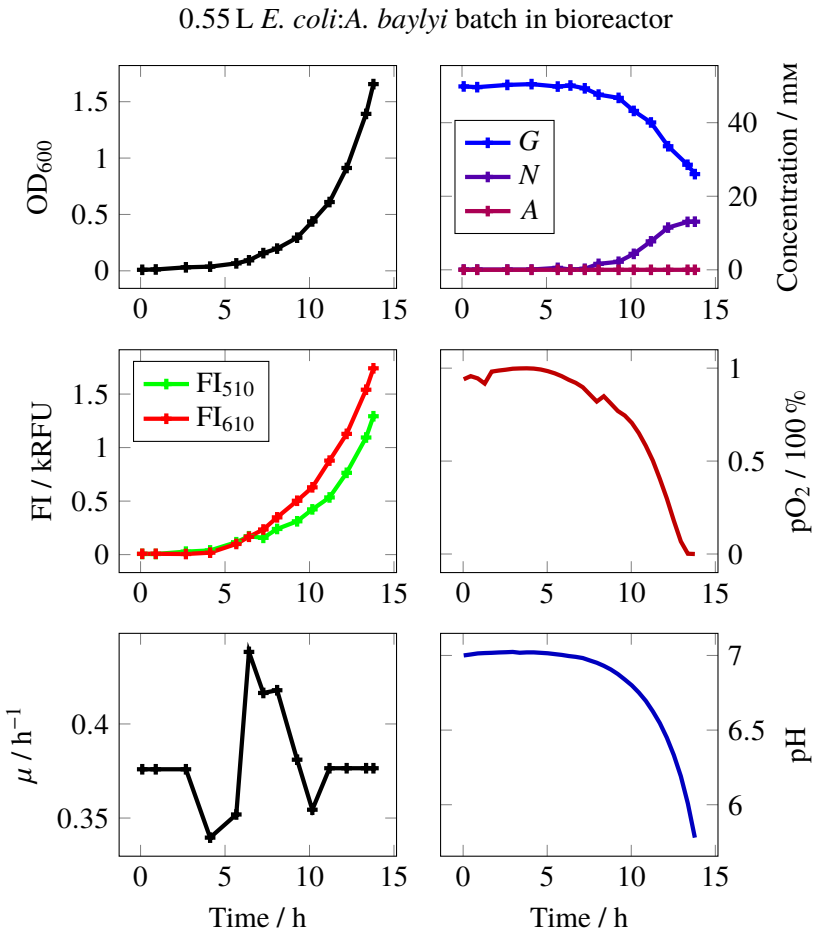

Figure 4.3 *EC:AB-batch had consistently highest specific growth rates in this work. It also achieved the highest glucose conversion of almost* 50 % *within* 14 h. *G stands for glucose, N for gluconate, and A for acetate. FI_{510} denotes fluorescence intensity corresponding to sfGFP wavelengths and FI_{610} corresponds to mScarlet.*

single strains, $0.12\,L^{-1}\,h^{-1}$, but the potential differences in OD_{600}-to-biomass-ratios make comparisons difficult. The yield was $0.37\,g^{-1}$, below that by either AB or EC. Mentioned in yield definition (Section 3.4.1), residual gluconate can influence yield values, and this also seems to be the case here with an estimated residual gluconate concentration of 13.09 mM.

The rising of pO_2 at the beginning of cultivation was unexpected. It was most likely caused by too early calibration of the pO_2 electrode. The sudden drop of pO_2 before at the beginning was in turn due to detachment of gas input hose. The surge corresponds to gas input reattachment and continuation of reactor aeration.

4.1.4 *E. coli* Δ*ptsI*:*A. baylyi* co-culture

EC Δ*ptsI*:AB-co-cultivation was similar to the EC:AB-co-culture in many respects: it also started with a very small biomass concentration in terms of OD_{600}, gluconate accumulated as glucose was consumed, no acetate was found, both FI_{610} and FI_{510} correlated quite

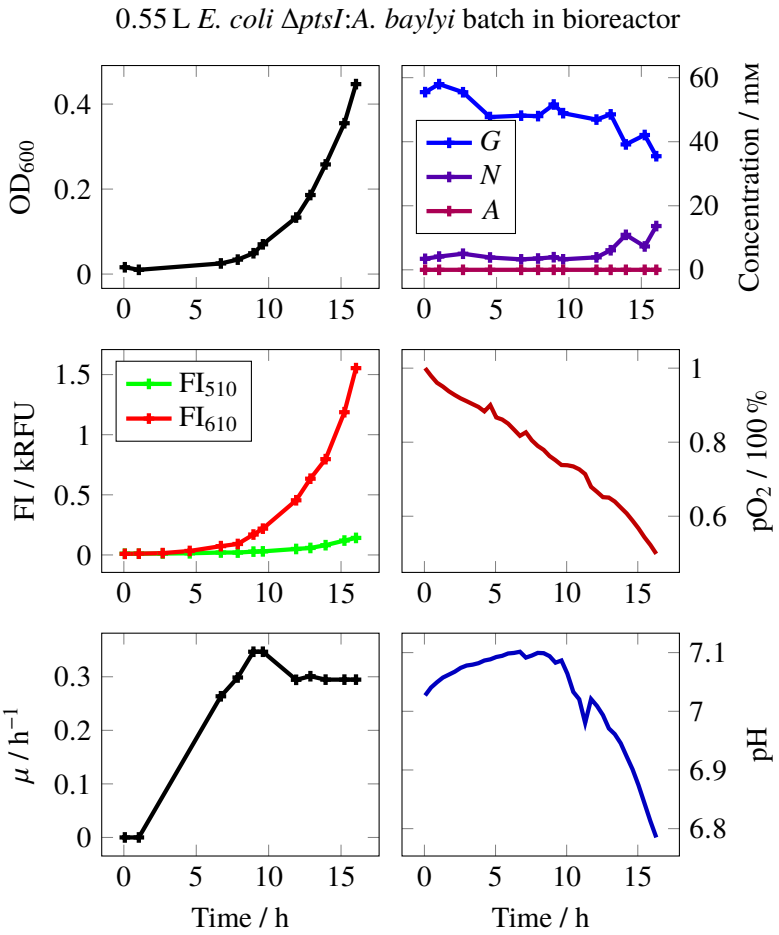

Figure 4.4 E. coli ΔptsI:A. baylyi-*batch had the longest lag phase of this work,* 5 h. *Unfortunately the* OD_{600} *measurements were mostly unsuccesful during the first* 5 h*, and consequently the specific growth rates during that interval could not be estimated. Like in AB cultivation, pH rose from the initial value. G stands for glucose, N for gluconate, and A for acetate.* FI_{510} *denotes fluorescence intensity corresponding to sfGFP wavelengths and* FI_{610} *corresponds to mScarlet.*

linearly with OD_{600}, and pH rose first steadily for the first 8 h, after which it started a steady descent. There were differences as well: pO_2 started to decline steadily right from inoculation, and the pH drop was not as remarkable. Also the final biomass concentration was much lower. Figure 4.4 shows the trajectory of EC*Δptsl*:AB cultivation.

The culture titer was only 0.45 in terms of OD_{600}, and yield was $0.11\,g^{-1}$ and productivity $0.03\,g\,L^{-1}\,h^{-1}$. Compared to AB, a similar oxygen consumption, a lower FI_{610}-to-FI_{510}-ratio, and a larger shift in pH are found despite the lower OD_{600}. These are taken to indicate the presence of EC*Δptsl*.

OD_{600} measurements between 1 h to 5 h were unsuccesful and consequently they were omitted from Figure 4.4 and specific growth rate calculations. The failed OD_{600} measurements were most likely due to sampling errors. However, metabolite concentrations as well as fluorescence intensities were still recoverable from the other sample. The zig-zag movement of glucose concentration was much stronger than in the previous three, EC, AB,

and EC:AB-cultivations, which implies that liquid chromatorgram sample preparation has been non-optimal. Most likely the reason has been in not letting the supernatants reach room temperature after thawing.

4.1.5 *E. coli*:*A. baylyi* Δ*gntT* co-culture

Co-culture of EC and ABΔ*gntT* grew almost exponentially for the whole cultivation time, and it reached the highest OD_{600} of all conducted experiments. Figure 4.5 contains the collected data of the cultivation. Towards the end of cultivation the medium became even more acidic than in the EC-monoculture: pH dropped below 5 by 14 h. Considerable fluorescence intensities were recorded, FI_{510} being stronger than FI_{610}. Residual gluconate and acetate seem to have come from inocula, but the residual acetate was consumed quickly, in almost 2 h. Acetate concentration exceeded the detection treshold again at 10 h, after which it accumulated. Estimated gluconate levels stayed fairly steady through the entire cultivation time. Glucose was consumed steadily throughout cultivation.

EC:ABΔ*gntT* reached an OD_{600} of 2.53, and correspondingly its productivity was also the highest of the six experiments, $0.17\,L^{-1}\,h^{-1}$. However, its specific growth rates were below those of EC:AB and even of ECΔ*ptsI*:AB. The yield of $0.61\,g^{-1}$ is close to the AB value of $0.79\,g^{-1}$, and higher than in either EC:AB or ECΔ*ptsI*:AB.

During the cultivation gas input rates had changed owing to equipment, which explains the zig-zagging movement of pO_2 signal. The sudden drop in specific growth rate after 5 h, however, was unexpected. Interestingly it corresponds to the time from which on foam started to accumulate considerably. Also the FI_{610} signal is seen to have stalled between 5 h to 7 h. These findings would suggest that some ABΔ*gntT* has lysed in the culture during that time, but this cannot be known with certainty.

4.1.6 *E. coli* Δ*ptsI*:*A. baylyi* Δ*gntT* co-culture

The co-culture of the two glucose-knock-out strains ECΔ*ptsI* and ABΔ*gntT* behaved in the most variable way, and its trajectory is shown in Figure 4.6. At first ECΔ*ptsI*:ABΔ*gntT* exhibited a quick burst of growth for the first 5 h, but decayed between 5 h and 8 h. The biomass concentration remained stationary during 8 h to 12 h, but started to grow again steadily until the end. The quick consumption of initial gluconate and acetate corresponds well to the initial surge in OD_{600}. Consequently the steady consumption of glucose and accumulation of gluconate along with rising FI_{510} and FI_{610} signals indicate that both ABΔ*gntT* and ECΔ*ptsI* indeed have grown despite the fact that neither could grow in monoculture. These findings suggest that the gluconate made available by ABΔ*gntT* is utilized by ECΔ*ptsI* and the subsequent side products of ECΔ*ptsI*, most likely acetate, is then utilized by ABΔ*gntT*.

ECΔ*ptsI*:ABΔ*gntT* displayed lowest performance in all three key parameters: the

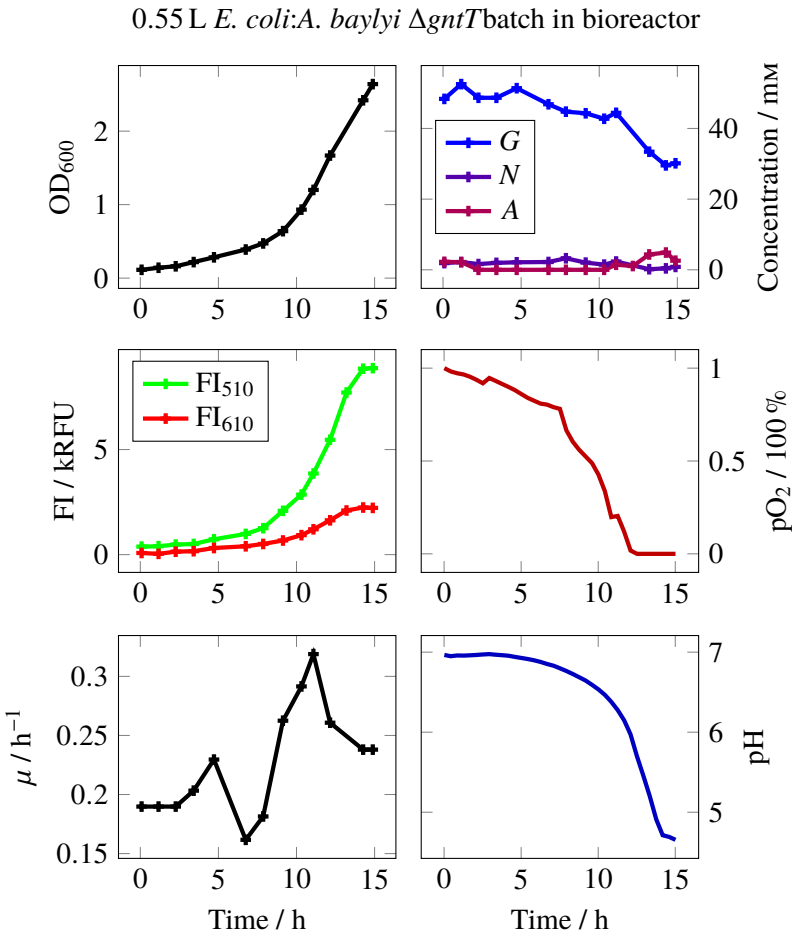

Figure 4.5 *EC:AB*ΔgntT*-batch reached the highest* OD_{600} *of this work, 2.64. The growth of both* FI_{510} *and* FI_{610} *signals indicate that both EC and AB*ΔgntT *have grown in the co-culture. Also the quick consumption of initial acetate and the late reoccurrence of it imply that AB*ΔgntT *has been active in the culture, consuming acetate excreted by EC. Oxygen limitation and possibly also low pH seem to have affected the culture towards the end of cultivation. G stands for glucose, N for gluconate, and A for acetate.* FI_{510} *denotes fluorescence intensity corresponding to sfGFP wavelengths and* FI_{610} *corresponds to mScarlet.*

final OD_{600} was 0.44, with a yield $0.10\,g^{-1}$ and a productivity $0.02\,L^{-1}\,h^{-1}$. It should be remembered, however, that this particular co-culture is not readily compared to any of the other tested cultures due to the fact that neither of the strains could grown in isolation. In a prior work by the author it was found that this co-culture is able to grow despite the fact that neither of the strains could grow in the given conditions by themselves, but the growth decline and stasis after initial acetate and gluconate depletion was unexpected. The previous experiments were carried out in microwell plates without any sampling for metabolite concentation analyses, though.

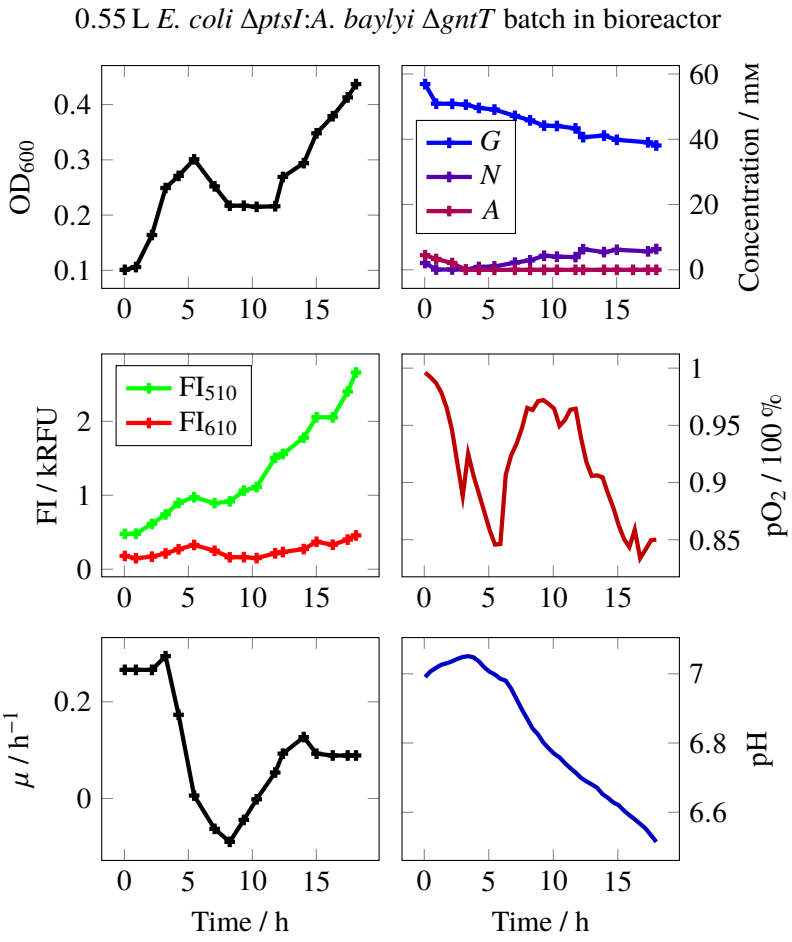

Figure 4.6 *EC*ΔptsI:*AB*ΔgntT*-batch was the most notable of the six cultures, because neither EC*ΔptsI *nor AB*ΔgntT *could grow by themselves. The pO_2 signal correlated well with the observed growth in OD_{600}. G stands for glucose, N for gluconate, and A for acetate. FI_{510} denotes fluorescence intensity corresponding to sfGFP wavelengths and FI_{610} corresponds to mScarlet.*

4.2 Batch simulations

All the six batch cultures were also simulated in a 1 L and 30 m^3 reactor, with working volumes of 0.55 L and 22 m^3. The small-scale batch simulations are shown in Figure A.1 and summarized in Table A.2. The main observations are the same as in the experiments: All cultures grew, co-cultures had the highest specific growth rates, EC was the only culture to accumulate acetate in considerable amounts, and gluconate was observed in cultures with AB or ABΔ*gntT*. The main differences were that ECΔ*ptsI*:AB underperformed relative to experiments, and that ECΔ*ptsI*:ABΔ*gntT* did not show the initial growth burst and decay. The model formulation is the likely reason for the worse than expected performance of ECΔ*ptsI*:AB, as any gluconate produced by *A. baylyi* is immediately equally available to ECΔ*ptsI* as well in the model, which is physically unrealistic. The lack of ECΔ*ptsI*:ABΔ*gntT* growth burst found in experimental batch is explained by the absence of initial gluconate and acetate. Another point worth noticing is that except for

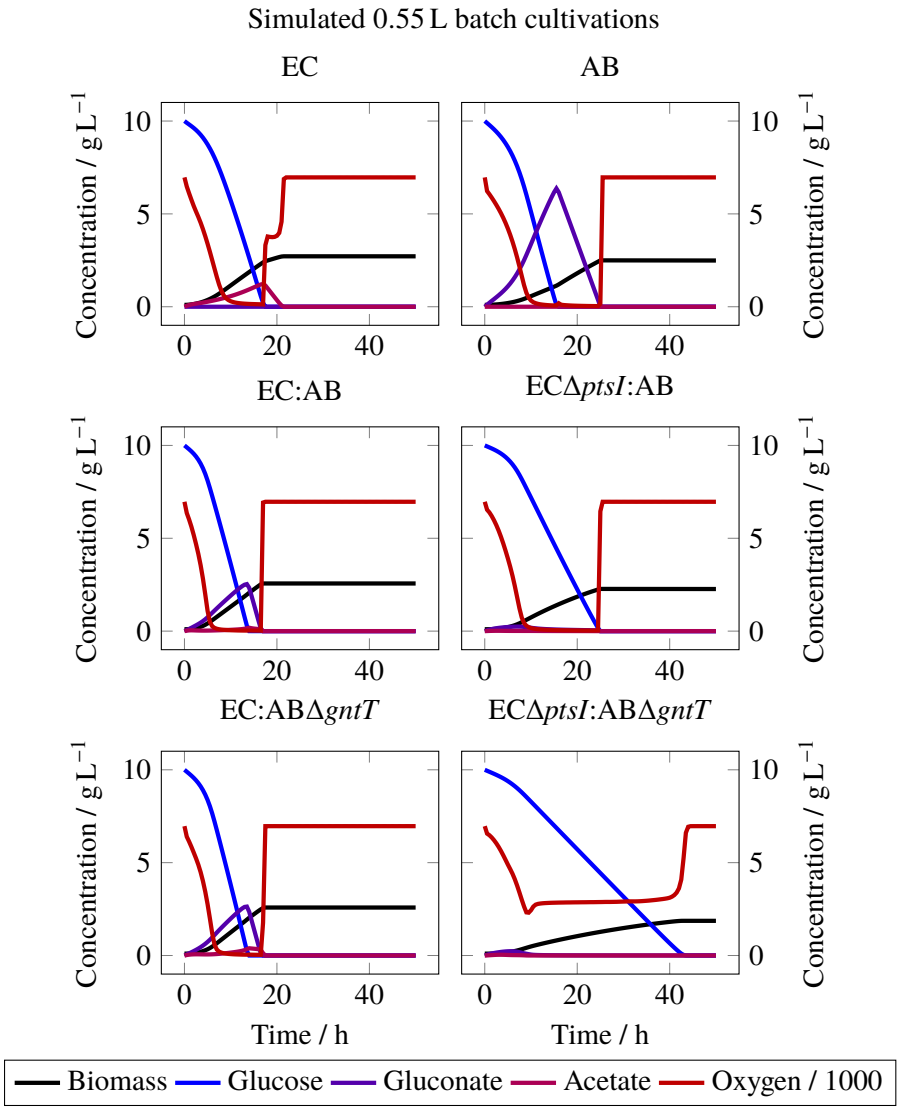

Figure 4.7 *Simulated batches in* 1 L *reactor. In general, the simulated batches were similar to the experimental ones. The greatest single difference is EC*ΔptsI*:AB*ΔgntT *co-culture, which did not show a quick growth burst followed by decay, unlike in experiments. However, the simulated batch did not either have any initial gluconate or acetate for the knock-out strains EC*ΔptsI *and AB*ΔgntT *to grow on.*

ECΔ*ptsI*:ABΔ*gntT* all of the cultures experienced oxygen limitation, to which the low k_La (below 0.01 s^{-1}) was the reason.

Figure A.1 shows the course of large-scale batch simulations, which are then summarized in Table A.3. The large-scale simulations showed exactly the same characteristics as small-scale simulations, with the difference that biomass titers, yields, and productivities were consistently lower due to more severe oxygen limitation. Acetate also accumulated to higher concentrations at large scale. As can be seen in Table 3.6, the overall oxygen transfer coefficient k_La is on average only half of the small-scale value (0.004 s^{-1} at large scale and 0.008 s^{-1} at small scale).

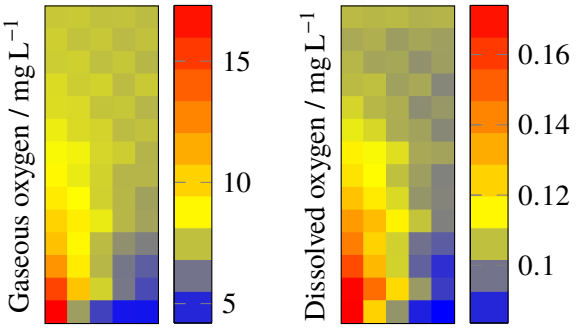

Figure 4.8 *Distribution of oxygen in the large reactor at* 10 h *during batch cultivation of* E. coli. *Clearly the oxygen transfer was limiting throughout the reactor, but even then the extent of limitation was heterogeneously distributed. An oxygen-deprived zone is found at bottom of the reactor next to the wall. Surface aeration is slightly visible at top of the reactor, but it's contribution to overall aeration is neglicible.*

A typical gaseous oxygen distribution to all large-scale cultivations is shown in Figure 4.8. Dissolved oxygen concentration dropped readily due to low transfer coefficients ($k_L a$ below 0.01 s^{-1}), and likewise due to the low transfer coefficients, gaseous oxygen stayed almost the same throughout culture time. As presented in Section 3.3.2, the time-scale of oxygen transfer was about 100 s in both small and large reactors, whereas the aeration time scales were 1 s for the small and 25 s for the large reactor. The time-scales are in agreement with the observed simulation behaviour: gaseous oxygen concentration was basically unaffected by transfer to liquid phase in the small reactor, but in the large reactor it was slightly decreased by transfer. In the large reactor, the amount of gaseous oxygen was heterogeneously distributed, which additionally affected the local oxygen transfer rates and consequently dissolved oxygen concentrations. The local differences in biomass, glucose, gluconate, and acetate concentrations were neglicible in large-scale batch simulations.

4.3 Fed-batch simulations

The six cultures were also simulated in fed-batch mode with feedings patterns based on small-scale batch performance. Like with batch simulations, both 1 L and 30 m^3 reactor fermentations were simulated. The simulated small-scale fed-batches are presented in Figure 4.9 and further summarized in Table A.4. Unlike in batch simulations, EC and AB were not limited by oxygen availability, and side products did not accumulate in any of the fed-batches. It seems therefore that the cultures could have supported higher glucose feeding rates, except for ECΔ*ptsI*:AB and ECΔ*ptsI*:ABΔ*gntT*.

Large-scale fed-batches are in turn presented in Figure A.2 and summarized in Table A.5. Like with batch simulations, the main difference between small- and large-scale was the more severe oxygen limitation at the large scale, which caused losses in biomass titers, yields, and productivities, and also accumulation of acetate and gluconate. In large-

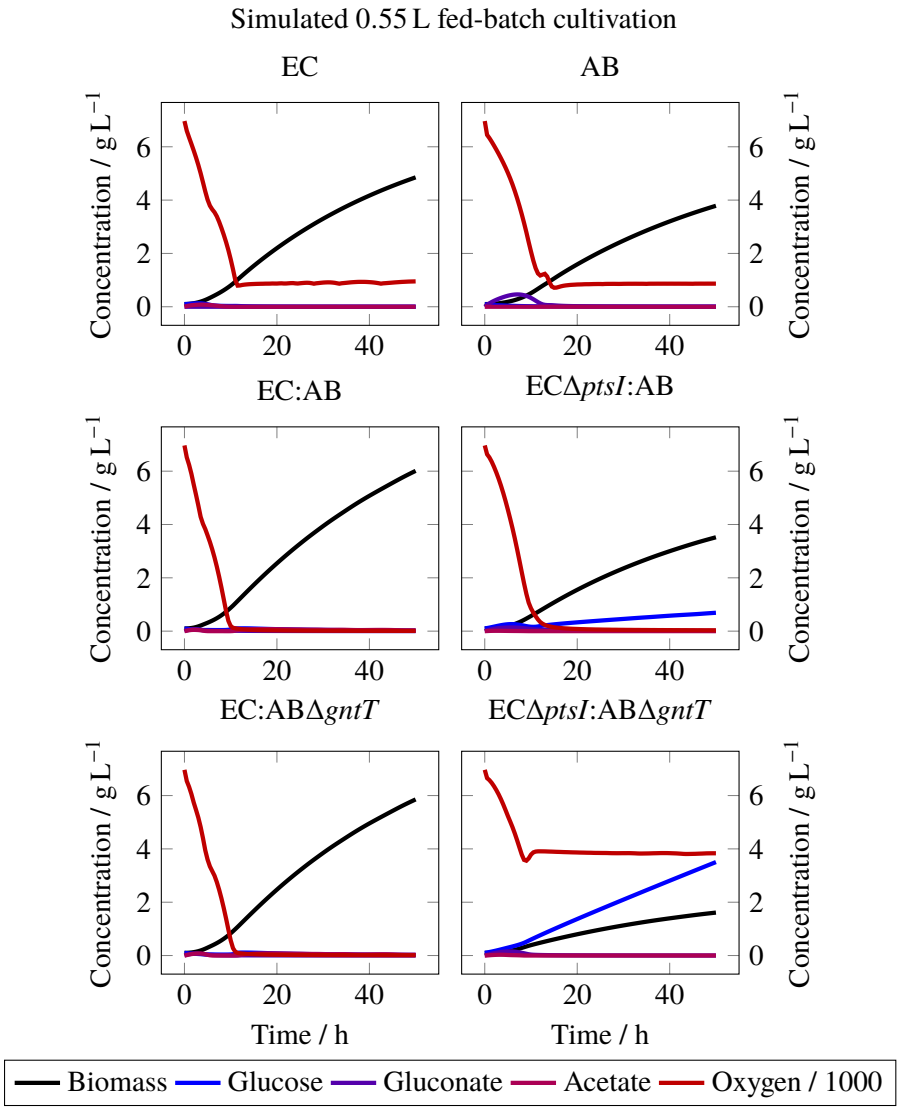

Figure 4.9 *Simulated fed-batches in* 1 L *reactor with* 0.55 L *working volume. Unlike the batch simulations in* 1 L *reactor, side products did not accumulate, and EC and AB were not limited by oxygen availability.*

scale fed-batches the oxygen limitation led also to considerable amounts of glucose left unconverted. The only culture not limited by oxygen availability was ECΔ*ptsI*:ABΔ*gntT*.

A typical glucose distribution during fed-batch cultivations is shown in Figure 4.10. The local differences in biomass, gluconate, and acetate concentrations were neglicible in fed-batch cultures. Oxygen concentrations acted very similarly to large-scale batch concentrations. Recognizing that the simulated biomass concentration did not exceed $4\,\mathrm{g\,L^{-1}}$ in any large-scale fed-batch, the glucose uptake time-scales have been over 4.5 s (assuming uptake rate of $2\,\mathrm{g_G\,g_X^{-1}\,h^{-1}}$ and considering glucose concentration of $10\,\mathrm{mg\,L^{-1}}$), which is within an order of magnitude from macromixing time-scales. Therefore only slight heterogeneity in glucose concentration was realized in these simulations.

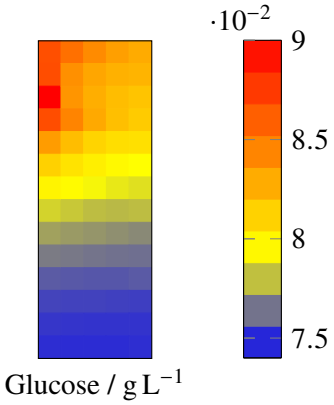

Figure 4.10 *Distribution of glucose at* 50 h *of EC fed-batch cultivation. The heterogeneity in glucose concentration was modest in the conducted large-scale fed-batch simulations.*

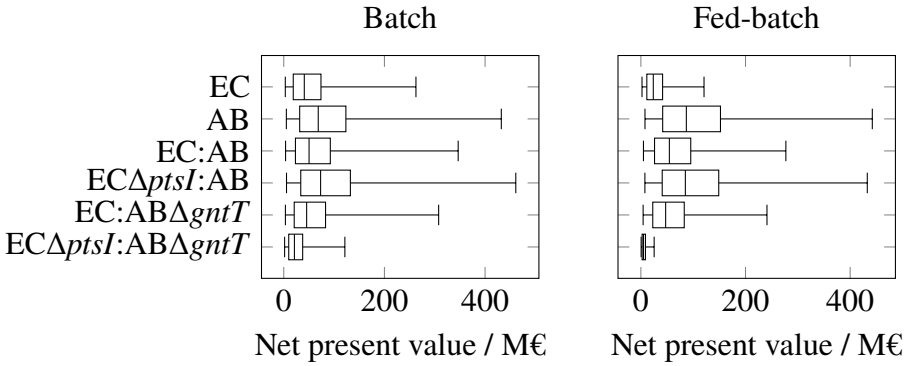

Figure 4.11 *Net present value lost in simulated scale-up. Apart from EC*ΔptsI:*AB*ΔgntT*, co-cultures cannot be said to have tolerated scale-up any better than the respective single strains. Majority of the parameter space resulted in relative net present values well below* 100 M€*. The left and right whiskers denote the minima and maxima, and the box covers the range from lower to upper quartile. Median is showed as a bar within the box.*

4.4 Relative economic potentials

The results of the economic potential assesment are shown for simulated batch and fed-batch cultivations in Figure 4.11. Table A.6 summarizes the results and additionally displays the biomass productivity of small scale relative to large scale.

On average there is no essential difference between mono- and co-cultures regarding the estimated losses of net present value. The losses ranged mostly between 10 M€ to 100 M€, depending on the evaluation parameters (see Section 3.4.2). The smaller losses of ECΔ*ptsI*:ABΔ*gntT* scale-up are noteworthy, but at least to some extent this is caused by the other cultures being more limited by oxygen availability.

5. DISCUSSION

The results presented in Chapter 4 are discussed followingly: Species interactions are considered in Section 5.1, Section 5.2 then compares co-culture performance to single strain performance based on both experiments and simulations, and Section 5.3 reviews simulated large and small-scale cultivations. Sections 5.4 and 5.5 conclude this chapter by assessing the reliability and validity of results and how they succeeded in meeting the objectives of this work, and by proposing future work.

5.1 Community dynamics of studied co-cultures

As was reviewed in Section 2.4, co-cultures can be constructed to utilize several substrates simultaneously or to remove inhibitory substances. In this work, both of these two functions were displayed along with cross-feeding. Acetate was formed by *E. coli* but consumed by *A. baylyi*, and gluconate was formed by *A. baylyi* but consumed by both *A. baylyi* and *E. coli*. Altogether this led to smaller amounts of side products acetate and gluconate, and consequently community dynamics ranged from commensialism to mutualism.

Given that EC monoculture accumulated formidable amounts of acetate in the bioreactor experiment (14.9 mM) as well as in simulations (up to 3.87 g L^{-1} in large-scale fed-batch), it is noteworthy that of all experimented co-cultures only EC:ABΔ*gntT* accumulated a small amount of acetate (4.88 mM) but with more than doubled biomass concentration in terms of OD_{600} (EC:ABΔ*gntT* 2.64, EC 0.97). In simulations also EC:AB accumulated small amounts of acetate, but the concentrations were consistently smaller than in EC:ABΔ*gntT* simulations. This implies that *A. baylyi* has consumed acetate excreted by *E. coli* in the EC:AB and EC:ABΔ*gntT* co-cultures. Considering that *A. baylyi* has been shown to grow faster on glucose in the presence of acetate [66] and also that ECΔ*ptsI*:AB co-culture had consistently higher specific growth rates than either EC or AB, it seems likely that AB received acetate, or possibly some other compound, from *E. coli* in ECΔ*ptsI*:AB. The quick consumption of residual precultivation acetate in ECΔ*ptsI*:ABΔ*gntT* experiment and the fact that FI_{610} rose during the cultivation imply that ABΔ*gntT* consumed acetate also in ECΔ*ptsI*:ABΔ*gntT*. Altogether the growth burst and subsequent decay of OD_{600} in ECΔ*ptsI*:ABΔ*gntT* bioreactor experiment resembled the quick bursts and decays found with another *A. baylyi* knock-out strain unable to utilize glucose [66]. As such, acetate removal by *A. baylyi* and the consequent removal of inhibition on *E. coli* have been demonstrated here in accordance with previous findings [131], but for a wider range of

co-culture configurations. Similar cross feeding of an inhibitory side product has been demonstrated in other studies as well, with acetate and ethanol being the most common compounds [6, 10, 169].

Similar to acetate, culture acidity rose to considerable levels (pH 5) in single strain EC cultivation. Consistent with the notion that acetate is most inhibitory to *E. coli* growth on glucose at low pH [90, 124], the growth of EC was observed to cease altogether after 10 h, when pH had descended almost to 5 and acetate had accumulated to 14 mM (see Figure 4.1). The only other culture to reach such a low low pH was EC:ABΔ*gntT*, but its growth did not visibly cease even when pH went below 5. Consistently, the highest acetate concentration in the EC:ABΔ*gntT* cultivation was three times smaller than in EC (see Figure 4.5). Compared to EC growth, all of the co-cultures showed only moderate pH drops during cultivation, even when the biomass concentration was above the maximum OD_{600} 0.97 reached by EC (see Table A.1). Such pH stabilization has also been found in other co-cultures which involve utilization of organic acids excreted by one of the community members [10, 131]. It is also noted that EC simulations were more optimistic than the actual bioreactor experiments, because pH and its effects were not accounted for in modelling. The demonstrated pH buffering possible within co-cultures has the advantage that it could reduce the required amount of pH controlling with concentrated acids and alkali, which induce potentially harmful pH gradients along the reactor in the macromixing length- and time-scales [26, 37, 51].

In addition to *E. coli* excreting acetate in cultivations, *A. baylyi* contributed gluconate according to experiments, simulations, and prior knowledge of *A. baylyi* metabolism [133]. Based on observed OD_{600} growth and FI_{510} increases in ECΔ*ptsI*:AB and ECΔ*ptsI*:ABΔ*gntT*, it is concluded that ECΔ*ptsI* grew on gluconate produced by *A. baylyi*. Keeping in mind that *E. coli* prefers glucose assimilation over other the use of other substrates and that changes in anabolic regulation take time [13, 38], it was unlikely that EC assimilated any gluconate in EC:AB and EC:ABΔ*gntT* co-cultures.

Based on the effects of acetate, pH, and gluconate observed in both experiments and simulations, it is concluded that EC:AB was the only synergistic co-culture. In other words, both AB and EC were useful to the other strain, but neither was dependent of or harmful to the other. This is in contrast with the study by Zhou, Qiao, Edgar, and Stephanopoulos [169], where *S. cerevisiae* inhibited *E. coli* when neither was dependent of the other. Unlike *E. coli* or *S. cerevisiae*, however, *A. baylyi* has not been found to release inhibitory side products but rather is known for preferring acetate as a substrate. ECΔ*ptsI*:AB on the other hand was commensialistic or possibly synergistic to AB but obligatorily so to ECΔ*ptsI*. Conversely, EC:ABΔ*gntT* was a synergistic co-culture, and obligatorily so to ABΔ*gntT*. Other synergistic and commensialistic co-cultures with cross feeding can be found in literature, with the common theme of at least one strain providing nutrients to another one [6, 10, 98, 131, 163, 169]. Last of the co-cultures, ECΔ*ptsI*:ABΔ*gntT*, was strictly mutualistic:

neither of the strains could grow on glucose without the other strain present. Examples of obligate mutualism based on cross feeding alone were not found in the conducted literature review; the only mutualistic co-culture found was based on simultaneous cross feeding and oxygen inhibition removal [172]. Considering then that in such co-cultures where the participating strains utilize different substrates, strain proportions adapt according to medium composition [36, 163, 168], it is concluded that ECΔ*ptsI* and ABΔ*gntT* strains in ECΔ*ptsI*:AB, EC:ABΔ*gntT*, and ECΔ*ptsI*:ABΔ*gntT* co-cultures grew according to the amount of gluconate or acetate made available by the other strain present.

5.2 Comparison of co-cultures to respective single strains

In short, EC:AB and EC:ABΔ*gntT* co-cultures outperformed EC and AB monocultures in terms of productivity and specific growth rates due to the positive interactions mentioned above. Side product accumulation was reduced considerably as well, also in ECΔ*ptsI*:AB. Of course, the performance of ECΔ*ptsI*:ABΔ*gntT* was not any better than that of either EC or AB, but it should be considered that this particular co-culture involved only knock-out strains incapable of growing on glucose by themselves. As such, the improvements of ECΔ*ptsI*:ABΔ*gntT* compared to the individual knock-out strains cannot even be quantified, much like in the work of Zuroff, Xiques, and Curtis where neither a yeast nor an obligately anaerobic bacterium could grow in isolation in the given conditions [172]. Regarding simulated fed-batch cultures, it should be remembered that each of the six cultures had its own feeding pattern determined by simulated small-scale performance, and therefore the biomass concentrations, yields, and productivities are not well comparable.

Considering the differing precultivations and consequently reactor start-up and process time differences, the biomass concentrations achieved in bioreactor experiments are hardly comparable to one another. Likewise, the fluorescence intensities measured are mostly applicable for demonstrating the presence of both strains in co-cultivations. Indeed it is noticed that a strong signal of both FI_{510} and FI_{610} relative to culture OD_{600} is present only in co-cultures (see Table A.1), which further verifies the growth of all strains in co-cultures. So far fluorescent proteins and also bioluminescence have not been used to infer exact community compositions, but instead they have been limited to noticing the presence and growth of strains involved in co-cultures [131, 168]. Nevertheless it is observed that in bioreactor experiments all three co-cultures with at least one wild-type strain (EC:AB, ECΔ*ptsI*:AB, and EC:ABΔ*gntT*) reached higher specific growth rates than EC or AB alone, and EC:AB and EC:ABΔ*gntT* also a considerably much higher OD_{600}. Similar findings of consistently better performance of co-cultures compared to respective monocultures have been demonstrated in other studies as well, with the co-cultured species ranging from bacteria to algae [6, 10, 66, 131].

Surprisingly, the simulated biomass concentrations in batch cultures were actually higher in single strain cultures than in co-cultures, if the comparison is done according

to the wild-type strains EC and AB. Both EC:AB and EC:ABΔ*gntT* reached a biomass concentration between AB and EC, but ECΔ*ptsI*:AB and ECΔ*ptsI*:ABΔ*gntT* a concentration below AB. Consequently the single strain biomass yields were higher. If the model biomass and energy yields on gluconate and acetate were too small relative to glucose, then it was inevitable that the EC and AB simulations reached higher biomass concentrations than the co-cultures, where a portion of glucose was always converted to gluconate or acetate before actual assimilation. On the other hand, it seems likely that due to higher specific growth rates the co-cultures were more severely oxygen limited than the respective monocultures (see Figures 4.7, A.1, 4.9, and A.2). To some extent similarly co-cultures that utilize several substrates simultaneously may also generate side products more efficiently than single strain cultures [36, 163]. However, simulated biomass productivities were higher in EC:AB and EC:ABΔ*gntT* in accordance with the consistently higher specific growth rates and shorter batch times of these co-cultures.

The most difficult culture to assess was ECΔ*ptsI*:AB, because the bioreactor cultivation started with very little biomass (OD_{600} 0.02), had an unusually long lag phase, and consequently reached only a low cell density (OD_{600} 0.45). The long lag phase of ECΔ*ptsI*:AB in bioreactor is in accordance with the fact that ECΔ*ptsI* could grow only on gluconate left over by AB and the general observation that glucose oxidation to gluconate by *A. baylyi* prior to actual assimilation causes a long lag phase in any case [133]. Additionally, AB glucose utilization modelling was problematic in this particular co-culture: In the model, all gluconate produced by AB was instantly equally available to ECΔ*ptsI*, which seems to have led to an unrealistic competition over gluconate. By virtue of being the actual gluconate producer AB should have the edge in subsequent gluconate utilization compared to ECΔ*ptsI* in the ECΔ*ptsI*:AB co-culture, which also seems to have been the case in the bioreactor experiment given the higher specific growth rates than with AB alone. A substrate assimilation model equivalent to heterogeneous catalysis, such as in [84, 85, 105, 121], could have avoided this defect. In the other co-cultures this modelling issue was not present as the strains did not assimilate gluconate simultaneously.

5.3 Comparison of large- and small-scale operation

As was expected, simulated large-scale performance of both batch and fed-batch cultures was sub-optimal compared to small-scale, which is in line with fermentations conducted in an actual 30 m^3 reactor, where about 20 % decreases in fed-batch biomass titer and productivity with 0.15 $g\,g^{-1}$ decreases on yield were observed compared to small scale (15 L) [165]. Studies on truly large reactors being scarce, numerous scale-down studies mimicking large-scale conditions at laboratory scale have similarly predicted 7 % to 25 % losses in average specific growth rate [5, 16, 83, 88], and both biomass and product yield losses [81, 82, 159]. These adverse effects of scale-up were consistently present in all the mono- and co-cultures studied in this work. As was reviewed in Section 2.3 concerning

fermentation scale-up, performance losses at production scale are in the end caused by physical heterogeneity.

Simulated batch cultures took on average 12 h longer to achieve total conversion of glucose to biomass in large scale. Maximum specific growth rates were not considerably much lower at large scale, but median specific growth rates were only 33 percent to 50 percent of the respective small-scale rates, with the only exception being the ECΔ*ptsI*:ABΔ*gntT* co-culture which was least affected by simulated transition to large-scale. Biomass titers were 0.27 $g\,L^{-1}$ smaller, and consequently biomass productivities were 0.045 $g\,L^{-1}\,h^{-1}$ smaller as well. However, biomass yields were relatively little affected, being on average 0.03 $g\,g^{-1}$ smaller than in small-scale.

In simulated fed-batches the specific growth rates were very similar across scales, but upper quartiles were notably lower (see Tables A.4 and A.5), which implies that growth limitations occurred earlier at large scale. Another observation is that large-scale fed-batches utilized slightly less glucose than the respective small-scale cultures, with ECΔ*ptsI*:AB consuming only half the glucose compared to small-scale. On average the fed-batch titers were 1.40 $g\,L^{-1}$ smaller, but it should be remembered that this mean value is affected by the different feeding patterns of cultures. Accordingly the productivities were on average 0.028 $g\,L^{-1}\,h^{-1}$ lower. Like in batch-cultures, fed-batch biomass yields were also relatively little affected, 0.04 $g\,g^{-1}$ on average. Comparing to the referenced experimental results, both at large-scale [165] and in scale-down simulators [5, 16, 83, 88], the growth rates were relatively little affected in simulations. This is likely due to the fact that already small scale simulations conducted in this work were oxygen limited.

As is evident from Figures 4.9 and A.2, the chosen glucose feeds were too much for almost all of the cultures at large scale. Only EC and EC:ABΔ*gntT* were capable of utilizing their feeds somewhat efficiently also at large scale, which is consistent with other simulations [120, 153] but somewhat inconsistent with the real experiments carried out in the modelled 30 m^3 reactor [165]. This implies that some phenomena relevant to the production-scale conditions have not been accounted for in the models. Nevertheless, residual glucose, gluconate, or acetate were present in each fed-batch culture at large scale. Likewise the large-scale batch cultures accumulated more gluconate and acetate than small-scale batches. Especially in the case of *E. coli* and acetate, such a cycle of accumulation and reassimilation wastes resources. Similar futile cycles have been demonstrated both in experiments and models [69, 120, 165].

Probably the major reason behind the decreased performance of both batch and fed-batch simulations at large-scale was the oxygen transfer rate. The average overall oxygen transfer coefficient $k_L a$ in the large reactor model was only 0.004 s^{-1}, which is very low compared to the range of 0.02 s^{-1} to 0.25 s^{-1} considered as an industrially relevant reference [31, 167]. It should also be noted that the small-scale ideal reactor was modelled to have a $k_L a$ of only 0.01 s^{-1}, making it also oxygen-limited. Therefore it seems that the choice of

simulation parameters has been unnecessarily pessimistic regarding oxygen transfer.

Substrate concentration gradients in fed-batches remained small in this work compared to the work of Pigou and Morchain [120]. Likewise the achieved cell densities were only 10 % of those simulated in the applicable references [120, 153]. This is attributed to the oxygen limitations present already at small scale, which in turn influenced the chosen feed rates for fed-batch production.

5.4 Assesment of results and methodology

A final assesment of both experimental and simulated results is made here by compiling some of the already discussed drawbacks, and by presenting some undiscussed ones. Despite the lacks of the conducted work, it is concluded that it has succeeded in providing answers to the research question.

Regarding the experimental results, it should be noted that none of the bioreactor experiments were replicated and that no replicate samples were drawn from the reactor for analysis. In other words, the measurement errors in OD_{600}, glucose, gluconate, and acetate concentrations, and fluorescence intensities cannot be quantified. Alleviating this shortcoming to some extent, the growth curves and metabolite concentrations obtained mostly advance smoothly as a function of time. In some sense showing internal consistency of results, each strain used in this work was cultivated at least twice: both knock-out strains in two co-cultures, and both wild-type strains in mono-culture and in two co-cultures. In hindsight, it is also evident that the chosen initial glucose level for batch experiments ($10\,\mathrm{g\,L^{-1}}$) was too high in the sense that none of the cultures was capable of achieving a full conversion of substrate within the experiment times. On the other hand, total sugar concentrations of even up to $50\,\mathrm{g\,L^{-1}}$ have been used in batch co-culture studies, but consequently with longer cultivation times [163].

Concerning simulations, the small-scale batch cultures and simulations were in reasonable agreement with each other, but validation of the biokinetic models would still be required. For example, biomass and energy yield coefficients were now estimated by flux balance analysis instead of experiments. The computationally estimated yield coefficients for *E. coli* were smaller but nevertheless in line with yields used by other authors. For example, *E. coli* was estimated by flux balance analysis to use $10.81\,\mathrm{mol_E\,mol_G^{-1}}$ ATP in biomass growth reaction on glucose, whereas the reference value was $12.05\,\mathrm{mol_E\,mol_G^{-1}}$ [120, 153, 166]. The used *A. baylyi* model, on the other hand, has the drawback that reference models for comparison were not found in literature. Though not an optimal way to infer yield coefficients for kinetic models, flux balance analysis has the merit of predicting in a mathematically concise way theoretical maximum yields allowed by a reaction network's stoichiometry. Mechanistically important improvements in *A. baylyi* model would be to incorporate the energy obtained in the form of electrons from glucose oxidation to gluconate, and possibly also a description of energy and carbon storage in

storage lipids such as triacylglycerols and wax esters [130].

As for the reactor modelling, gas holdups were assumed according to a general estimation of reactor average corrected by hydrostatic pressure [107]. A more realistic approach would be to simulate them first with a bubble size distribution [106, 167]. Also the turbulent power dissipation ε ($\mathrm{W\,kg^{-1}}$) was considered to be equal to the mean value throughout the large reactor even though up to 100-fold differences have been reported between regions near and far away from impellers [29]. Considering the way oxygen transfer coefficient in reactor compartments was obtained (Equations 2.5, 3.21, and 2.7), these simplifications of holdup and power dissipation made oxygen transfer rates far more uniform than they would otherwise have been. Quite uniform oxygen transfer and dissolved oxygen concentration in the large reactor influenced the simulated results, making them undoubtedly more optimistic than if the simulated large reactor had a greater degree of heterogeneity.

Altogether, this work has met the main objectives set for this work. The goal was to assess up-scaling of microbial co-culture fermentations. To make a successful assesment, it was necessary to demonstrate the differences of mono- and co-cultures, and the difference of large- and small-scale performance. To achieve the goal, co-cultures were cultivated in laboratory, and large-scale performance was estimated with simulations. Clear differences between mono- and co-cultures and between scales were realized: co-cultures were more productive than monocultures, and small-scale reactor operated better than the large one. To additionally estimate industrial relevance, the difference of large- and small-scale performance was also projected to monetary units.

5.5 Proposal for future work

This thesis has combined for the first time fermentation scale-up and microbial co-culture research, both established fields in their own right. Future work should include designing co-culture systems with realistic products, appropriate scale-down studies in laboratory, and improvements to the modelling framework utilized here. Perhaps first and foremost, a comprehensive economic assessment should be made to establish generalized criteria for titers, yields, and productivities required of economically feasible production of different product types, such as microbial biomass, recombinant proteins, fuels, and chemicals. Only then can the scalability of any bioprocess be reasonably evaluated, as economics ultimately dictate whether a proposed process is industrially relevant.

Following then a retro-design mindset [112], future research should pick both established and unestablished products and devise co-culture setups which either could replace an existing monoculture production scheme by virtue of superior performance or provide an altogether new one. It is proposed here that some of the commodity chemical fermentations reviewed in [143] should be redesigned as co-cultures to test whether they truly can compete with existing monoculture fermentations in terms of the key parameters titer, yield, and

productivity.

Regardless of how co-culture setups are devised, scale-down studies should be conducted with them and the single strains involved to experimentally assess whether co-cultures tolerate the conditions expected to exist at industrial scale any better than single strains. Scale-down systems with oscillating pH, substrate concentration, or oxygen tension are numerous in literature [5, 13, 15, 16, 26, 50, 67–69, 75, 81–83, 138, 140, 155, 156, 159], yet not a single co-culture scale-down study was found in the literature review of this thesis. Care should be taken in estimating relevant large-scale conditions in order to design an actually representative scale-down setup [51]. Such studies should also be carried out with complex media and carbon sources, for it has been pointed out that industrially used fermentation media are often complex in composition in contrast to the defined minimal media regularly used in laboratory studies [80].

Given that published literature already contains validated models of industrially relevant reactors [28, 106, 151, 167], it is proposed here that several of them should be used in simulating production-scale performance of any devised co-culture fermentations. For reasons discussed earlier (Sections 5.2 and 5.4), emphasis should be laid in not treating gas holdups and turbulence power dissipations as evenly distributed as in this work. As to the modelling of the biological phase, population balance models seem very applicable, and their distinct advantage is in providing the concepts of biological equilibrium, disequilibrium, and adaptation, which all enable heterogeneous metabolic responses within a population [103–105, 120, 121]. Future use and extension of them is therefore recommended, and particularly in conjuction with a substrate assimilation model equivalent to heterogeneous catalysis is encouraged [84, 85, 105, 121]. Another interesting possibility would be to couple flux balance analysis of genome-scale models with population balances even though the resulting models would likely be too costly computationally to combine with other than ideal reactor models.

This thesis already demonstrated an attempt at quantifying relative economic potential of microbial fermentations across cultivation scales, but the derived framework should be extended to account for the effects of product type, yield, titer, and productivity on production costs. It would be particularly useful to generalize downstream processing costs of the major fermentation product types as functions of the key parameters. The economic assessment carried out in this thesis had to assume that the chosen reference cultivations would make up profitable investments, but the comprehesive review of commodity and bulk chemical fermentations could serve as an actually appopriate reference of economically sound and profitable processes [143]. Another major improvement would be to consider already established processes or plant designs proposed in literature [25, 86, 87, 91, 97, 123, 142] and their characteristics as a reference of economically feasible fermentations.

6. CONCLUSIONS

Microbial co-cultures have been associated with promising properties, such as simultaneous utilization of different substrates, robustness to environmental conditions, and side-product inhibition removal in several laboratory-scale studies [6, 10, 36, 131, 163, 168, 169]. Accordingly the objective of this work was to make a generalized assessment whether co-cultures could scale-up from laboratory- to production-scale. More specifically the goal was to evaluate whether co-cultures would tolerate the physical adversities of scale-up better than the respective single strain cultures. As such, the scope of this study was limited to a few generalized cases rather than any specific production schemes.

In order to then meet these objectives, altogether four co-cultures and the two respective monocultures of *Escherichia coli* and *Acinetobacter baylyi* were studied and compared to each other as an extension of an earlier study [131]. The assessment was based on laboratory experiments with a 1 L stirred bioreactor and simulations of the same cultures in 1 L and 30 m^3 reactors. The simulations utilized a compartment-based representation of the reactors and population balances of microbial biomass to which unstructured kinetic models were coupled similarly to another study [120]. To additionally provide order of magnitude estimations of economics involved in scale-up, a simple method was derived to approximate the relative profitability of fermentations.

Based on experiments alone, co-cultures with internal utilization of inhibitory side-product, in this work acetate, showed 10 % to 50 % increases in maximal specific growth rate compared to single strains. This notion was on a qualitative level further supported by simulations of small- and large-scale bioreactors, with 3 % to 20 % increases. As for the biomass titers and yields, experiments were not amenable for comparison, but simulations suggested a slight advantage for the single strains, but the relatively small differences were likely to be caused by yield coefficients used in models. Based on the conducted simulations alone, it cannot be said that co-cultures would tolerate the physical heterogeneity caused by scale-up any better than the respective single strains. Simulated scale-up caused co-cultures productivity losses proportional to those caused to monocultures, estimated to translate into 1 M€ to 100 M€ decreases in net present value of a hypothetical plant. However, the simulations were considerably much oxygen limited already at the small scale and the experiments suggested higher relative performance of co-cultures. Therefore it is still an open question whether co-cultures would tolerate scale-up better than monocultures.

Future work on this subject should move from a generalized approach presented here onto real process schemes, in which the actual product and the according economical

Table 6.1 *Summary of the conducted work. The objective, methods, results, and their relevance are briefly presented. Owing to internal recycling of inhibitory side-products, co-cultures may redirect some of the otherwise lost substrate back into the desired products.*

Objective	Assess scale-up of co-cultures and respective monocultures
Methods	Experiments and simulations
Results	Co-cultures have greater biomass productivity Inhibitory side-products internally removed by co-cultures
Significance	Fermentation processes may lose 1 M€ to 100 M€ potential net present value in scale-up Co-cultures may recover some of the lost economic value

constraints are defined. The use of co-cultures should consequently be evaluated for different product types: biomass itself, commodity and specialty chemicals, fuels, and proteins. As to the modelling aspects, combining heterogeneous catalysis models of substrate assimilation [84, 85, 105, 121] with detailed kinetic models [120, 166] requires further work. Likewise the simple economic assessment devised in this work should be extended by using real production schemes [143] as a reference. The limitation of academia having almost exclusively only laboratory- or at best pilot-scale equipment on hand is ever present, and therefore co-cultures should be experimented with by applying appropriate scale-down simulators [108].

Table 6.1 provides a final summary of this thesis. Based on the simulations performed on all six cultures at both scales and in both batch and fed-batch operation, co-cultures were affected by scale-up just as much as the monocultures. Overall it is then concluded that microbial co-cultures should not be any less scalable than the conventional single strain cultures. To the contrary, the experimental results suggest that they might even withstand scale-up better than the respective strains in isolation.

REFERENCES

[1] A. R. Allman, “Fermentors: Design, Operation and Applications”, in *Fermentation Microbiology and Biotechnology*, M. El-Mansi and C. Bryce, Eds. Taylor & Francis, 1999, pp. 9–47.

[2] E. Almaas, B. Kovács, T. Vicsek, Z. N. Oltval, and A.-L. Barabási, “Global organization of metabolic fluxes in the bacterium *Escherichia coli*”, *Nature*, vol. 427, pp. 839–843, 2004.

[3] E. Anane, D. C. López, P. Neubauer, and M. N. C. Bournazou, “Modelling overflow metabolism in *Escherichia coli* by acetate cycling”, *Biochemical Engineering Journal*, vol. 125, pp. 23–30, 2017.

[4] T. Baba, T. Ara, M. Hasegawa, Y. Takai, Y. Okumura, M. Baba, K. A. Datsenko, M. Tomita, B. L. Wanner, and H. Mori, “Construction of *Escherichia coli* K-12 in-frame, single-gene knockout mutants: the Keio collection”, *Molecular Systems Biology*, vol. 2, no. 2006.0008, 2006.

[5] J. Baert, A. Delepierre, S. Telek, P. Fickers, D. Toye, A. Delamotte, A. R. Lara, K. E. Jaén, G. Gosset, P. R. Jensen, and F. Delvigne, “Microbial population heterogeneity versus bioreactor heterogeneity: Evaluation of Redox Sensor Green as an exogenous metabolic biosensor”, *Engineering in Life Sciences*, vol. 16, pp. 643–651, 2016.

[6] T. S. Bayer, D. M. Widmaier, K. Temme, E. A. Mirsky, D. V. Santi, and C. A. Voigt, “Synthesis of Methyl Halides from Biomass Using Engineered Microbes”, *Journal of the American Chemical Society*, vol. 131, pp. 6508–6515, 2009.

[7] A. Beloqui, P. D. de María, P. N. Golyshin, and M. Ferrer, “Recent trends in industrial microbiology”, *Current Opinion in Microbiology*, vol. 11, pp. 240–248, 2008.

[8] V. de Berardinis, D. Vallenet, V. Castelli, M. Besnard, A. Pinet, C. Cruaud, S. Samair, C. Lechaplais, G. Gyapay, C. Richez, M. Durot, A. Kreimeyer, F. L. Fèvre, V. Schächter, V. Pezo, V. Döring, C. Scarpelli, C. Médigue, G. N. Cohen, P. Marlière, M. Salanoubat, and J. Weissenbach, “A complete collection of single-gene deletion mutants of *Acinetobacter baylyi* ADP1”, *Molecular Systems Biology*, vol. 4, no. 174, 2008.

[9] S. M. Bhajaravu, T. W. F. Russell, and H. W. Blanch, “The design of gas sparged devices for viscous liquid systems”, *AIChE Journal*, vol. 24, no. 3, 1978.

[10] S. K. Bhatia, D. Ki, Y. Kim, H. Kim, H. Seo, J. Lee, J. Kim, J. Jeon, K. Jang, Y. Kim, and Y. Yang, “Development of semi-synthetic microbial consortia of *Streptomyces coelicolor* for increased production of biodiesel (fatty acid methyl esters)”, *Fuel*, vol. 159, pp. 189–196, 2015.

[11] D. S. Bindels, L. Haarbosch, L. van Weeren, M. Postma, K. E. Wiese, M. Mastop, S. Aumonier, G. Gotthard, A. Royant, M. A. Hink, and T. W. J. Gadella Jr, "mScarlet: a bright monomeric red fluorescent protein for cellular imaging", *Nature Methods*, vol. 14, pp. 53–56, 2017.

[12] P. Bogacki and L. F. Shampine, "A 3(2) Pair of Runge-Kutta Formulas", *Applied Mathematics Letters*, vol. 2, no. 4, pp. 321–325, 1989.

[13] E. Brand, S. Junne, E. Anane, M. N. Cruz-Bournazou, and P. Neubauer, "Importance of the cultivation history for the response of *Escherichia coli* to oscillations in scale-down experiments", *Bioprocess and Biosystems Engineering*, vol. 41, no. 9, pp. 1305–1313, 2018.

[14] K. Brenner, L. You, and F. H. Arnold, "Engineering microbial consortia: a new frontier in synthetic biology", *Trends in Biotechnology*, vol. 26, no. 9, pp. 483–489, 2008.

[15] A. Brognaux, F. Francis, J. Twizere, P. Thonart, and F. Delvigne, "Scale-down effect on the extracellular proteome of *Escherichia coli*: correlation with membrane permeability and modulation according to substrate heterogeneities", *Bioprocess and Biosystems Engineering*, vol. 37, pp. 1469–1485, 2014.

[16] J. Buchholz, M. Graf, A. Freund, T. Busche, J. Kalinowski, B. Blombach, and R. Takors, "CO_2/HCO_3^- perturbations of simulated large scale gradients in a scale-down device cause fast transcriptional responses in *Corynebacterium glutamicum*", *Applied Microbiology and Biotechnology*, vol. 98, pp. 8563–8572, 2014.

[17] A. Castan and S. Enfors, "Characteristics of a DO-controlled fed-batch culture of *Escherichia coli*", *Bioprocess Engineering*, vol. 22, pp. 509–515, 2000.

[18] A. Castan and S. Enfors, "Formate Accumulation Due to DNA Release in Aerobic Cultivations of *Escherichia coli*", *Biotechnology and Bioengineering*, vol. 77, pp. 324–328, 2002.

[19] A. Castan, A. Näsman, and S. Enfors, "Oxygen enriched air supply in *Escherichia coli* processes: production of biomass and recombinant human growth hormone", *Enzyme and Microbial Technology*, vol. 30, pp. 847–854, 2002.

[20] F. Ceroni, R. Algar, G. Stan, and T. Ellis, "Quantifying cellular capacity identifies gene expression designs with reduced burden", *Nature Methods*, vol. 12, no. 5, pp. 415–418, 2015.

[21] S. H. J. Chan, M. N. Simons, and C. D. Maranas, "SteadyCom: Predicting microbial abundances while ensuring community stability", *PLoS Computational Biology*, vol. 13, no. 5, e1005539, 2017.

[22] T. Charoenrat, M. Ketudat-Cairns, M. Jahic, A. Veide, and S. Enfors, "Increased total air pressure versus oxygen limitation for enhanced oxygen transfer and product formation in a *Pichia pastoris* recombinant protein process", *Biochemical Engineering Journal*, vol. 30, pp. 205–211, 2006.

[23] T. Charoenrat, M. Ketudat-Cairns, H. Stendahl-Andersen, M. Jahic, and S. Enfors, "Oxygen-limited fed-batch process: An alternative control for *Pichia pastoris* recombinant protein processes", *Bioprocess and Biosystems Engineering*, vol. 27, pp. 399–406, 2005.

[24] A. Ciranna, R. Ferrari, V. Santala, and M. Karp, "Inhibitory effects of substrate and soluble end products on biohydrogen production of the alkalithermophile *Caloramator celer*: Kinetic, metabolic and transcription analyses", *International Journal of Hydrogen Energy*, vol. 39, pp. 6391–6401, 2014.

[25] J. T. Claypool, D. R. Raman, L. R. Jarboe, and D. R. Nielsen, "Technoeconomic evaluation of bio-based styrene production by engineered *Escerichia coli*", *J Ind Microbiol Biotechnol*, vol. 41, no. 8, pp. 1211–1216, 2014.

[26] J. T. Cortés, N. Flores, F. Bolívar, A. R. Lara, and O. T. Ramírez, "Physiological Effects of pH Gradients on *Escherichia coli* During Plasmid DNA Production", *Biotechnology and Bioengineering*, vol. 113, no. 3, pp. 598–611, 2016.

[27] Y. Q. Cui, R. G. J. M. van der Lans, and K. C. A. M. Luyben, "Local Power Uptake in Gas-Liquid Systems with Single and Multiple Rushton Turbines", *Chemical Engineering Science*, vol. 51, no. 11, pp. 2631–2636, 1996.

[28] A. Delafosse, M. Collignon, S. Calvo, F. Delvigne, M. Crine, P. Thonart, and D. Toye, "CFD-based compartment model for description of mixing in bioreactors", *Chemical Engineering Science*, vol. 106, pp. 76–85, 2014.

[29] A. Delafosse, A. Line, J. Morchain, and P. Guiraud, "LES and URANS simulations of hydrodynamics in mixing tank: Comparison to PIV experiments", *Chemical Engineering Research and Design*, vol. 86, pp. 1322–1330, 2008.

[30] Z. T. Dobroth, S. Hu, E. R. Coats, and A. G. McDonald, "Polyhydroxybutyrate synthesis on biodiesel wastewater using mixed microbial consortia", *Bioresource Technology*, vol. 102, pp. 3352–3359, 2011.

[31] P. M. Doran, *Bioprocess engineering principles*, 2nd ed. Oxford, UK: Academic Press, 2013, p. 926.

[32] R. Du, J. Yan, S. Li, L. Zhang, S. Zhang, J. Li, G. Zhao, and P. Qi, "Cellulosic ethanol production by natural bacterial consortia is enhanced by *Pseudoxanthomonas taiwanensis*", *Biotechnology for Biofuels*, vol. 8, no. 10, 2015.

[33] M. Durot, F. L. Fèvre, V. de Berardinis, A. Kreimeyer, D. Vallenet, C. Combe, S. Smidtas, M. Salanoubat, J. Weissenbach, and V. Schachter, "Iterative reconstruction of a global metabolic model of *Acinetobacter baylyi* ADP I using high-throughput growth phenotype and gene essentiality data", *BMC Systems Biology*, vol. 2, no. 85, 2008.

[34] A. Ebrahim, J. A. Lerman, B. O. Palsson, and D. R. Hyduke, "COBRApy: COnstraints-Based Reconstruction and Analysis for Python", *BMC Systems Biology*, vol. 7, no. 74, 2013.

[35] M. A. Eiteman and E. Altman, "Overcoming acetate in *Escherichia coli* recombinant protein fermentations", *Trends in Biotechnology*, vol. 24, no. 11, pp. 530–536, 2006.

[36] M. A. Eiteman, S. A. Lee, and E. Altman, "A co-fermentation strategy to consume sugar mixtures effectively", *Journal of Biological Engineering*, vol. 2, no. 3, 2008.

[37] S. Enfors, M. Jahic, A. Rozkov, B. Xu, M. Hecker, B. Jürgen, E. Krüger, T. Schweder, G. Hamer, D. O'Beirne, N. Noisommit-Rizzi, M. Reuss, L. Boone, C. Hewitt, C. McFarlane, A. Nienow, T. Kovacs, C. Trägårdh, L. Fuchs, J. Revstedt, P. Friberg, B. Hjertager, G. Blomsten, H. Skogman, S. Hjort, F. Hoeks, H. Lin, P. Neubauer, R. van der Lans, K. Luyben, P. Vrabel, and Å. Manelius, "Physiological responses to mixing in large scale bioreactors", *Journal of Biotechnology*, vol. 85, pp. 175–185, 2001.

[38] B. Enjalbert, M. Cocaign-Bousquet, J. Portais, and F. Letisse, "Acetate Exposure Determines the Diauxic Behavior of Escherichia coli during the Glucose-Acetate Transition", *Journal of Bacteriology*, vol. 197, no. 19, pp. 3173–3181, 2015.

[39] B. Enjalbert, P. Millard, M. Dinclaux, J. Portais, and F. Letisse, "Acetate fluxes in *Escherichia coli* are determined by the thermodynamic control of the Pta-AckA pathway", *Scientific Reports*, vol. 7, no. 42135, 2017.

[40] A. E. Escalante, M. Rebolleda-Gomez, M. Benitez, and M. Travisano, "Ecological perspectives on synthetic biology: insights from microbial population biology", *Frontiers in Microbiology*, vol. 6, no. 143, 2015.

[41] A. M. Feist, C. S. Henry, J. L. Reed, M. Krummenacker, A. R. Joyce, P. D. Karp, L. J. Broadbelt, V. Hatzimanikatis, and B. Ø. Palsson, "A genome-scale metabolic reconstruction for *Escherichia coli* K-12 MG1655 that accounts for 1260 ORFs and thermodynamic information", *Molecular Systems Biology*, vol. 3, no. 121, 2007.

[42] J. Gabelle, F. Augier, A. Carvalho, R. Rousset, and J. Morchain, "Effect of Tank Size on $k_{\mathrm{L}}a$ and Mixing Time in Aerated Stirred Reactors with Non-Newtonian Fluids", *The Canadian Journal of Chemical Engineering*, vol. 89, pp. 1139–1153, 2011.

[43] F. Garcia-Ochoa and E. Gomez, "Bioreactor scale-up and oxygen transfer rate in microbial processes: An overview", *Biotechnology Advances*, vol. 27, pp. 153–176, 2009.

[44] R. Gelves, A. Dietrich, and R. Takors, "Modeling of gas-liquid mass transfer in a stirred tank bioreactor agitated by a Rushton turbine or a new pitched blade impeller", *Bioprocess and Biosystems Engineering*, vol. 37, pp. 365–375, 2014.

[45] R. González-Cabaleiro, A. M. Mitchell, W. Smith, A. Wipat, and I. D. Ofiţeru, "Heterogeneity in Pure Microbial Systems: Experimental Measurements and Modeling", *Frontiers in Microbiology*, vol. 8, no. 1813, 2017.

[46] A. Haldimann and B. L. Wanner, "Conditional-Replication, Integration, Excision, and Retrieval Plasmid-Host Systems for Gene Structure-Function Studies of Bacteria", *Journal of Bacteriology*, vol. 183, no. 21, pp. 6384–6393, 2001.

[47] L. Han, S. Enfors, and L. Häggström, "*Escherichia coli* high-cell-density culture: carbon mass balances and release of outer membrane components", *Bioprocess and Biosystems Engineering*, vol. 25, pp. 205–212, 2003.

[48] T. J. Hanly and M. A. Henson, "Unstructured modeling of a synthetic microbial consortium for consolidated production of ethanol", in *IFAC Proceedings Volumes (IFAC-PapersOnline)*, vol. 12, 2013, pp. 157–162.

[49] T. J. Hanly, M. Urello, and M. A. Henson, "Dynamic flux balance modeling of *S. cerevisiae* and *E. coli* co-cultures for efficient consumption of glucose/xylose mixtures", *Applied Microbiology and Biotechnology*, vol. 93, pp. 2529–2541, 2012.

[50] C. Haringa, A. T. Deshmukh, R. F. Mudde, and H. J. Noorman, "Euler-Lagrange analysis towards representative down-scaling of a 22 m^3 aerobic *S. cerevisiae* fermentation", *Chemical Engineering Science*, vol. 170, pp. 653–669, 2017.

[51] C. Haringa, W. Tang, A. T. Deshmukh, J. Xia, M. Reuss, J. J. Heijnen, R. F. Mudde, and H. J. Noorman, "Euler-Lagrange computational fluid dynamics for (bio)reactor scale down: An analysis of organism lifelines", *Engineering in Life Sciences*, vol. 16, pp. 652–663, 2016.

[52] C. Haringa, W. Tang, G. Wang, A. T. Deshmukh, W. A. van Winden, J. Chu, W. M. van Gulik, J. J. Heijnen, R. F. Mudde, and H. J. Noorman, "Computational fluid dynamics simulation of an industrial *P. chrysogenum* fermentation with a coupled 9-pool metabolic model: Towards rational scale-down and design optimization", *Chemical Engineering Science*, vol. 175, pp. 12–24, 2018.

[53] S. Hartmans, J. D. Smits, M. J. van der Werf, F. Volkering, and J. A. de Bont, "Metabolism of Styrene Oxide and 2-Phenylethanol in the Styrene-Degrading *Xanthobacter* Strain 124X", *Applied and Environmental Microbiology*, vol. 55, no. 11, pp. 2850–2855, 1989.

[54] S. G. Hays, W. G. Patrick, M. Ziesack, N. Oxman, and P. A. Silver, "Better together: engineering and application of microbial symbioses", *Current Opinion in Biotechnology*, vol. 36, pp. 40–49, 2015.

[55] H. He, C. Edlich-Muth, S. N. Lindner, and A. Bar-Even, "Ribulose Monophosphate Shunt Provides Nearly All Biomass and Energy Required for Growth of *E. coli*", *ACS Synthetic Biology*, vol. 7, pp. 1601–1611, 2018.

[56] A. Hecht, D. Endy, M. Salit, and M. S. Munson, "When Wavelengths Collide: Bias in Cell Abundance Measurements Due to Expressed Fluorescent Proteins", *ACS Synthetic Biology*, vol. 5, pp. 1024–1027, 2016.

[57] M. A. Henson and T. J. Hanly, "Dynamic flux balance analysis for synthetic microbial communities", *IET Systems Biology*, vol. 8, no. 5, pp. 214–229, 2014.

[58] A. Ho, K. de Roy, O. Thas, J. D. Neve, S. Hoefman, P. Vandamme, K. Heylen, and N. Boon, "The more, the merrier: heterotroph richness stimulates methanotrophic activity", *The ISME Journal*, vol. 8, pp. 1945–1948, 2014.

[59] E. Hochuli, W. Bannwarth, H. Döbeli, R. Gentz, and D. Stüber, "Genetic Approach to Facilitate Purification of Recombinant Protein with a Novel Metal Chelate Adsorbent", *Nature Biotechnology*, vol. 6, pp. 1321–1323, 1988.

[60] I. S. Hunter, "Microbial Synthesis of Commercial Products and Strain Improvement", in *Fermentation Microbiology and Biotechnology*, M. El-Mansi and C. Bryce, Eds. Taylor & Francis, 1999, pp. 121–145.

[61] M. Jahic, J. Rotticci-Mulder, M. Martinelle, K. Hult, and S. Enfors, "Modeling of growth and energy metabolism of *Pichia pastoris* producing a fusion protein", *Bioprocess and Biosystems Engineering*, vol. 24, pp. 385–393, 2002.

[62] M. Jahic, F. Wallberg, M. Bollok, P. Garcia, and S.-O. Enfors, "Temperature limited fed-batch technique for control of proteolysis in *Pichia pastoris* bioreactor cultures", *Microbial Cell Factories*, vol. 2, no. 6, 2003.

[63] S. S. de Jesus, J. M. Neto, and R. M. Filho, "Hydrodynamics and mass transfer in bubble column, conventional airlift, stirred airlift and stirred tank bioreactors, using viscous fluid: A comparative study", *Biochemical Engineering Journal*, vol. 118, pp. 70–81, 2017.

[64] D. R. Johnson, F. Goldschmidt, E. E. Lilja, and M. Ackermann, "Metabolic specialization and the assembly of microbial communities", *The ISME Journal*, vol. 6, pp. 1985–1991, 2012.

[65] E. Jones, T. Oliphant, P. Peterson, *et al.*, *SciPy: Open source scientific tools for Python*, 2001–. [Online]. Available: http://www.scipy.org/.

[66] M. S. Kannisto, R. K. Mangayil, A. Shrivastava-Bhattacharya, B. I. Pletschke, M. T. Karp, and V. P. Santala, "Metabolic engineering of *Acinetobacter baylyi* ADP1 for removal of *Clostridium butyricum* growth inhibitors produced from lignocellulosic hydrolysates", *Biotechnology for Biofuels*, vol. 8, no. 198, 2015.

[67] T. Kar, J. Destain, P. Thonart, and F. Delvigne, "Scale-down assessment of the sensitivity of *Yarrowia lipolytica* to oxygen transfer and foam management in bioreactors: investigation of the underlying physiological mechanisms", *Journal of Industrial Microbiology and Biotechnology*, vol. 39, pp. 337–346, 2012.

[68] F. Käß, I. Hariskos, A. Michel, H. Brandt, R. Spann, S. Junne, W. Wiechert, P. Neubauer, and M. Oldiges, "Assessment of robustness against dissolved oxygen/substrate oscillations for *C. glutamicum* DM1933 in two-compartment bioreactor", *Bioprocess and Biosystems Engineering*, vol. 37, pp. 1151–1162, 2014.

[69] F. Käß, S. Junne, P. Neubauer, W. Wiechert, and M. Oldiges, "Process inhomogeneity leads to rapid side product turnover in cultivation of *Corynebacterium glutamicum*", *Microbial Cell Factories*, vol. 13, no. 6, 2014.

[70] Y. Kawase and M. Moo-Young, "The effect of antifoam agents on mass transfer in bioreactors", *Bioprocess Engineering*, vol. 5, pp. 169–173, 1990.

[71] Y. Kawase, B. Halard, and M. Moo-Young, "Liquid-Phase Mass Transfer Coefficients in Bioreactors", *Biotechnology and Bioengineering*, vol. 39, pp. 1133–1140, 1992.

[72] R. A. Khandelwal, B. G. Olivier, W. F. M. Röling, B. Teusink, and F. J. Bruggeman, "Community Flux Balance Analysis for Microbial Consortia at Balanced Growth", *PLoS ONE*, vol. 8, no. 5, e64567, 2013.

[73] K. Kiviharju, K. Salonen, M. Leisola, and T. Eerikäinen, "Modeling and simulation of *Streptomyces peucetius* var. caesius N47 cultivation and ϵ-rhodomycinone production with kinetic equations and neural networks", *Journal of Biotechnology*, vol. 126, pp. 365–373, 2006.

[74] S. Koch, D. Benndorf, K. Fronk, U. Reichl, and S. Klamt, "Predicting compositions of microbial communities from stoichiometric models with applications for the biogas process", *Biotechnology for Biofuels*, vol. 9, no. 17, 2016.

[75] C. Korneli, C. J. Bolten, T. Godard, E. Franco-Lara, and C. Wittmann, "Debottlenecking Recombinant Protein Production in *Bacillus megaterium* Under Large-Scale Conditions—Targeted Precursor Feeding Designed From Metabolomics", *Biotechnology and Bioengineering*, vol. 109, no. 6, pp. 1538–1550, 2012.

[76] M. Kuschel, F. Siebler, and R. Takors, "Lagrangian Trajectories to Predict the Formation of Population Heterogeneity in Large-Scale Bioreactors", *Bioengineering*, vol. 4, no. 27, 2017.

[77] A. de Lamotte, A. Delafosse, S. Calvo, F. Delvigne, and D. Toye, "Investigating the effects of hydrodynamics and mixing on mass transfer through the free-surface in stirred tank bioreactors", *Chemical Engineering Science*, vol. 172, pp. 125–142, 2017.

[78] A. R. Lara, L. A. Palomares, and O. T. Ramírez, "Scale-Down: Simulating Large-Scale Cultures in the Laboratory", in *Industrial Biotechnology: Products and Processes*, C. Wittmann and J. C. Liao, Eds., 1st ed. Wiley-VCH Verlag GmbH & Co. KGaA, 2017, pp. 55–79.

[79] N. Lebaz, A. Cockx, M. Spérandio, and J. Morchain, "Population Balance Approach for the Modelling of Enzymatic Hydrolysis of Cellulose", *The Canadian Journal of Chemical Engineering*, vol. 93, pp. 276–284, 2015.

[80] A. Lemoine, M. H. Limberg, S. Kästner, M. Oldiges, P. Neubauer, and S. Junne, "Performance loss of *Corynebacterium glutamicum* cultivations under scale-down conditions using complex media", *Engineering in Life Sciences*, vol. 16, pp. 620–632, 2016.

[81] A. Lemoine, N. M. Martínez-Iturralde, R. Spann, P. Neubauer, and S. Junne, "Response of *Corynebacterium glutamicum* Exposed to Oscillating Cultivation Conditions in a Two- and a Novel Three-Compartment Scale-Down Bioreactor", *Biotechnology and Bioengineering*, vol. 112, pp. 1220–1231, 2015.

[82] J. Li, J. Jaitzig, P. Lu, R. D. Süssmuth, and P. Neubauer, "Scale-up bioprocess development for production of the antibiotic valinomycin in *Escherichia coli* based on consistent fed-batch cultivations", *Microbial Cell Factories*, vol. 14, no. 83, 2015.

[83] M. H. Limberg, V. Pooth, W. Wiechert, and M. Oldiges, "Plug flow versus stirred tank reactor flow characteristics in two-compartment scale-down bioreactor: Setup-specific influence on the metabolic phenotype and bioprocess performance of *Corynebacterium glutamicum*", *Engineering in Life Sciences*, vol. 16, pp. 610–619, 2016.

[84] M. Linkès, M. M. Afonso, P. Fede, J. Morchain, and P. Schmitz, "Numerical study of substrate assimilation by a microorganism exposed to fluctuating concentration", *Chemical Engineering Science*, vol. 81, pp. 8–19, 2012.

[85] M. Linkès, P. Fede, J. Morchain, and P. Schmitz, "Numerical investigation of subgrid mixing effects on the calculation of biological reaction rates", *Chemical Engineering Science*, vol. 116, pp. 473–485, 2014.

[86] H. Listewnik, K. Wendlandt, M. Jechorek, and G. Mirschel, "Process Design for the Microbial Synthesis of Poly-β-hydroxybutyrate (PHB) from Natural Gas", *Engineering in Life Sciences*, vol. 7, no. 3, pp. 278–282, 2007.

[87] G. Liu, J. Zhang, and J. Bao, "Cost evaluation of cellulase enzyme for industrial-scale cellulosic ethanol production based on rigorous Aspen Plus modeling", *Bioprocess and Biosystems Engineering*, vol. 39, no. 1, pp. 133–140, 2016.

[88] M. Löffler, J. D. Simen, G. Jäger, K. Schäferhoff, A. Freund, and R. Takors, "Engineering *E. coli* for large-scale production – Strategies considering ATP expenses and transcriptional responses", *Metabolic Engineering*, vol. 38, pp. 73–85, 2016.

[89] H. Lu, C. Li, W. Tang, Z. Wang, J. Xia, S. Zhang, Y. Zhuang, J. Chu, and H. Noorman, "Dependence of fungal characteristics on seed morphology and shear stress in bioreactors", *Bioprocess and Biosystems Engineering*, vol. 38, pp. 917–928, 2015.

[90] G. W. Luli and W. R. Strohl, "Comparison of Growth, Acetate Production, and Acetate Inhibition of *Escherichia coli* Strains in Batch and Fed-Batch Fermentations", *Applied and Environmental Microbiology*, vol. 56, no. 4, pp. 1004–1011, 1990.

[91] S. Macrelli, M. Galbe, and O. Wallberg, "Effects of production and market factors on ethanol profitability for an integrated first and second generation ethanol plant using the whole sugarcane as feedstock", *Biotechnology for Biofuels*, vol. 7, no. 26, 2014.

[92] R. Mangayil, T. Aho, M. Karp, and V. Santala, "Improved bioconversion of crude glycerol to hydrogen by statistical optimization of media components", *Renewable Energy*, vol. 75, pp. 583–589, 2015.

[93] R. Mangayil, S. Rajala, A. Pammo, E. Sarlin, J. Luo, V. Santala, M. Karp, and S. Tuukkanen, "Engineering and Characterization of Bacterial Nanocellulose Films as Low Cost and Flexible Sensor Material", *ACS Applied Materials & Interfaces*, vol. 9, pp. 19 048–19 056, 2017.

[94] E. M. T. El-Mansi, "Microbiology of Industrial Fermentation", in *Fermentation Microbiology and Biotechnology*, M. El-Mansi and C. Bryce, Eds. Taylor & Francis, 1999, pp. 49–68.

[95] K. Marisch, K. Bayer, T. Scharl, J. Mairhofer, P. M. Krempl, K. Hummel, E. Razzazi-Fazeli, and G. Striedner, "A Comparative Analysis of Industrial *Escherichia coli* K-12 and B Strains in High-Glucose Batch Cultivations on Process-, Transcriptome- and Proteome Level", *PLoS ONE*, vol. 8, no. 8, e70516, 2013.

[96] W. McKinney, "Data Structures for Statistical Computing in Python", in *Proceedings of the 9th Python in Science Conference*, 2010, pp. 51–56.

[97] E. M. de Medeiros, J. A. Posada, H. Noorman, P. Osseweijer, and R. M. Filho, "Hydrous bioethanol production from sugarcase bagasse via energy self-sufficient gasification-fermentation hybrid route: Simulation and financial analysis", *Journal of Cleaner Production*, vol. 168, pp. 1625–1635, 2017.

[98] M. T. Mee, J. J. Collins, G. M. Church, and H. H. Wang, "Syntrophic exchange in synthetic microbial communities", *Proceedings of the National Academy of Sciences*, vol. 111, no. 20, E2149–E2156, 2014.

[99] J. J. Minty, M. E. Singer, S. A. Scholz, C. Bae, J. Ahn, C. E. Foster, J. C. Liao, and X. N. Lin, "Design and characterization of synthetic fungal-bacterial consortia for direct production of isobutanol from cellulosic biomass", *Proceedings of the National Academy of Sciences*, vol. 110, no. 36, pp. 14 592–14 597, 2013.

[100] J. Morchain, "Numerical Tools for Scaling Up Bioreactors", in *Current Developments in Biotechnology and Bioengineering: Bioprocesses, Bioreactors and Controls*, C. Larroche, M. Á. Sanromán, G. Du, and A. Pandey, Eds. Elsevier, 2017, pp. 495–523.

[101] J. Morchain, *Bioreactor Modeling, Interactions between Hydrodynamics and Biology*, 1st ed. London, UK: ISTE Press Ltd, 2017, p. 218.

[102] J. Morchain and C. Fonade, "A Structured Model for the Simulation of Bioreactors Under Transient Conditions", *AIChE Journal*, vol. 55, no. 11, pp. 2973–2984, 2009.

[103] J. Morchain, J. Gabelle, and A. Cockx, "A Coupling of Biokinetic and Population Balance Models to Account for Biologial Heterogeneity in Bioreactors", *AIChE Journal*, vol. 59, no. 2, pp. 369–379, 2013.

[104] J. Morchain, J. Gabelle, and A. Cockx, "A Coupled Population Balance Model and CFD Approach for the Simulation of Mixing Issues in Lab-Scale and Industrial Bioreactors", *AIChE Journal*, vol. 60, no. 1, pp. 27–40, 2014.

[105] J. Morchain, M. Pigou, and N. Lebaz, "A population balance model for bioreactor combining interdivision time distributions and micromixing concepts", *Biochemical Engineering Journal*, vol. 126, pp. 135–145, 2017.

[106] E. K. Nauha, Z. Kálal, J. M. Ali, and V. Alopaeus, "Compartmental modeling of large stirred tank bioreactors with high gas volume fractions", *Chemical Engineering Journal*, vol. 334, pp. 2319–2334, 2018.

[107] E. K. Nauha, O. Visuri, R. Vermasvuori, and V. Alopaeus, "A new simple approach for the scale-up of aerated stirred tanks", *Chemical Engineering Research and Design*, vol. 95, pp. 150–161, 2015.

[108] P. Neubauer and S. Junne, "Scale-down simulators for metabolic analysis of large-scale bioprocesses", *Current Opinion in Biotechnology*, vol. 21, pp. 114–121, 2010.

[109] J. Nielsen, "Fermentation Kinetics", in *Fermentation Microbiology and Biotechnology*, M. El-Mansi and C. Bryce, Eds. Taylor & Francis, 1999, pp. 69–120.

[110] A. W. Nienow, "Agitators for mycelial fermentations", *Trends in Biotecnology*, vol. 8, pp. 224–233, 1990.

[111] A. Nieß, M. Löffler, J. D. Simen, and R. Takors, "Repetitive Short-Term Stimuli Imposed in Poor Mixing Zones Induce Long-Term Adaptation of *E. coli*, Cultures in Large-Scale Bioreactors: Experimental Evidence and Mathematical Model", *Frontiers in Microbiology*, vol. 8, no. 1195, 2017.

[112] H. J. Noorman and J. J. Heijnen, "Biochemical engineering's grand adventure", *Chemical Engineering Science*, vol. 170, pp. 677–693, 2017.

[113] K. Novak, L. Flöckner, A. M. Erian, P. Freitag, C. Herwig, and S. Pflügl, "Characterizing the effect of expression of an acetyl-CoA synthetase insensitive to acetylation on co-utilization of glucose and acetate in batch and continuous cultures of *E. coli* W", *Microbial Cell Factories*, vol. 17, no. 109, 2018.

[114] J. D. Orth, I. Thiele, and B. Ø. Palsson, "What is flux balance analysis?", *Nature Biotechnology*, vol. 28, no. 3, pp. 245–248, 2010.

[115] R. Palmen and K. J. Hellingwerf, "Uptake and processing of DNA by *Acinetobacter calcoaceticus* – a review", *Gene*, vol. 192, pp. 179–190, 1997.

[116] J. D. Pédelacq, S. Cabantous, T. Tran, T. C. Terwilliger, and G. S. Waldo, "Engineering and characterization of a superfolder green fluorescent protein", *Nature Biotechnology*, vol. 24, no. 1, pp. 79–88, 2006.

[117] M. S. Peters, K. D. Timmerhaus, and R. E. West, *Plant Design and Economics for Chemical Engineers*, 5th ed. New York, NY, US: McGraw-Hill, 2003, p. 988.

[118] H. T. B. Pham, G. Larsson, and S. Enfors, "Growth and Energy Metabolism in Aerobic Fed-Batch Cultures of *Saccharomyces cerevisiae*: Simulation and Model Verification", *Biotechnology and Bioengineering*, vol. 60, pp. 474–482, 1998.

[119] R. Phillips and R. Milo, "A feeling for the numbers in biology", *Proceedings of the National Academy of Sciences*, vol. 106, no. 51, pp. 21 465–21 471, 2009.

[120] M. Pigou and J. Morchain, "Investigating the interactions between physical and biological heterogeneities in bioreactors using compartment, population balance and metabolic models", *Chemical Engineering Science*, vol. 126, pp. 267–282, 2015.

[121] V. Quedeville, H. Ouazaite, B. Polizzi, R. O. Fox, P. Villedieu, P. Fede, F. Létisse, and J. Morchain, "A two-dimensional population balance model for cell growth including multiple uptake systems", *Chemical Engineering Research and Design*, vol. 132, pp. 966–981, 2018.

[122] V. V. Ranade and V. R. Deshpande, "Gas–liquid flow in stirred reactors: Trailing vortices and gas accumulation behind impeller blades", *Chemical Engineering Science*, vol. 54, pp. 2305–2315, 1999.

[123] S. Redl, S. Sukumara, T. Ploeger, L. Wu, T. Ø. Jensen, A. T. Nielsen, and H. Noorman, "Thermodynamics and economic feasibility of acetone production from syngas using the thermophilic production host *Moorella thermoacetica*", *Biotechnology for Biofuels*, vol. 10, no. 150, 2017.

[124] A. J. Roe, C. O'Byrne, D. McLaggan, and I. R. Booth, "Inhibition of *Escherichia coli* growth by acetic acid: a problem with methionine biosynthesis and homocysteine toxicity", *Microbiology*, vol. 148, pp. 2215–2222, 2002.

[125] A. Rosseburg, J. Fitschen, J. Wutz, T. Wucherpfennig, and M. Schlüter, "Hydrodynamic inhomogeneities in large scale stirred tanks – Influence on mixing time", *Chemical Engineering Science*, vol. 188, pp. 208–220, 2018.

[126] P. Rugbjerg, N. Myling-Petersen, A. Porse, K. Sarup-Lytzen, and M. O. Sommer, "Diverse genetic error modes constrain large-scale bio-based production", *Nature Communications*, vol. 9, no. 787, 2018.

[127] J. R. Rumble, Ed., *CRC Handbook of Chemistry and Physics*, 99th ed. Boca Raton, FL: CRC Press/Taylor & Francis, 2018, Internet Version.

[128] R. Sander, "Compilation of Henry's law constants (version 4.0) for water as solvent", *Atmospheric Chemistry and Physics*, vol. 15, pp. 4399–4981, 2015.

[129] S. Santala, E. Efimova, M. Karp, and V. Santala, "Real-Time monitoring of intracellular wax ester metabolism", *Microbial Cell Factories*, vol. 10, no. 75, 2011.

[130] S. Santala, E. Efimova, V. Kivinen, A. Larjo, T. Aho, M. Karp, and V. Santala, "Improved Triacylglycerol Production in *Acinetobacter baylyi* ADP1 by Metabolic Engineering", *Microbial Cell Factories*, vol. 10, no. 36, 2011.

[131] S. Santala, M. Karp, and V. Santala, "Rationally Engineered Synthetic Coculture for Improved Biomass and Product Formation", *PLoS ONE*, vol. 9, no. 12, e113786, 2014.

[132] P. Satyamurthy and N. Vigneshwaran, "A novel process for synthesis of spherical nanocellulose by controlled hydrolysis of microcrystalline cellulose using anaerobic microbial consortium", *Enzyme and Microbial Technology*, vol. 52, pp. 20–25, 2013.

[133] B. J. van Schie, R. J. Rouwenhorst, J. P. van Dijken, and J. G. Kuenen, "Selection of glucose-assimilating variants of *Acinetobacter calcoaceticus* LMD 79.41 in chemostat culture", *Antonie van Leeuwenhoek*, vol. 55, no. 1, pp. 39–52, 1989.

[134] J. K. Schmidt, C. Riedele, L. Regenstein, J. Rausenberger, and U. Reichl, "A Novel Concept Combining Experimental and Mathematical Analysis for the Identification of Unknown Interspecies Effects in a Mixed Culture", *Biotechnology and Bioengineering*, vol. 108, pp. 1900–1911, 2011.

[135] J. J. Seppälä, A. Larjo, T. Aho, O. Yli-Harja, M. T. Karp, and V. Santala, "Prospecting hydrogen production of *Escherichia coli* by metabolic network modeling", *International Journal of Hydrogen Energy*, vol. 38, pp. 11 780–11 789, 2013.

[136] J. J. Seppälä, J. A. Puhakka, O. Yli-Harja, M. T. Karp, and V. Santala, "Fermentative hydrogen production by *Clostridium butyricum* and *Escherichia coli* in pure and cocultures", *International Journal of Hydrogen Energy*, vol. 36, pp. 10 701–10 708, 2011.

[137] J. Sheng, H. Meng, and R. O. Fox, "Validation of CFD Simulations of a Stirred Tank Using Particle Image Velocimetry Data", *The Canadian Journal of Chemical Engineering*, vol. 76, pp. 611–625, 1998.

[138] J. D. Simen, M. Löffler, G. Jäger, K. Schäferhoff, A. Freund, J. Matthes, J. Müller, R. Takors, and RecogNice-Team, "Transcriptional response of *Escherichia coli* to ammonia and glucose fluctuations", *Microbial Biotechnology*, vol. 10, no. 4, pp. 858–872, 2017.

[139] M. J. H. Simmons, H. Zhu, W. Bujalski, C. J. Hewitt, and A. W. Nienow, "Mixing in a Model Bioreactor Using Agitators with a High Solidity Ratio and Deep Blades", *Chemical Engineering Research and Design*, vol. 85, no. 5, pp. 551–559, 2007.

[140] J. Soini, K. Ukkonen, and P. Neubauer, "Accumulation of amino acids deriving from pyruvate in *Escherichia coli* W3110 during fed-batch cultivation in a two-compartment scale-down bioreactor", *Advances in Bioscience and Biotechnology*, vol. 2, pp. 336–339, 2011.

[141] S. Stolyar, S. V. Dien, K. L. Hillesland, N. Pinel, T. J. Lie, J. A. Leigh, and D. A. Stahl, "Metabolic modeling of a mutualistic microbial community", *Molecular Systems Biology*, vol. 3, no. 92, 2007.

[142] C. C. Stowers, B. M. Cox, and B. A. Rodriguez, "Development of an industrializable fermentation process for propionic acid production", *Journal of Industrial Microbiology and Biotechnolgy*, vol. 41, pp. 837–852, 2014.

[143] A. J. J. Straathof, "Transformation of Biomass into Commodity Chemicals Using Enzymes or Cells", *Chemical Reviews*, vol. 114, no. 3, pp. 1871–1908, 2014.

[144] M. Svensson, L. Han, G. Silfversparre, L. Häggström, and S. Enfors, "Control of endotoxin release in *Escherichia coli* fed-batch cultures", *Bioprocess and Biosystems Engineering*, vol. 27, pp. 91–97, 2005.

[145] M. Svensson, I. Svensson, and S. Enfors, "Osmotic stability of the cell membrane of *Escherichia coli* from a temperature-limited fed-batch process", *Applied Microbiology and Biotechnology*, vol. 67, pp. 345–350, 2005.

[146] R. Taffs, J. E. Aston, K. Brileya, Z. Jay, C. G. Klatt, S. McGlynn, N. Mallette, S. Montross, R. Gerlach, W. P. Inskeep, D. M. Ward, and R. P. Carlson, "*In silico* approaches to study mass and energy flows in microbial consortia: a syntrophic case study", *BMC Systems Biology*, vol. 3, no. 114, 2009.

[147] W. Tang, A. T. Deshmukh, C. Haringa, G. Wang, W. van Gulik, W. van Winden, M. Reuss, J. J. Heijnen, J. Xia, J. Chu, and H. J. Noorman, "A 9-Pool Metabolic Structured Kinetic Model Describing Days to Seconds Dynamics of Growth and Product Formation by *Penicillium chrysogenum*", *Biotechnology and Bioengineering*, vol. 114, pp. 1733–1743, 2017.

[148] W. Tang, A. Pan, H. Lu, J. Xia, Y. Zhuang, S. Zhang, J. Chu, and H. Noorman, "Improvement of glucoamylase production using axial impellers with low power consumption and homogeneous mass transfer", *Biochemical Engineering Journal*, vol. 99, pp. 167–176, 2015.

[149] M. B. Ternbach, C. Bollman, C. Wandrey, and R. Takors, "Application of Model Discriminating Experimental Design for Modeling and Development of a Fermentative Fed-Batch L-Valine Production Process", *Biotechnology and Bioengineering*, vol. 91, no. 3, 2005.

[150] I. Valdez-Vazquez, M. Perez-Rangel, A. Tapia, G. Buitron, C. Molina, G. Hernandez, and L. Amaya-Delgado, "Hydrogen and butanol production from native wheat straw by synthetic microbial consortia integrated by species of *Enterococcus* and *Clostridium*", *Fuel*, vol. 159, pp. 214–222, 2015.

[151] P. Vrábel, R. G. J. M. van der Lans, Y. Q. Cui, and K. C. A. M. Luyben, "Compartment Model Approach: Mixing in Large Scale Aerated Reactors with Multiple Impellers", *Trans IChemE*, vol. 77, pp. 291–302, 1999.

[152] P. Vrábel, R. G. J. M. van der Lans, K. C. A. M. Luyben, L. Boon, and A. W. Nienow, "Mixing in large-scale vessels stirred with multiple radial or radial and axial up-pumping impellers: modelling and measurements", *Chemical Engineering Science*, vol. 55, pp. 5881–5896, 2000.

[153] P. Vrábel, R. G. J. M. van der Lans, F. N. van der Schot, K. C. A. M. Luyben, B. Xu, and S. Enfors, "CMA: integration of fluid dynamics and microbial kinetics in modelling of large-scale fermentations", *Chemical Engineering Journal*, vol. 84, pp. 463–474, 2001.

[154] J. de Vries and W. Wackemagel, "Integration of foreign DNA during natural transformation of *Acinetobacter* sp. by homology-facilitated illegitimate recombination", *Proceedings of the National Academy of Sciences*, vol. 99, no. 4, pp. 2094–2099, 2002.

[155] J. Wallenius, D. Barth, and T. Eerikäinen, "The effects of pH oscillations on *Lactobacillus rhamnosus* batch cultivation", *Applied Microbiology and Biotechnology*, vol. 95, pp. 1265–1273, 2012.

[156] J. Wallenius, T. Uuksulainen, K. Salonen, J. Rautio, and T. Eerikäinen, "The effect of temperature and pH gradients of *Lactobacillus rhamnosus* gene expression of stress-related genes", *Bioprocess and Biosystems Engineering*, vol. 34, pp. 1169–1176, 2011.

[157] S. van der Walt, S. C. Colbert, and G. Varoquaux, "The NumPy Array: A Structure for Efficient Numerical Computation", *Computing in Science & Engineering*, vol. 13, pp. 22–30, 2011.

[158] G. Wang, B. Wu, J. Zhao, C. Haringa, J. Xia, J. Chu, Y. Zhuang, S. Zhang, J. J. Heijnen, W. van Gulik, A. T. Deshmukh, and H. J. Noorman, "Power input effects on degeneration in prolonged penicillin chemostat cultures: A systems analysis at flux, residual glucose, metabolite, and transcript levels", *Biotechnology and Bioengineering*, vol. 115, pp. 114–125, 2018.

[159] G. Wang, J. Zhao, C. Haringa, W. Tang, J. Xia, J. Chu, Y. Zhuang, S. Zhang, A. T. Deshmukh, W. van Gulik, J. J. H. 4, and H. J. Noorman, "Comparative performance of different scale-down simulators of substrate gradients in *Penicillium chrysogenum* cultures: the need of a biological systems response analysis", *Microbial Biotechnology*, vol. 11, no. 3, pp. 486–497, 2018.

[160] E. Wang, M. Ding, Q. Mia, X. Dong, and Y. Yuan, "Reorganization of a synthetic microbial consortium for one-step vitamin C fermentation", *Microbial Cell Factories*, vol. 15, no. 21, 2016.

[161] J. von Wulffen, RecogNice-Team, O. Sawodny, and R. Feuer, "Transition of an Anaerobic *Escherichia coli* Culture to Aerobiosis: Balancing mRNA and Protein Levels in a Demand-Directed Dynamic Flux Balance Analysis", *PLoS ONE*, vol. 11, no. 7, e0158711, 2016.

[162] J. Wutz, A. Lapin, F. Siebler, J. E. Schäfer, T. Wucherpfennig, M. Berger, and R. Takors, "Predictability of $k_L a$ in stirred tank reactors under multiple operating conditions using an Euler-Lagrange approach", *Engineering in Life Sciences*, vol. 16, pp. 633–642, 2016.

[163] T. Xia, M. A. Eiteman, and E. Altman, "Simultaneous utilization of glucose, xylose and arabinose in the presence of acetate by a consortium of *Escherichia coli* strains", *Microbial Cell Factories*, vol. 11, no. 77, 2012.

[164] M. Xie, J. Xia, Z. Zhou, G. Zhou, J. Chu, Y. Zhuang, S. Zhang, and H. Noorman, "Power consumption, local and average volumetric mass transfer coefficient in multiple-impeller stirred bioreactors for xanthan gum solutions", *Chemical Engineering Science*, vol. 106, pp. 144–156, 2014.

[165] B. Xu, M. Jahic, G. Blomsten, and S. Enfors, "Glucose overflow metabolism and mixed-acid fermentation in aerobic large-scale fed-batch processes with *Escherichia coli*", *Applied Microbiology and Biotechnology*, vol. 51, pp. 564–571, 1999.

[166] B. Xu, M. Jahic, and S. Enfors, "Modeling of Overflow Metabolism in Batch and Fed-Batch Cultures of *Escherichia coli*", *Biotechnology Progress*, vol. 15, pp. 81–90, 1999.

[167] J. Zahradník, R. Mann, M. Fialová, D. Vlaev, S. D. Vlaev, V. Lossev, and P. Seichter, "A networks-of-zones analysis of mixing and mass transfer in three industrial bioreactors", *Chemical Engineering Science*, vol. 56, pp. 485–492, 2001.

[168] H. Zhang, B. Pereira, Z. Li, and G. Stephanopoulos, "Engineering *Escherichia coli* coculture systems for the production of biochemical products", *Proceedings of the National Academy of Sciences*, vol. 112, no. 27, pp. 8266–8271, 2015.

[169] K. Zhou, K. Qiao, S. Edgar, and G. Stephanopoulos, "Distributing a metabolic pathway among a microbial consortium enhances production of natural products", *Nature Biotechnology*, vol. 33, no. 4, pp. 377–383, 2015.

[170] A. R. Zomorrodi, M. M. Islam, and C. D. Maranas, "d-OptCom: Dynamic Multi-level and Multi-objective Metabolic Modeling of Microbial Communities", *ACS Synthetic Biology*, vol. 3, pp. 247–257, 2014.

[171] A. R. Zomorrodi and C. D. Maranas, "OptCom: A Multi-Level Optimization Framework for the Metabolic Modeling and Analysis of Microbial Communities", *PLoS Computational Biology*, vol. 8, no. 2, e1002363, 2012.

[172] T. R. Zuroff, S. B. Xiques, and W. R. Curtis, "Consortia-mediated bioprocessing of cellulose to ethanol with a symbiotic *Clostridium phytofermentas*/yeast co-culture", *Biotechnology for Biofuels*, vol. 6, no. 59, 2013.

APPENDIX A. SUPPLEMENTARY FIGURES AND TABLES

Supplementary tables and figures omitted from Chapter 4 are provided here:

1. Table A.1 summarizes the batch experiments performed (Section 4.1)
2. Table A.2 summarizes the 0.55 L batch simulations (Section 4.2)
3. Table A.3 summarizes the 22 L batch simulations (Section 4.2)
4. Figure A.1 shows the course of the 22 m^3 batch simulations (Section 4.2)
5. Table A.4 summarizes the 0.55 L fed-batch simulations (Section 4.3)
6. Table A.5 summarizes the 22 L fed-batch simulations (Section 4.3)
7. Figure A.2 shows the course the 22 m^3 fed-batch simulations (Section 4.3)
8. Table A.6 summarizes results of the economic assessment (Section 4.4).

Table A.1 *Summary of* 0.55 L*-batch cultivations.* Δ_m*-notation is used as a shorthand for* $\max(x) - \min(x)$*, not for* $x_1 - x_0$*.*

	Unit	EC	AB	EC:AB	ECΔ*ptsI*:AB	EC:ABΔ*gntT*	ECΔ*ptsI*:ABΔ*gntT*
OD_0		0.07	0.12	0.01	0.02	0.11	0.10
OD_1		0.91	1.14	1.66	0.45	2.64	0.44
$\Delta_m OD$		0.90	1.04	1.65	0.44	2.53	0.34
G_0	mM	52.14	55.91	49.86	55.49	48.36	56.90
G_1	mM	38.97	50.67	26.02	35.48	30.14	38.09
$\Delta_m G$	mM	13.17	7.34	24.47	22.51	23.00	18.82
N_0	mM	0.67	0.07	0.07	3.44	1.89	2.08
N_1	mM	0.07	0.07	13.09	13.67	0.82	6.37
$\Delta_m N$	mM	0.59	4.23	13.01	10.40	3.09	6.30
A_0	mM	0.00	0.00	0.00	0.00	2.26	4.48
A_1	mM	14.86	0.00	0.00	0.00	2.58	0.00
$\Delta_m A$	mM	14.86	0.00	0.00	0.00	4.88	4.48
pO_{20}		0.99	1.00	0.94	1.00	1.00	1.00
pO_{21}		0.73	0.40	0.00	0.50	0.00	0.83
$\Delta_m pO_2$		0.37	0.60	1.00	0.50	1.00	0.17
pH_0		6.93	7.03	7.00	7.03	6.96	6.99
pH_1		4.95	6.92	5.58	6.79	4.63	6.50
$\Delta_m pH$		1.99	0.15	1.45	0.32	2.34	0.55
FIg_0	kRFU	0.70	0.00	0.01	0.01	0.38	0.48
FIg_1	kRFU	6.72	0.28	1.29	0.14	8.87	2.66
Δ_mFIg	kRFU	6.19	0.27	1.29	0.13	8.49	2.18
FIr_0	kRFU	0.00	0.14	0.01	0.01	0.08	0.18
FIr_1	kRFU	0.00	6.40	1.74	1.55	2.22	0.46
Δ_mFIr	kRFU	0.00	6.26	1.74	1.54	2.20	0.31
Q_{OD}	$L^{-1}\,h^{-1}$	0.08	0.09	0.12	0.03	0.17	0.02
Y_{ODG}	g^{-1}	0.38	0.79	0.37	0.11	0.61	0.10
μ_{max}	h^{-1}	0.29	0.25	0.44	0.35	0.32	0.29
$\mu_{75\,\%}$	h^{-1}	0.28	0.24	0.38	0.30	0.26	0.17
μ_{med}	h^{-1}	0.26	0.23	0.38	0.29	0.23	0.09
$\mu_{25\,\%}$	h^{-1}	0.22	0.10	0.38	0.28	0.19	0.01
μ_{min}	h^{-1}	0.17	0.10	0.34	0.00	0.16	−0.09
t	h	11.93	12.00	13.68	15.97	14.80	18.07

Table A.2 *Summary of small-scale batch simulations. Like in the experiment summary (Table A.1),* Δ_m *corresponds to the difference of maximum and minimum,* $\max x - \min x$.

	Unit	EC	AB	EC:AB	ECΔ*ptsI*:AB	EC:ABΔ*gntT*	ECΔ*ptsI*:ABΔ*gntT*
$\Delta_\mathrm{m}X$	$\mathrm{g\,L^{-1}}$	2.62	2.40	2.47	2.17	2.48	1.77
$\Delta_\mathrm{m}G$	$\mathrm{g\,L^{-1}}$	10.00	10.00	10.00	10.00	10.00	10.00
$\Delta_\mathrm{m}N$	$\mathrm{g\,L^{-1}}$	0.00	6.37	2.53	0.24	2.63	0.23
$\Delta_\mathrm{m}A$	$\mathrm{g\,L^{-1}}$	1.22	0.00	0.18	0.02	0.39	0.04
$\Delta_\mathrm{m}O$	$\mathrm{mg\,L^{-1}}$	6.84	6.93	6.94	6.93	6.93	4.66
Q_X	$\mathrm{g\,L^{-1}\,h^{-1}}$	0.12	0.09	0.15	0.09	0.14	0.04
Y_XG	$\mathrm{g\,g^{-1}}$	0.26	0.24	0.25	0.22	0.25	0.18
μ_max	$\mathrm{h^{-1}}$	0.30	0.21	0.36	0.26	0.34	0.22
$\mu_{75\,\%}$	$\mathrm{h^{-1}}$	0.27	0.18	0.28	0.20	0.27	0.10
μ_med	$\mathrm{h^{-1}}$	0.16	0.13	0.20	0.13	0.23	0.04
$\mu_{25\,\%}$	$\mathrm{h^{-1}}$	0.08	0.10	0.11	0.06	0.11	0.02
μ_min	$\mathrm{h^{-1}}$	0.02	0.03	0.05	0.03	0.04	0.01
Δt	h	21.50	25.50	17.00	25.00	17.50	43.00

Table A.3 *Summary of large-scale batch simulations.*

	Unit	EC	AB	EC:AB	ECΔ*ptsI*:AB	EC:ABΔ*gntT*	ECΔ*ptsI*:ABΔ*gntT*
$\Delta_\mathrm{m}X$	$\mathrm{g\,L^{-1}}$	2.35	2.02	2.21	1.82	2.24	1.63
$\Delta_\mathrm{m}G$	$\mathrm{g\,L^{-1}}$	10.00	10.00	10.00	10.00	10.00	9.82
$\Delta_\mathrm{m}N$	$\mathrm{g\,L^{-1}}$	0.00	5.97	2.57	0.23	2.68	0.23
$\Delta_\mathrm{m}A$	$\mathrm{g\,L^{-1}}$	1.87	0.00	0.27	0.02	0.54	0.04
$\Delta_\mathrm{m}O$	$\mathrm{mg\,L^{-1}}$	8.77	8.83	8.84	8.83	8.83	8.62
Q_X	$\mathrm{g\,L^{-1}\,h^{-1}}$	0.08	0.05	0.08	0.04	0.08	0.03
Y_XG	$\mathrm{g\,g^{-1}}$	0.23	0.20	0.22	0.18	0.22	0.17
μ_max	$\mathrm{h^{-1}}$	0.29	0.20	0.31	0.23	0.30	0.21
$\mu_{75\,\%}$	$\mathrm{h^{-1}}$	0.17	0.11	0.18	0.12	0.22	0.09
μ_med	$\mathrm{h^{-1}}$	0.07	0.05	0.08	0.04	0.08	0.03
$\mu_{25\,\%}$	$\mathrm{h^{-1}}$	0.04	0.04	0.05	0.02	0.05	0.02
μ_min	$\mathrm{h^{-1}}$	0.01	0.01	0.02	0.01	0.02	0.01
Δt	h	31.00	42.50	28.00	43.00	27.50	50.00

Table A.4 *Summary of small-scale fed-batch simulations. $\Delta_m G$ stands here for the amount of glucose fed into the reactor.*

	Unit	EC	AB	EC:AB	ECΔ*ptsI*:AB	EC:ABΔ*gntT*	ECΔ*ptsI*:ABΔ*gntT*
$\Delta_m X$	$g\,L^{-1}$	4.75	3.69	5.91	3.42	5.76	1.51
$\Delta_m G$	$g\,L^{-1}$	21.45	16.77	27.42	17.55	26.24	7.83
$\Delta_m N$	$g\,L^{-1}$	0.00	0.46	0.07	0.14	0.07	0.16
$\Delta_m A$	$g\,L^{-1}$	0.08	0.00	0.08	0.01	0.08	0.03
$\Delta_m O$	$mg\,L^{-1}$	6.17	6.25	6.96	6.93	6.96	3.41
Q_X	$g\,L^{-1}\,h^{-1}$	0.10	0.07	0.12	0.07	0.12	0.03
Y_{XG}	$g\,g^{-1}$	0.22	0.22	0.22	0.19	0.22	0.19
μ_{max}	h^{-1}	0.27	0.20	0.28	0.23	0.28	0.19
$\mu_{75\,\%}$	h^{-1}	0.14	0.12	0.14	0.12	0.15	0.08
μ_{med}	h^{-1}	0.04	0.04	0.04	0.04	0.04	0.04
$\mu_{25\,\%}$	h^{-1}	0.02	0.02	0.02	0.02	0.02	0.02
μ_{min}	h^{-1}	0.01	0.02	0.02	0.01	0.02	0.01
Δt	h	50.00	50.00	50.00	50.00	50.00	50.00

Table A.5 *Summary of large-scale fed-batch simulations. Like in Table A.4, $\Delta_m G$ denotes the amount of glucose fed during cultivation.*

	Unit	EC	AB	EC:AB	ECΔ*ptsI*:AB	EC:ABΔ*gntT*	ECΔ*ptsI*:ABΔ*gntT*
$\Delta_m X$	$g\,L^{-1}$	3.82	1.94	3.78	1.82	3.86	1.44
$\Delta_m G$	$g\,L^{-1}$	21.37	13.65	24.94	8.62	25.62	7.41
$\Delta_m N$	$g\,L^{-1}$	0.00	6.31	6.58	0.14	6.25	0.16
$\Delta_m A$	$g\,L^{-1}$	3.87	0.00	0.99	0.01	1.52	0.03
$\Delta_m O$	$mg\,L^{-1}$	8.80	8.84	8.84	8.83	8.84	7.99
Q_X	$g\,L^{-1}\,h^{-1}$	0.08	0.04	0.08	0.04	0.08	0.03
Y_{XG}	$g\,g^{-1}$	0.18	0.14	0.15	0.21	0.15	0.19
μ_{max}	h^{-1}	0.26	0.19	0.28	0.21	0.27	0.19
$\mu_{75\,\%}$	h^{-1}	0.10	0.10	0.10	0.09	0.11	0.08
μ_{med}	h^{-1}	0.04	0.04	0.04	0.03	0.04	0.03
$\mu_{25\,\%}$	h^{-1}	0.02	0.02	0.02	0.02	0.02	0.02
μ_{min}	h^{-1}	0.02	0.02	0.02	0.01	0.02	0.01
Δt	h	50.00	50.00	50.00	50.00	50.00	50.00

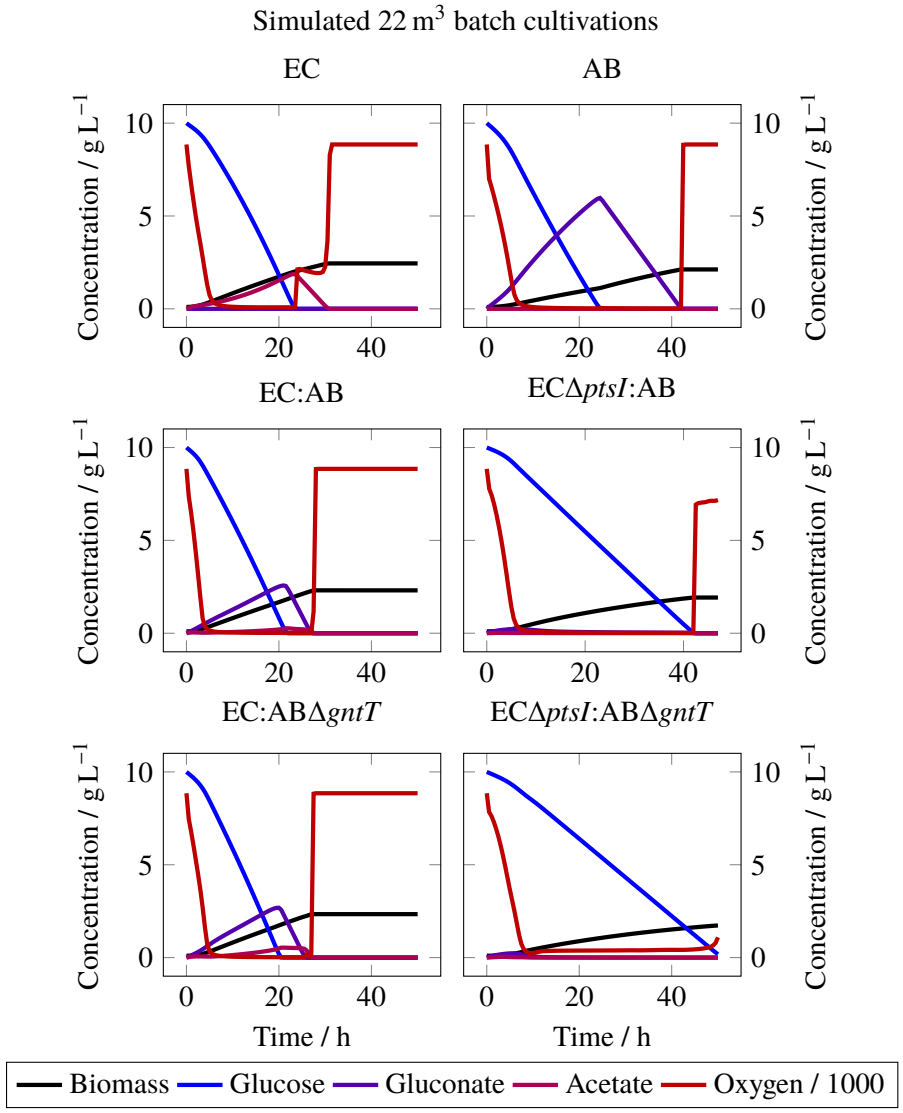

Figure A.1 *Simulated batches in* $30\,\mathrm{m}^3$ *reactor with* $22\,\mathrm{m}^3$ *working volume. The main difference to small-scale simulations is the consistently lower dissolved oxygen concentration. This is caused by a lower overall oxygen transfer coefficient* $k_\mathrm{L}a$ *in the large reactor.*

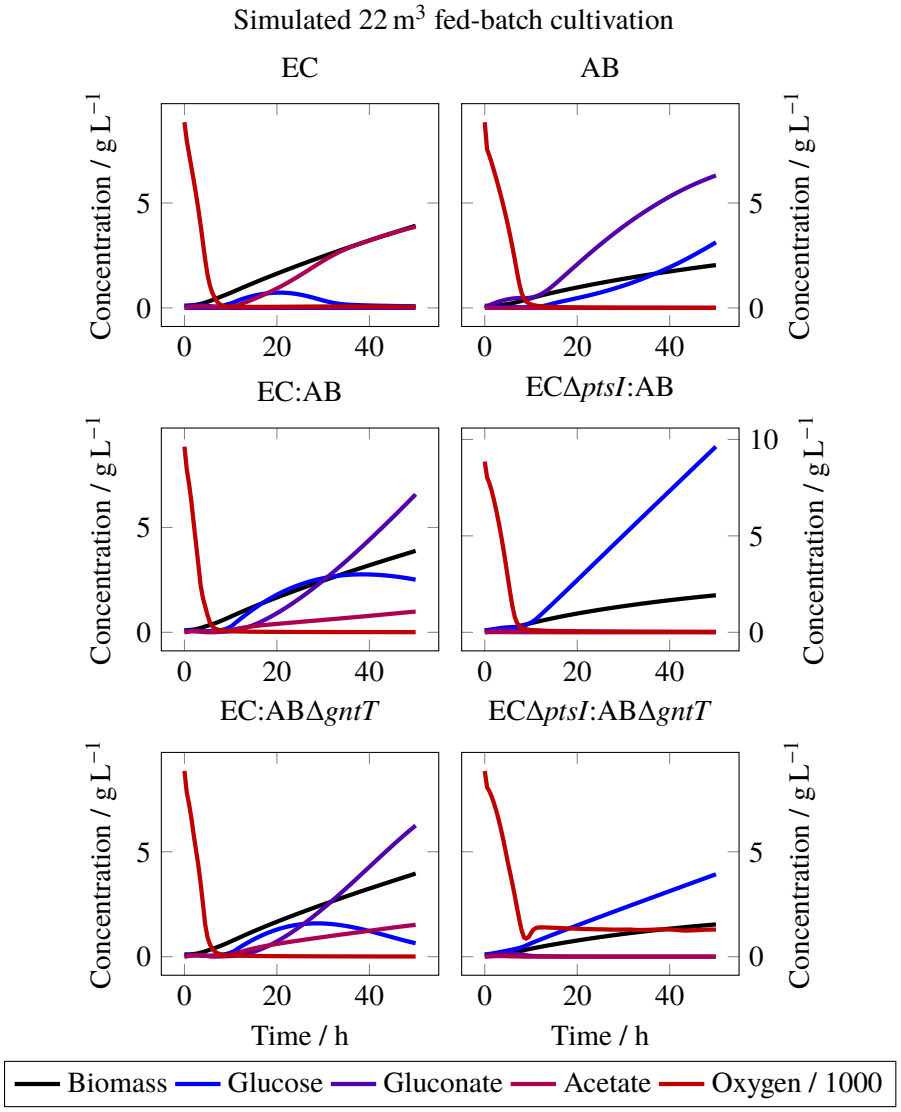

Figure A.2 *Simulated fed-batches in* $30\,m^3$ *reactor. The oxygen limitation caused accumulation of glucose, acetate, and gluconate.*

Table A.6 *Lost net present value in simulated scale-up of the six studied cultures. Small-scale biomass productivity relative to large-scale Q_S/Q_L is also shown. The co-culture EC*ΔptsI:*AB*ΔgntT *seems to have lost least amounts of net present value, but this is to some extent affected by the considerable oxygen limitation encountered by the other cultures. The losses were consistent between batch and fed-batch production modes.*

	EC	AB	EC:AB	ECΔ*ptsI*:AB	EC:ABΔ*gntT*	ECΔ*ptsI*:ABΔ*gntT*
Batch						
Minimum	3.05	5.14	3.61	5.46	3.25	1.70
25 %	18.8	31.6	23.2	33.8	20.8	9.87
Median	40.8	68.5	50.3	73.2	45.5	21.2
75 %	73.9	123	92.5	132	83	37.6
Maximum	263	432	347	461	308	121
Q_S/Q_L	1.61	1.98	1.84	2.05	1.74	1.26
Fed-batch						
Minimum	2.14	7.83	4.91	7.66	4.27	0.449
25 %	11.4	41.7	26.1	40.8	22.7	2.39
Median	23.7	86.9	54.4	85	47.3	4.98
75 %	41.5	152	95.3	149	82.9	8.72
Maximum	121	442	277	433	241	25.4
Q_S/Q_L	1.25	1.90	1.56	1.88	1.49	1.05